2016

Single molecule analysis of integrin-ligand interactions

Chenyu Wu
Lehigh University

Single molecule analysis of integrin-ligand interactions

by

Chenyu Wu

Presented to the Graduate and Research
Committee of Lehigh University
in Candidacy for the Degree
of Doctor of Philosophy

in

Bioengineering

Lehigh University

May 2016

Approved and recommended for acceptance as a dissertation in partial fulfillment of the requirements for the degree of Doctor of Philosophy.

Student name: Chenyu Wu

Dissertation title: Single molecule analysis of integrin-ligand interactions

May 2nd, 2016

Dr. Xiaohui (Frank) Zhang, Dissertation advisor

Accepted Date

Committee Members:

Dr. Yevgeny Berdichevsky

Dr. Bryan Berger

Dr. Daniel Ou-Yang

Dr. Chao Zhou

Acknowledgments

I would like to express my deepest gratitude to my advisor, Dr. Xiaohui (Frank) Zhang for his financial support, guidance and encouragement throughout out my doctoral study. He was always available and provided me the opportunity to learn and apply the most advanced techniques in single-molecule study.

I would also like to thank all my dissertation committee members: Dr. Yevgeny Berdichevsky, Dr. Bryan Berger, Dr. Daniel Ou-Yang and Dr. Chao Zhou for their discussions and suggestions during the projects.

I would like to give a special thanks to Dr. Susan Perry. I worked as her teaching assistant in class BIOE 357 for five semesters. She is one of the best people I have ever worked with and has an extraordinary passion for teaching.

I would also like to thank my current and former colleagues: Dr. Wei Zhang, Matthew Dragovich, Dr. Yan Xu, Steven Bach, Dr. Yizhen Wang and Yan Guo for their suggestions and assistance. It was a pleasure to work with every one of them.

I would like to thank all my friends at Lehigh: Yu song, Jing Liu, Yang Zhou, Yuanyuan Wang, Shunqiang Wang, Shuo Zhang and Whitney Lai, thank you for your accompaniment.

Lastly, I would like to thank my mother Lifang Zhou, my father Zhenghong Wu, my aunt Dr. Jun Zhou and other family members for their love, understanding, encouragement and support.

Table of Contents

List of Tables

List of Figures

Abstract

Precisely regulated lymphocyte trafficking plays very important roles in immune surveillance and host defense. The adhesive interaction between leukocyte integrin $\alpha_4\beta_7$ and its endothelial ligand, mucosal addressin cell adhesion molecule-1 (MAdCAM-1), mediates the rolling and firm adhesion of leukocytes to the high endothelial venules of mucosal tissues. A key property of $\alpha_4\beta_7$ is that it mediates rolling on resting leukocytes. Upon leukocyte activation, $\alpha_4\beta_7$ is induced to adopt a high-affinity conformation and thus mediates firm adhesion. We used single-molecule force spectroscopy (SMFS) and single-cell force spectroscopy (SCFS) to determine the mechanical strength of the low- and high-affinity $\alpha_4\beta_7$/MAdCAM-1 complexes. An atomic force microscope (AFM) was used to pull individual $\alpha_4\beta_7$/MAdCAM-1 complexes to determine their mechanical strength and force-dependent dissociation kinetics under ionic conditions that produce low- and high-affinity complexes, which mediate leukocyte rolling and firm adhesion, respectively. Integrin $\alpha_4\beta_7$ also binds to vascular cell adhesion molecule-1 (VCAM-1) expressed in other tissues. To regulate the adhesion of lymphocytes to target tissues, integrin $\alpha_4\beta_7$ must be able to distinguish different ligands. Here we used SCFS to pull individual $\alpha_4\beta_7$/MAdCAM-1 or $\alpha_4\beta_7$/VCAM-1 complexes under different chemokine stimulations and demonstrated that the chemokine CCL25 promotes $\alpha_4\beta_7$-mediated lymphocyte adhesion to MAdCAM-1 but suppresses adhesion to VCAM-1, whereas the chemokine CXCL10 regulates adhesion in the opposite way at the single molecule level. In addition, Sin Nombre Hantavirus (SNVs) bind to the Plexin Semaphorin Integrin (PSI) domain of inactive, bent conformation β_3 integrins. We used SMFS to pull individual integrin $\alpha_{IIb}\beta_3$ and $P2Y_2R$ complexes, with or without SNVs binding, and demonstrated that binding of SNV to the PSI domain induces

an increase in the affinity of the integrin's RGD binding site, and stimulates activation of several heterotrimeric G-proteins, Rho GTPases and infection.

In conclusion, this work provides new insights into the kinetic mechanism of integrin-mediated leukocyte rolling and firm adhesion, but also provides a mechanism for lymphocyte homing through the unique ligand-specific regulation of integrin adhesion by different chemokines. Our findings are also fundamental to understanding integrin-GPCR transactivation, and Hantavirus pathogenesis.

1 Introduction

Leukocytes in the immune system not only protect the human body from infectious disease and foreign invaders, but also facilitate the repair of damaged tissues. Leukocytes circulate in blood vessels looking for signs of inflammation or tissue damage. The complicated mechanism involved in recruiting leukocytes from blood vessel to inflammation or tissue damage sites has been investigated for more than 40 years. There is a recognized multistep paradigm, which describes the process of recruiting leukocytes. The recruitment involves leukocytes's tethering and rolling, activation, firm adhesion, crawling and transendothelial migration [1] (Figure 1.1). During the process, biochemical signals released or produced from the tissue damage site activate leukocytes and endothelium to aid monocyte recruitment. Chemokines, a group of biochemical signals that induce leukocyte activation, increase the binding of adhesion molecules expressed on the leukocytes surface and their ligands expressed on the vascular endothelium [2]. These signals may also increase the expression of adhesion molecules on the endothelium [3]. Cell adhesion molecules are crucial in regulating leukocyte adhesion and movement. The interactions between integrins and their ligands play important roles in leukocyte migration in inflamed vessels of many organs. Integrins receive outside-in and inside-out transmembrane signals, which regulate leukocytes to perform their functions appropriately. Integrin are also major players in mediating leukocyte migration directly.

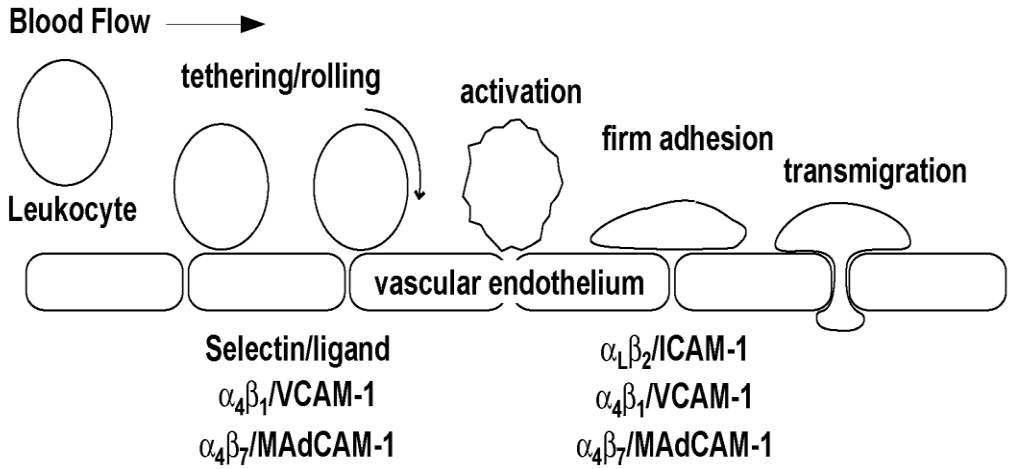

Figure 1.1 Recruitment of leukocytes in inflamed tissues. Multiple cell adhesion molecules, including selectins, immunoglobulin superfamily members, and integrin, mediate the initial tethering/rolling, firm adhesion, and transmigration of leukocytes. Leukocytes are captured from the circulating blood by transient α_4 integrin-ligand or selectin-glycan-based interactions. Following activation by chemokines, the leukocytes adhere firmly to the endothelial cells via integrin-mediated (i.e., α_4 integrin or α_L β_2) adhesion.

1.1 Overview of leukocytes recruitment to the endothelium

Leukocytes circulating in the bloodstream are first captured to the vascular endothelium by adhesion molecules named selectins expressed on the surface of leukocytes [4]. Selectins have very high on-(association) and off-(dissociation) rates (100 fold faster than antibodies), which allow leukocytes to rapidly and reversibly bind to the endothelium [5]. The leukocytes first overcome the shear stress exerted by blood flow, then tether and roll on the endothelium as the bonds between leukocytes and endothelium are constantly formed and broken during the rapid binding and unbinding process. Damaged vascular tissue can release biochemical signals to trigger leukocyte adhesion, and rolling of leukocytes on the endothelium allow theses adhesive signals to be detected [6].

Chemokines are a group of proteins released from damaged tissue that activate integrins [7] and may also upregulate the expression of ligands for integrins on the endothelium [8]. The integrin activation may involve the following: the increase of integrin

expression [9, 10], the increase of integrin affinity to its ligands [7, 11-13], and integrin clustering [14]. In general, integrins can resist larger forces than selectins, thus can strop leukocyte rolling and arrest them to the endothelium [5]. Once leukocytes are arrested, they firmly adhere to the endothelium, crawl and extravagate across the endothelium, and infiltrate the inflamed tissue.

1.1.1 Integrins

In 1986 Tamkun and co-workers named an integral membrane protein "integrin" because it maintained the "integrity" of the linkage between the Extra Cellular Matrix (ECM) and the actin cytoskeleton [15, 16]. Integrins are constitutively expressed on a wide variety of cells and their main function is to facilitate cell adhesion [17]. Integrins serve as mediators in transducing both outside-in and inside-out signals [17, 18]. Extracellular ligands binding to integrins trigger outside-in signals [19-23], whereas chemokine and cytokine stimulation trigger inside-out signals and result in intracellular regulation of integrin adhesiveness [2, 11, 13, 24-28].

Integrins are heterodimeric transmembrane molecules, held together by strong non-covalent interactions. Integrins mediate cell adhesion by binding to components of the extracellular matrix or to another cell by binding to members of the IgSF. The N-terminal region of all integrin alpha subunits is made up of seven repeats that form a 'beta-propeller' structure. In half of the integrin, a 200-residue, Rossmann fold 'I-domain' is inserted between the beta-propeller repeats 2 and 3. A divalent cation coordination site, designated the metal ion-dependent adhesion site in the I-domain, binds negatively charged residues in ligands. A similar 'beta I-domain' structure is found in the N-terminal of the beta subunit, which is directly involved in ligand binding in integrins that lack I-domains in the alpha

subunits (Figure 1.2) [29]. Other domains of the alpha and beta chain are important in regulating the integrin's global conformation, affinity, and the bidirectional mechanical signals crossing through the cell membranes [30, 31]. Affinity regulation is an important functional feature of all integrins. The strength of the integrin-ligand bond is drastically increased when the integrin molecule is activated by intracellular signals. Although the detailed molecular mechanism of affinity regulation is still obscure, it is shown that integrin activation is associated with a dramatic change of its overall global conformation [30, 31].

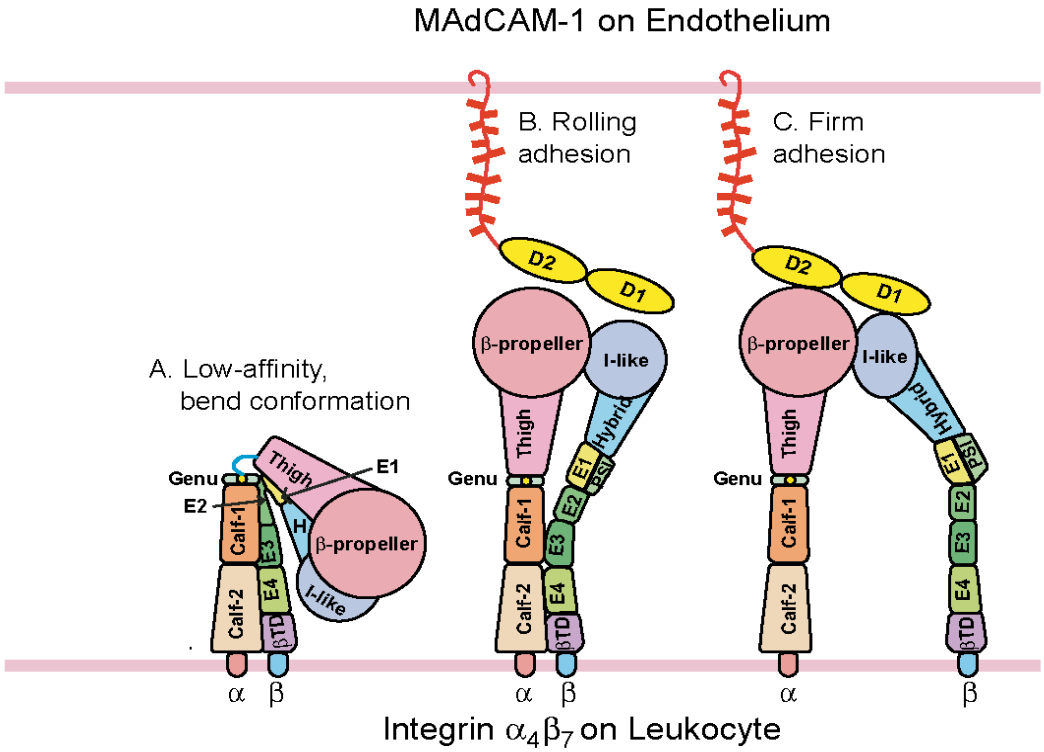

Figure 1.2 Different affinity conformations of integrin and their supports on leukocyte rolling and firm adhesion. Integrin exist in three different conformational states: (A) Bend low-affinity conformation, (B) Extended low affinity that regulates leukocytes rolling adhesion, (C) Extended high affinity that regulates leukocytes firm adhesion

α_4 integrin expressed on leukocyte membrane, including $\alpha_4\beta_1$ and $\alpha_4\beta_7$, are prominently important in the trafficking of leukocytes from the blood to sites of inflammation [32]. The biggest difference between α_4 integrins and others is their multistep

functions in leukocyte recruitment and the ability of α_4 integrins to both mediate leukocyte rolling and firm adhesion under different conditions. For example, integrin $\alpha_4\beta_7$, also known as LPAM-1 (lymphocyte Peyer's patch adhesion molecule-1), can mediate transient and reversible leukocyte rolling along the vascular endothelium under physiologic flow *in vivo* and *in vitro*. After leukocyte activation, which is induced by chemokines acting through G-protein coupled receptors on the cell membrane and a sequential signal cascade that is still not well defined, $\alpha_4\beta_7$-mediated leukocyte adhesion can be enhanced. The increased adhesion supports the leukocyte's stable arrest and spreading on the endothelium [33]. Some structural basis of the regulation of $\alpha_4\beta_7$ adhesiveness has previously been further elucidated through biochemical study [34]. However, the kinetic properties and mechanical mechanism of $\alpha_4\beta_7$- mediated different leukocyte adhesion have been unknown.

1.2 The mechanical strength of a ligand-receptor bond

1.2.1 Force spectroscopy

Single-molecule force spectroscopy (SMFS) and single-cell force spectroscopy (SCFS) are techniques used in this study to determine the mechanical strength and the lifetime of a ligand-receptor bond in response to a spectrum of applied forces. By attaching biomolecules to atomic force microscopy (AFM) tips, AFM based SMFS has been intensively used to study protein-protein interactions since 1994 [35-38]. Later, SCFS was developed by attaching a single living cell to an AFM tip and using the AFM system to detect the mechanics between the cells on the tip and the other cells or molecules on the substrates [39-45]. These methods are widely used to study the mechanical properties of

single polymer proteins, or individual ligand-receptor bonds. Force spectra can reveal the intrinsic kinetics and mechanical strength of the ligand-receptor bond.

1.2.2 Bell model

All of the theories and models characterizing force spectra are derived from Kramers' transitions state theory. The Bell and Bell-Evans model were used in this study to characterize the ligand-receptor bond force spectra.

George Bell was one of the first scientists to apply kinetic models to study the rate of bond dissociation under applied forces in 1978 [46, 47]. The kinetic model Bell proposed describes the influence of external forces on the rate of bonds dissociation, referred to as the Bell model:

$$k_{off}(f) = k^{o} \exp\{\frac{f\gamma}{k_B T}\} \qquad [1\text{-}1]$$

where f is force, k^o is the dissociation rate constant in the absence of the applied force, k_B is the Boltzmann's constant, T is absolute temperature and γ is the distance between the bound state and the transition state along the reaction coordinate.

The Bell model describes the lifetime of a single molecular ligand-receptor bond complex using a single energy barrier theory. It proposes that the dissociation rate of the adhesion complex increases to an external pulling force exponentially, and thus can be used to characterize the free energy changes in a biological single molecular adhesion bond under external forces (Figure 1.3). Although there is no rigorous theoretical justification for the exponential relationship proposed by Bell, recent experimental studies lend support and general acceptance of this model [48, 49].

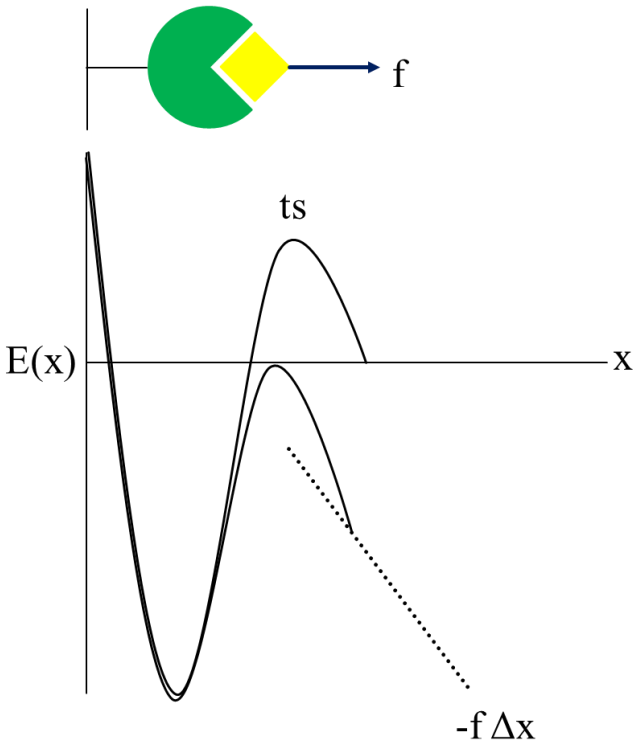

Figure 1.3 Bell-Evans model based on transition theory. Free energy plotted against receptor-ligand bond separation along the reaction coordinate. An external force tending to separate the bond will decrease the free energy linearly with distance.

Based on the Bell model, a ligand and its receptor exist in the bound state at equilibrium because the energy configuration for the bound complex is much lower than that of the unbound state. Once the applied energy from the external force exceeds the energy barrier height, the ligand-receptor bond will dissociate. The parameters k^o and γ are referred to as the Bell model parameters. These two parameters describe the energy potential of the ligand-receptor bond. k^o describes the depth and γ describes the width of the energy potential. The off rate k^o is equivalent to the dissociation rate of the bound ligand-receptor complex. The energy barrier width γ dictates the minimum separation distance required to completely break the bound ligand-receptor bond, or the force resistance of the adhesion bond. The energy barrier width scaled by the external force $f\gamma$

dictates the amount of work needed to lower the energy barrier. If the γ value of a bond is small, the external force will have little effect on the bond's off rate $k_{off}(f)$ since fγ is small. But if the γ value is large, the bond will be very sensitive to applied force since fγ adds a larger term to the activation energy potential. The parameter γ was later named as the "mechanical strength' of a receptor-ligand bond and is a function of the shape of the energy barrier during bond dissociation [46].

1.2.3 Bell-Evans model

The Bell model describes the change of a ligand-receptor bond under constant force over time. However, experimentally a constant pulling force is hard to achieve in the past, while a linearly increasing force is more feasible by setting up a constant pulling speed of the force probe. The Bell-Evans model was then developed to fit the case where a linearly increasing force is applied to the ligand-receptor bond and expressed as:

$$f^* = \frac{k_B T}{\gamma} \ln\{\frac{\gamma}{k^o k_B T}\} + \frac{k_B T}{\gamma} \ln\{r_f\} \qquad [1\text{-}2]$$

where f* is the most probable force f and r_f (rf=df/dt)is the loading rate, all other terms are the same as in Equation 1-1.

The Bell-Evans model shows that the most probable unbinding force f* is a linear function of the natural logarithm of r_f. Experimentally the most probable unbinding force f* is obtained from the mode of the unbinding force histogram. The loading rate is the rate of application of external force on the ligand-receptor bond and can be calculated from the pulling velocity and the system spring, which includes the mechanical stiffness of the ligand-receptor bond itself and the probe that pulls the bond.

In the plot of f* vs. ln(r_f), the Bell model parameters can be obtained from the slope and the y-intercept of the linear fit. The plot of f* vs. ln(r_f) was then named "Dynamic Force Spectrum" [47].

1.3 Overview of Atomic Force Microscopy

Conventional biochemical techniques cannot extrapolate the mechanical strength of a ligand-receptor bond from its binding affinities. Special devices such as atomic force microscopy (AFM) [50], optical tweezers/optical trap [51], the biomembrane force probe (BFP) [52], or transient tether measurements using the flow chamber [53] can measure the mechanical strength of a ligand-receptor bond from the dissociation rates as a function of pulling force. One of the major advantages of the AFM over the other devices is that the AFM can follow the trajectory of a single molecular interaction with ultra-high spatial and temporal resolutions. AFM can apply and measure forces over a range from 10 pico-newtons up to several nano-newtons. AFM can also achieve sub-second temporal control of substrates interactions and resolve sub-second adhesion events. The major device to be used in this study to measure the mechanical strength is a custom built AFM.

1.3.1 AFM components

The custom built AFM consists of several key components: laser, piezoelectric element, AFM cantilever, and a 2-segment photodiode shown in Figure 1.4. A cantilever is positioned on the sample surface; a beam of laser light is directed onto the cantilever and is reflected onto a photo detector, a 2-segment photodiode.

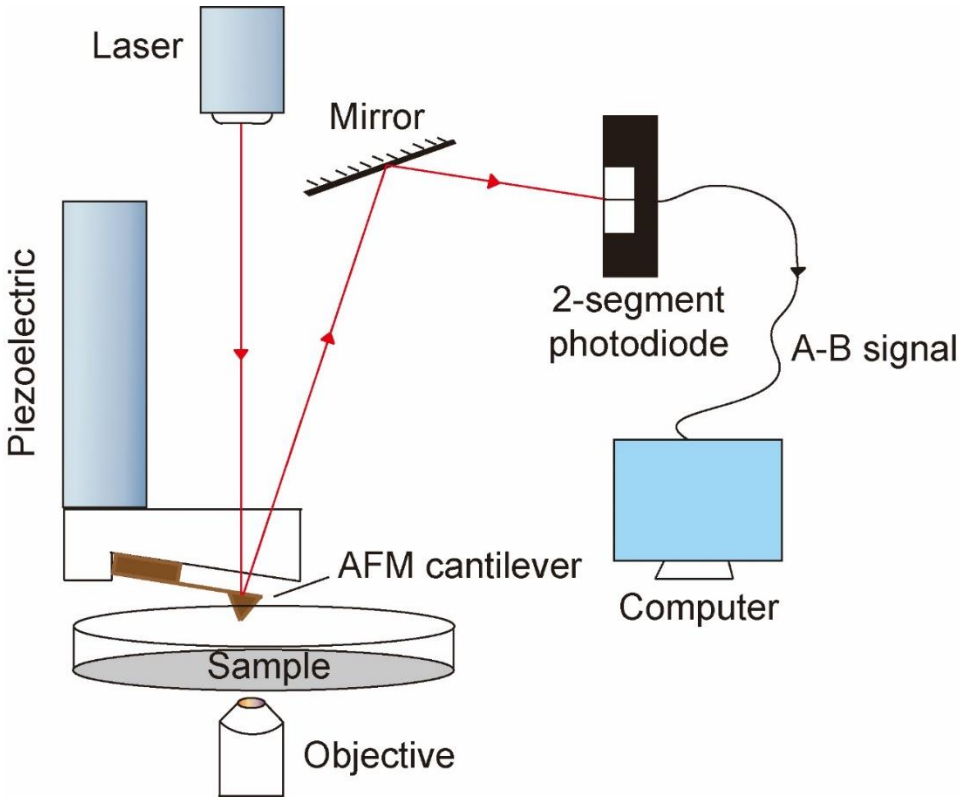

Figure 1.4 AFM schematics. A beam of laser light is directed onto the cantilever and is reflected onto a photo detector, a split photodiode. The difference (A–B) signal from the photodiode reports the bending of the cantilever due to forces exerted on the tip.

The cantilever is the transducer through which forces are applied and measured. It is flexible and behaves like a spring, which tends to oscillate at a natural frequency when no external perturbations are exerted. The frequency of the oscillation is refereed to as resonant frequency. The cantilevers used in this study are V-shaped Veeco MLCT-UC and MLCT-O10. The factory suggested spring constant is 0.01 N/m and the resonant frequency is 4-10 kHz. The cantilevers are composed of a thin layer of silicon nitride (Si_3N_4). For the MLCT-UC cantilever, at the apex of a triangular cantilever lies a small pyramidal tip (Figure 1.5). The tip or bottom side of the cantilever comes into contact with the substrate; for the MLCT-O10 cantilever, there is no tip at the apex, and it is used to pick up a cell (Figure 1.5). A focused fiber-coupled diode laser (Pegasus Optical Systems) is positioned

on the top side of the cantilever and reflected through a mirror onto a photodiode to monitor the cantilever deflection. When a force is applied to the cantilever, the reflected laser light path changes and cause the displacement of the reflected laser signal.

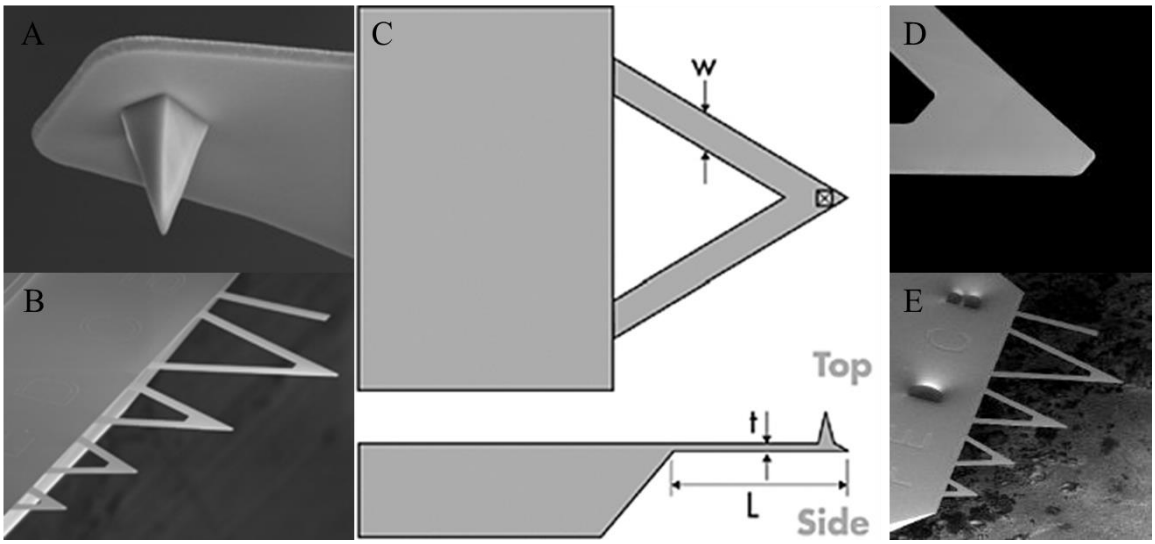

Figure 1.5 MCLT cantilever schematics. (A) MCLT-UC cantilever with a small pyramidal tip. (B) Overview of MCLT-UC cantilever. (C) Top and side view of an MLCT-UC cantilever. (Width: 20um, Thickness: 0.55umm, Length: 310um). (D) MCLT-O10 cantilever with no tip. (E) Overview of MCLT-O10 cantilever. (Figure is adapted with permission from Bruker Corporation website: www.BrukerAFMProbes.com)

The method to detect the displacement of the reflected laser signal is through a two-segment, position-sensitive photo diode (PSPD). Photons from reflected laser light impart energy onto a silicon semiconductor material and the measured current is proportional to the photon power. The 2-segments photodiode is divided into segments A and B. The displacement of the laser can be detected by comparing the light intensity difference between segments A and B (A-B signal) (Figure 1.6). The voltage difference between segments A and B is 0 when the laser spot is centered on the photodiode; the A-B signal becomes positive when the laser spot moves towards segment A and the A-B signal becomes negative when the laser spot moves towards segment B.

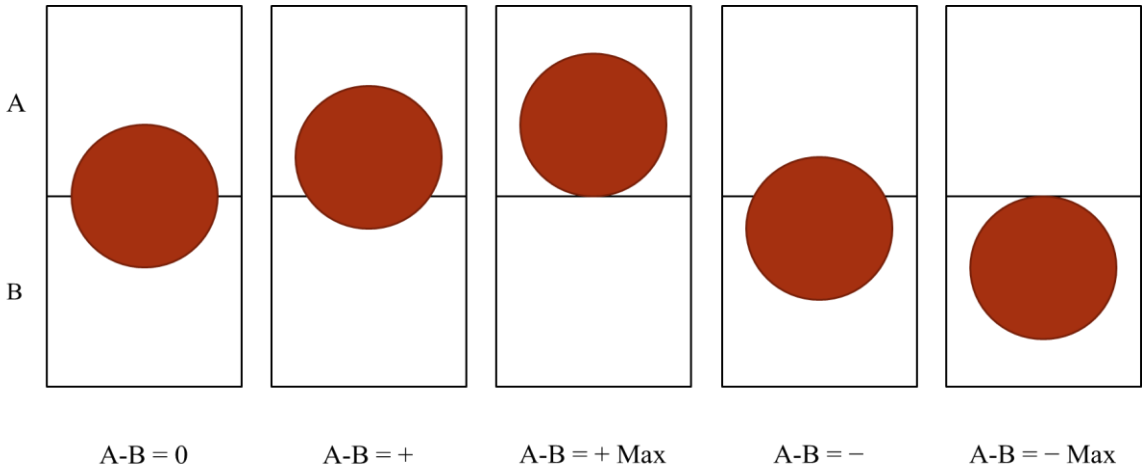

Figure 1.6 Detection of cantilever reflection with PSPD. The PSPD is divided into two segments A and B. The red circle represents the reflected laser spot. The A-B signal shows the displacement of the laser spot and is used to calculate the deflection of the cantilever tip.

The piezoelectric element makes it possible to accurately move the cantilever up and down and control the distance between the cantilever and the sample. An electric field is applied to a piezoelectric material causing either the compression or expansion of the material based on the polarity of the electric field. The extent of compression or expansion is monitored with a position sensor. The sample holder was designed to hold a standard 35-mm tissue culture dish. The whole AFM apparatus was suspended inside a refrigerator housing unit to minimize both the mechanical and thermal instabilities.

1.3.2 Measurement of forces

A force exerted on the cantilever causes the bending of the cantilever, resulting in the displacement of the reflected laser light spot on the 2-segment photodiode. The extent of cantilever bending is measured by determining the A-B signal. Because the cantilever obeys Hooke's Law for small displacements, the interaction force between the cantilever tip and the sample can be determined from the photodiode signal after a proper calibration of the spring constant of the cantilever using a thermal fluctuation method. In our AFM

setup, both the AFM and the sample stage can be moved in the x and y directions to make sure the sample is directly below the cantilever tip. Figure 1.7 depicts the representative force scans with adhesion or without adhesion. The two interacting surfaces are the AFM tip functionalized with streptavidin and a cell culture Petri dish immobilized with biotin. The amount of force exerted on the cantilever tip can be calculated from the deflection of the cantilever after calibration. When the measurements start, the cantilever is far away from the substrate and there is no force exerted on cantilever. The piezoelectric first expands and lowers the cantilever toward the biotin substrate. Before the cantilever touches the biotin substrate, the deflection signal maintains a stable baseline level. Once the cantilever tip eventually comes into contact with the biotin surface, the cantilever bends upward and results in a change in deflection signal. The piezo stops expanding when a preset compression force is reached. Then the piezo contracts and the cantilever is retracted from the substrate to its initial position. During the contact duration, the streptavidin and biotin may form bond(s). If there is adhesion between the cantilever tip and biotin surface, further upward movement of the cantilever results in an increase of tension applied to the streptavidin-biotin bond(s) until the bond(s) break. A sharp vertical transition in the retraction trace indicates bond rupture. If there is no adhesion between the cantilever tip and the biotin surface, the retraction trace will overlap with the approach trace. During the measurement, the piezoelectric is operated under a constant expansion/retraction velocity and the tension that increases to break the bonds is proportional to the time. The rate of change of tension $r_f = df/dt$, is the 'loading rate' and can be achieved by changing the piezoelectric retraction velocity.

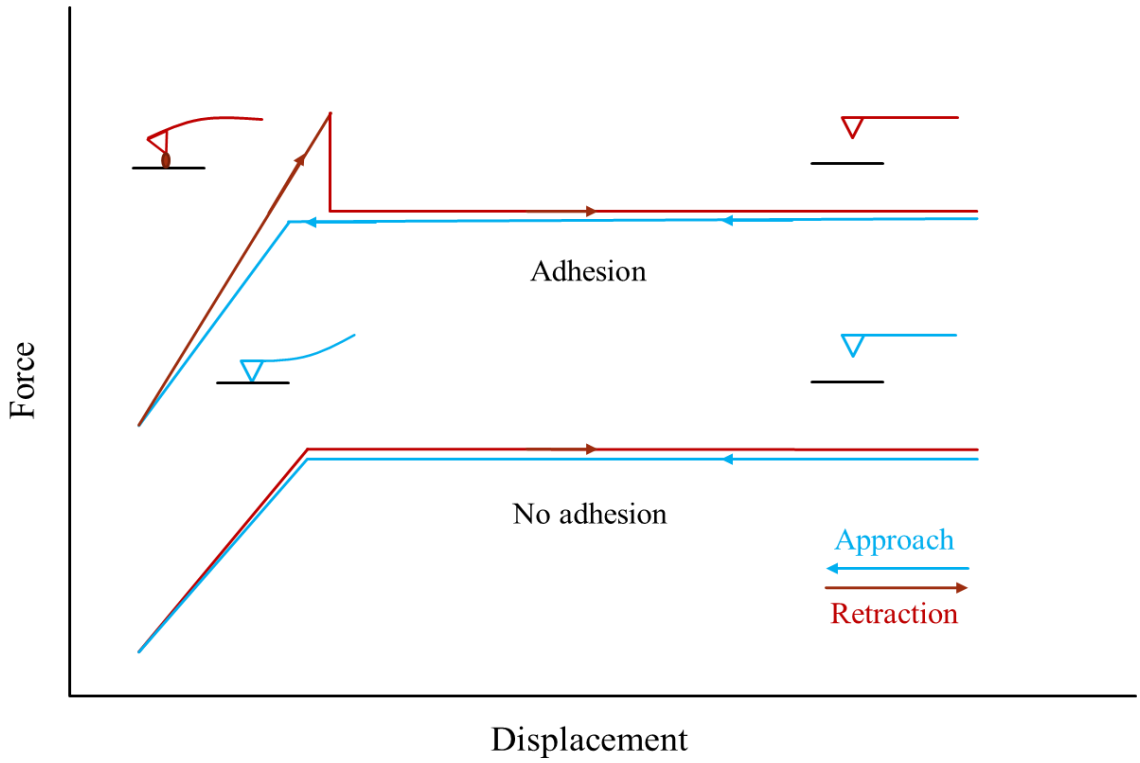

Figure 1.7 Cantilever deflection during a reprehensive force scan of biotin-streptavidin interaction. Blue lines represent approach curves and red lines represent retraction curves.

1.3.3 Acquisition of single molecule measurements

The key to successful single molecule measurements is to ensure that a single ligand-receptor bond is being picked and measured. In order to increase the probability of measuring a single bond, several factors can be controlled during the experiment: 1) protein concentration, 2) indentation force, and 3) contact time. Changes in the protein concentration will affect the chance of ligand and receptor binding; changes in the indentation force will affect the contact area formed between the substrates; changes in the contact time will not only affect the contact area formed between the substrates but also the binding probability. The single molecule measurements generally require a lower amount of protein concentration, small indentation forces and shorter contact times. Previous arguments for single-molecule measurements were justified statistically. When

the frequency of interaction between a ligand and a receptor is reduced to less than 30%, there is more than 80% probability that the adhesion event is mediated by a single bond [49].

1.3.4 Calibration

Two steps are required to calibrate an AFM cantilever for force measurements: 1) calibrate the photodiode position sensitivity of PSPD and 2) determine the spring constant of the cantilever tip. With the position sensitivity of PSPD, the electrical signal of the voltage difference can be converted into the distance of cantilever deflection. With the spring constant, the measured cantilever deflection can be converted to a force.

As described before, the raw electrical signal of cantilever deflection measured from the two segments photodiode is the voltage difference between the two segments. When an AFM cantilever comes into contact with a hard surface, the displacement of the cantilever is equal to the displacement of the piezoelectric element. In order to calibrate the position sensitivity, an AFM cantilever is pressed against a hard surface (cell culture Petri dish) and the slope of the contact region in the force scan is calculated (Figure 1.8A). The inverse of the slope, also called the inverse optical lever sensitivity (InvOLS), is the factor to convert the voltage difference between the photodiode and the actual distance of the cantilever deflection.

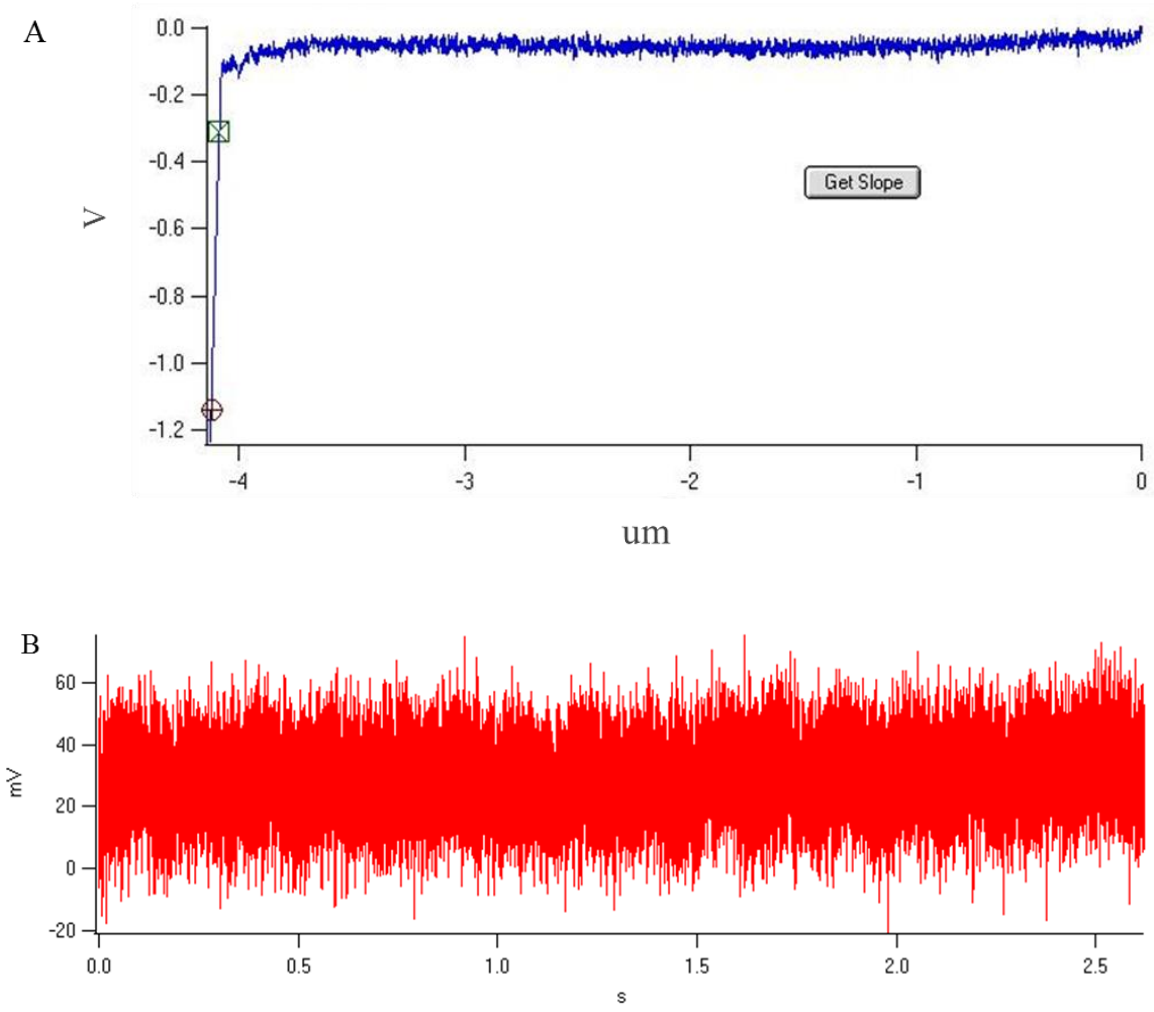

Figure 1.8 Determination of the position sensitivity of PSPD and cantilever spring constant, (A) Two open cursors represent the contact region where the InvOLS is determined. (B) Oscillation of a freely cantilever in PBS approximately 50 um above the cell culture Petri dish.

The spring constant varies from different sizes and shapes of the cantilever. The manufacturer reported cantilever spring constant is determined from a parallel beam approximation [54]. Although cantilevers are precisely made at the microscopic level during the manufacturing process, there is large variability between cantilevers from different batches. In addition, functionalization of cantilevers with molecules may also affect the cantilever spring constant. As a result, the thermal fluctuation method is used in this study to determine the spring constant of each cantilever.

The thermal fluctuation method is the most convenient and non-destructive method to experimentally determine the cantilever spring constant [55]. The oscillations or fluctuations of the cantilever at equilibrium with the surroundings in a free environment are mainly driven by thermal noise (Figure 1.8B). The cantilever spring constant (k) is determined by:

$$k = \frac{K_B T}{<q^2>} \qquad [1\text{-}3]$$

where K_B is Boltzmann's constant, T is the temperature in Kelvins and (q^2) is the rms displacement of the free oscillating cantilever, which can be determined by integrating the area under the power spectral density of the cantilever oscillations.

1.3.5 Hydrodynamic force measurements

In order to calculate the actual rupture force of the ligand-receptor bond, the hydrodynamic force of the AFM tips needs to be considered. Cantilevers without adhering cells that were manipulated by the AFM system didn't contact with the Petri dish surface at different speeds below 30 μm/s. Forces between approaching and retracting curves were calculated. Hydrodynamic forces were half of those forces. With a linear fitting curve in Figure 1.9, we obtained the hydrodynamic force value as a function of cantilever moving speed.

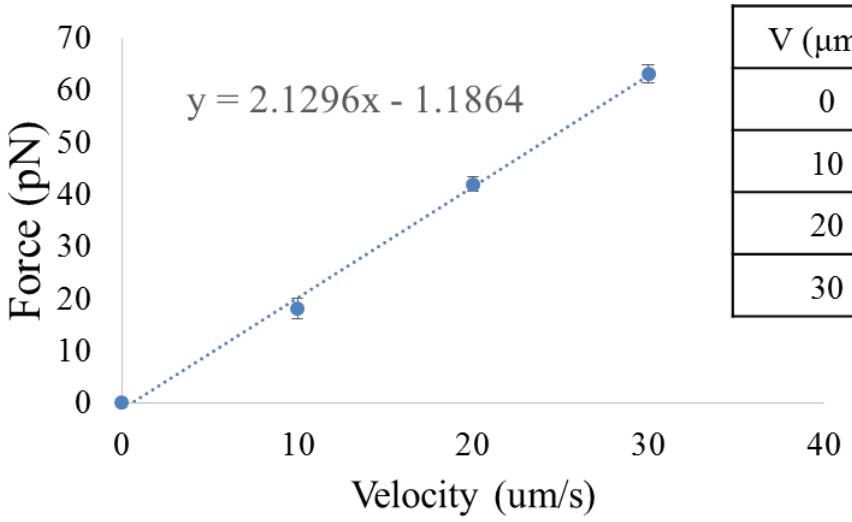

V (μm/s)	F (pN)
0	0
10	18.05570
20	41.95585
30	63.02150

Figure 1.9 Linear fitting of hydrodynamic force. The forces were recorded when the cantilever was moving at different speeds below 30 μm/s without adhering cells.

1.4 AFM cantilevers and substrate functionalization

1.4.1 Functionalization of AFM cantilevers and substrates via a polyethylene glycol (PEG) linker

Adhesion molecules are attached to an AFM cantilever via a flexible PEG linker. By inserting a long, flexible PEG chain between the cantilever surface and the adhesion molecules, the attached adhesion molecule is flexibly linked to the cantilever and can reorient itself to facilitate specific binding. The method to functionalize an AFM cantilever with flexible PEG linkers involves four steps. Firstly, amino groups (NH_2) are generated on the AFM cantilever surface. Secondly, at one end of the PEG linker, NHS ester groups react with these amino groups and form amide bonds. Thirdly, the acetal groups on the other side of the PEG linker are converted into an aldehyde groups. Lastly, the adhesion molecules attach to the aldehyde groups on the free-hanging end of the PEG chain.

1.4.2 Attaching cells to AFM cantilevers

The basic principle behind attaching cells to AFM cantilevers is functionalizing the cantilever surface with adhesion molecules such as Concanavalin A (Con A) or Poly-L-Lysine. This makes AFM cantilevers adhesive to cells and enables cells to be picked up by cantilever tip. Cantilever functionalization is achieved by increasing the cantilever surface pH to at least 9.0 and imparting a partial negative charge to cantilever. At high pH conditions, the primary amine group in the adhesion molecule binds to the negatively charged cantilever.

Con A specifically binds to the mannose on the cell membrane and can be used to functionalize the cantilever for cell capture. The process of coupling Con A to an AFM cantilever tip involves the following steps: First, a high pH $NaHCO_3$ buffer is used to increase the cantilever surface pH. Then the cantilever is functionalized with Biotin-BSA, The BSA couples with the cantilever surface due to the positive charged amino group in BSA adhered to the cantilever surface. Once the cantilever is functionalized with Biotin-BSA, streptavidin is introduced into the system as a linker for the Biotin-Con A coupling. Because streptavidin has four binding sites to biotin, the Biotin-Con A can be bound to the streptavidin-functionalized cantilever. Finally the cantilever is functionalized with Con A and is ready to pick up cells.

Poly-L-Lysine is commonly used to coat cell culture ware or the AFM cantilever tip as an attachment factor that promotes cell adherence. This is due to the interactions between negatively charged proteins on the cell membrane and positive charged Poly-L-Lysine. Functionalizing the cantilever with Poly-L-Lysine is achieved by treatting the cantilever with a high pH $NaHCO_3$ buffer to increasing the cantilever surface pH and

imparting a partial negative charge to the cantilever. At high pH conditions, the Poly-L-Lysine binds to the negatively charged cantilever. The functionalized cantilever is then mounted on an AFM cantilever holder and pressed against a cell to pick it up.

2 Biophysical mechanisms of Human integrin $\alpha_4\beta_7$ mediated leukocyte rolling and firm adhesion

2.1 Motivation

A complicated and efficient mechanism is involved in recruiting leukocytes from the blood stream to sites where inflammation or tissue damage has happened [56]. The mechanism of leukocyte recruitment has been investigated for more than 40 years. There is a recognized multistep paradigm describing the process of leukocyte recruitment. The recruitment involves leukocytes' tethering and rolling, activation, firm adhesion, crawling and transendothelial migration [57, 58]. During the process, cell adhesion molecules, such as selectins and integrins on leukocyte membranes, play critical roles in the regulation of leukocyte adhesion and movement [5]. The interactions between integrins, especially α_4 and β_2 integrins, and their ligands (cellular adhesion molecules, CAMs) are crucial for the leukocyte migration in inflamed vessels of many organs [57]. Integrins serve as mediators of exchanging outside-in and inside-out transmembrane signals [18]. These signals instruct leukocytes to perform their functions appropriately. And at the same time, integrins are major players in mediating leukocyte migration directly [32].

Herein, we applied AFM based single-molecule force spectroscopy (SMFS) and single cell force spectroscopy (SCFS) technologies to study the mechanical properties of interactions between human integrin $\alpha_4\beta_7$ and its preferred ligand human mucosal vascular addressin cell adhesion molecule 1 (MAdCAM-1) while governing leukocyte rolling and firm adhesion in vitro. By attaching biomolecules to AFM tips, AFM based SMFS has been intensively used to study protein-protein interactions since 1994 [35-38]. And later, the

method called SCFS was developed by attaching a single living cell to the AFM tip and using AFM system to detect the mechanics between cells on tip and other cells or molecules on substrates [39-45]. The development of SCFS has provided us new insight into biological interactions mechanics under physiological external forces which is fruitful in understanding cell adhesion processes.

To study the biophysical properties of human integrin $\alpha_4\beta_7$-mediated leukocyte rolling and firm adhesion, we first used SMFC to detect the mechanics of interactions between purified integrin $\alpha_4\beta_7$ and its preferred ligand MAdCAM-1 protein. Integrin $\alpha_4\beta_7$ is functionalized on an AFM cantilever tip and MAdCAM-1 is coated on the dish via long, flexible polyethylene glycol (PEG) chains (http://www.jku.at/biophysics/content). This approach not only avoided nonspecific interactions to the most extent, but also facilitated the specific binding to the target molecules [59-61].

Then we used SCFS method to detect the mechanics of interactions between integrin $\alpha_4\beta_7$ expressed on cell membranes of stable K562 transfectants and its ligand MAdCAM-1 protein coated on substrate. Full-length α_4 andβ_7 subunits expressing vectors were transfected into K562 cells and stable cell lines were screened. A significant property of $\alpha_4\beta_7$ is that its adhesiveness is regulated by metal ions [62]. In addition to wild type (WT) integrin $\alpha_4\beta_7$ K562 transfectants, we have also mutants including a metal ion-dependent adhesion site (MIDAS) mutant (S121A), an adjacent site to MIDAS (ADMIDAS) mutant (D126A) and a ligand-induced metal binding site (LIMBS) mutant (D217A) [34]. Human MAdCAM-1 protein containing domains 1 and 2 (D1 and D2) [63] with a His-tag was expressed and purified via the 293T expressing system and the Ni-NTA column. Previous studies indicated that D1 and D2 domains of MAdCAM-1 are responsible for interacting

with $\alpha_4\beta_7$ directly [63-65]. Integrin $\alpha_4\beta_7$/MAdCAM-1 mediated leukocyte slow rolling and firm adhesion after activation can be mimicked by manipulating metal cation as Ca^{2+}+Mg^{2+} and Mg^{2+} in the environment, respectively [34]. We applied AFM-based SCFS approach to detect the mechanical strength of $\alpha_4\beta_7$/MAdCAM-1 interactions under different affinity. Our research focused on the mechanical forces to rupture $\alpha_4\beta_7$/MAdCAM-1 complexes when they mediate leukocyte rolling and firm adhesion. Through Bell model [66] analysis, we have obtained new findings about the biophysical properties of this complex dissociation under physiological force in these conditions.

2.2 Materials and Methods

2.2.1 AFM setup

Single molecule rupture force measurements for integrin $\alpha_4\beta_7$/MAdCAM-1 were conducted using a custom built AFM as described in Chapter 1. All experiments were conducted at room temperature about 25℃ unless noted otherwise. Cantilevers were calibrated over a clean culture dish in PBS buffer using the Igor program. The photodiode position sensitivity was determined by indenting a non-compliant surface. Then a thermal fluctuation method was used to determine the spring constant of the cantilevers. The spring constant values of MLCT cantilevers (Bruker) used in this study were typically 0.01-0.02 N/m.

2.2.2 SMFC experiment

2.2.2.1 MAdCAM-1 D1, D2 construction and expression

The MAdCAM-1 D1, D2 cDNA was cloned into pHLsec mammalian expression vector. The pHLsec construct is based on the pLEXm backbone, and contains a signal

sequence for secretion of the protein fused with a C- terminal His6 tag. The MAdCAM-1 was cloned into pHLsec between the AgeI and KpnI cloning sites, in which MAdCAM-1 protein was fused with the C-terminal 6X His-tag (Figure 2.1). Transient protein expression was performed in Human embryonic kidney (HEK) 293T cells (ATCC) using MegaTran 1.0 Transfection Reagent (OriGene). HEK 293T Cells were cultured in Dulbecco's Modified Eagle Medium (DMEM) (Gibco Invitrogen) containing 10% Fetal Bovine Serum (FBS) (Biochrom, German), and 100U/mL Penicillin-Streptomycin (Gibco), 37°C, 5% CO_2. Supernatants were collected and MAdCAM-1 D1, D2 protein was isolated by nickel-NTA chromatography. Integrin $\alpha_4\beta_7$ was purchased from BD Biosciences.

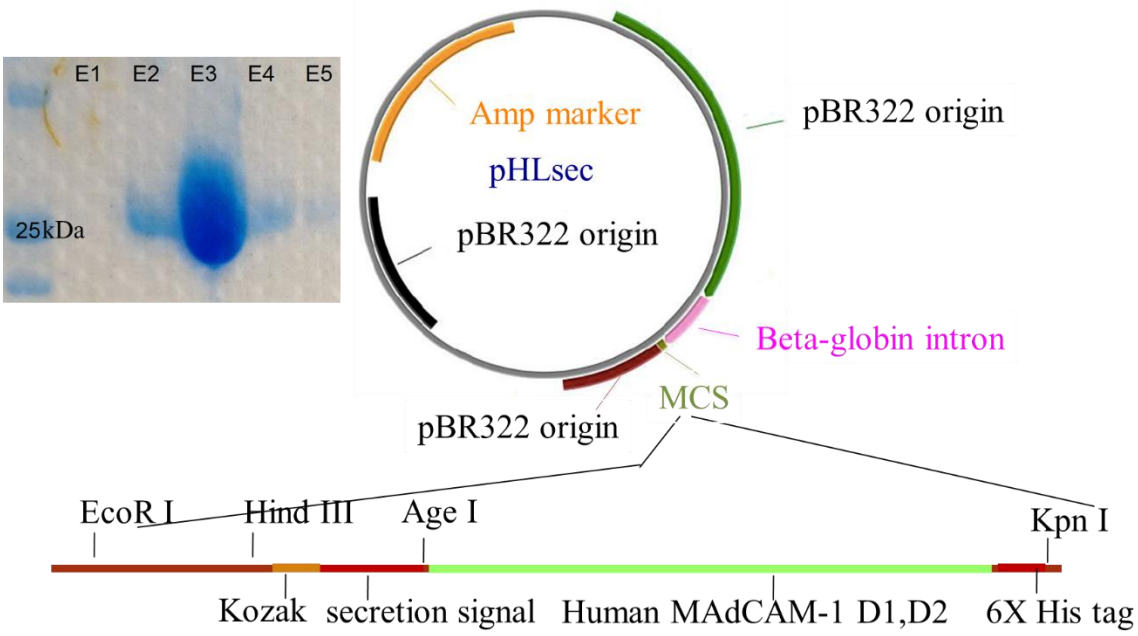

Figure 2.1 MAdCAM-1 D1, D2 plasmid construction and protein expression. The MAdCAM-1 was cloned into pHLsec between the AgeI and KpnI cloning sites, in which MAdCAM-1 protein was fused with the C-terminal 6X His-tag. Insert: Gel image of isolated MAdCAM-1 D1, D2. The majority of the MAdCAM-1 D1, D2 protein elute out in the 3rd fraction (1/2 column volume for each fraction).

2.2.2.2 AFM cantilever functionalization via polyethylene glycol (PEG) chains.

AFM cantilevers were functionalized with integrin $\alpha_4\beta_7$ using a bifunctional Polyethylene Glycol (PEG) crosslinker (Hinterdorfer and Dufrene, 2006). Silicon nitride cantilevers (MLCT: Bruker Nano, Camarillo, CA) were first cleaned using a UV-Ozone cleaner (ProCleaner Plus, Bioforce Nanosciences, Ames, IA) for 15 min and silanized with 2% v/v APTES (3-aminopropyltriethoxysilane) in toluene by incubation for 2 h at room temperature. The silanized cantilevers were rinsed thoroughly with toluene and ethanol and then immersed for 1 h in sodium borate (SB) buffer (50 mM, pH 8.5) to deprotonate the amino groups. NHS-PEG-acetal (N-hydroxysuccinimide-polyethylene glycol-acetal, MW 5000, Jenkem Technology, P.R. China), a polyethylene glycol spacer containing an amino-reactive group (NHS) at one end and an unreactive acetal group on the other end, was used to link integrin $\alpha_4\beta_7$ in a flexible state. The NHS-PEG-acetal was dissolved to a concentration of 50 mM, incubated on the sulfinyl modified cantilevers for 2 h at room temperature, and subsequently rinsed thoroughly with SB buffer to remove unbound NHS-PEG-acetal. Then the acetal group was converted into aldehyde group by incubation in 1% citric acid in water for 10 min. The integrin $\alpha_4\beta_7$ was coupled to the PEG-modified cantilevers though the aldehyde group by incubating the cantilevers in 100 ug/mL integrin $\alpha_4\beta_7$ solution with 20 uM $NaCNBH_3$ for 2 h at room temperature. The cantileverss were finally quenched with 50uM ethanolamine for 10 min and rinsed in phosphate-buffered saline (PBS) for 3 times before mount into AFM setup.

2.2.2.3 Substrate functionalization

For substrate treatments, glass coverslips were cleaned by sonication in a solution of 50% v/v ethanol for 10 min, followed by an additional 15 min irritation in the UV-Ozone

cleaner. The cleaned coverslips were silanized with 2% v/v APTMS (3-mercaptopropyl trimethoxysilane) in toluene during an incubation for 2 h at room temperature. Then, the coverslips were functionalized according to the similar procedures used for the cantilevers. The NHS-PEG-acetal was dissolved to a concentration of 50 mM, incubated on the sulfinyl modified coverslips for 2 h at room temperature, and subsequently rinsed thoroughly with SB buffer to remove unbound NHS-PEG-acetal. Then the acetal group was converted to aldehyde group by incubation in 1% citric acid in water for 10 min. The PEG-modified coverslips were immersed in MAdCAM-1 D1, D2 solution at 15 ug/mL to link the MAdCAM-1 D1, D2 to the coverslips through the aldehyde group. The coverslips were finally quenched with 50uM ethanolamine for 10 min and rinsed in PBS for 3 times before mount to the AFM setup.

2.2.2.4 AFM SMFS force measurements of individual integrin $\alpha_4\beta_7$ and MAdCAM-1 D1, D2 interactions

The indentation force and contact time between the cantilever tip and the sample were minimized to obtain measurements of the unitary integrin $\alpha_4\beta_7$/MAdCAM-1 D1, D2 unbinding force. An adhesion frequency of ~30% in the force measurements ensured that there was a >83% probability that the adhesion event was mediated by a single $\alpha_4\beta_7$/MAdCAM-1 D1, D2 bond [49]. Typically, a contact duration of 0-50 ms and a compression force of 50-150 pN satisfied these conditions. AFM measurements were collected at cantilever retraction speeds ranging from 0.6 to 10 μm/s to achieve the desired loading rate (50-5,000 pN/s). All measurements were conducted at 25^0C in Tris buffer (50 mM Tris, 0.15 M NaCl).

2.2.3 Cell adhesion experiment

2.2.3.1 Tissue culture of K562 cells

All K562 stable cell lines (WT, D126A, D217A and S121A transfectants) and K562 cells came from Dr. J. Chen [34]. cDNA construction and expression approaches were described previously [34]. Cells were cultured in RPMI 1640 media (Gibco Invitrogen) containing 10% FBS (Biochrom, German), 100U/mL Penicillin-Streptomycin (Gibco), 0.5 mg/mL G418 (Amresco) in PBS and 0.2 mg/mL Hygromycin B (Amresco).

2.2.3.2 Flow cytometry

One million of each kind of K562 cells were centrifuged at 1200 rpm for 5 minutes. The supernatant was then pipetted out and the cell pellet was washed once with 1 mL PBA buffer (PBS containing 1% BSA). After incubation with primary antibody human integrin $\alpha_4\beta_7$ specific monoclonal antibody Act-1 [67, 68] or isotype antibody X63 and second antibody goat anti-mouse Alexa-488 diluted in PBA, and the cells were then washed once with PBS, cells were suspended in 500 μL PBS for BD Calibur machine detection.

2.2.3.3 Protein immobilization

MAdCAM-1 D1, D2 protein cDNA was constructed into secreting plasmid pHLsec [69]. Constructs were transiently transfected into HEK 293T cells via MegaTran 1.0 reagent (Origene) according to the manufacturer's instructions. Secreted MAdCAM-1 protein with a His-tag protein in EX-Cell serum-free media (JRH biosciences) was purified with Ni-NTA resins (IBA). 20 μL of 15μg/mL purified MAdCAM-1 protein (diluted in PBS containing 10 mM $NaHCO_3$, pH 8.6) were dropped onto a 35mm Petri dish (Corning) surface and incubated in a wet box at 37℃ for 2 hours. After being washed twice with PBS, the surface was blocked by 1% bovine serum albumin (BSA) in PBS in a wet box at 37℃

for 1 hour. Before usage, the surface was washed twice with PBS and switched to 2 mL HBS buffer (150 mM NaCl, 5 mM HEPES, pH 7.4) containing 1mM Ca^{2+} and 1 mM Mg^{2+} or 1 mM Mg^{2+}.

2.2.3.4 Functionalization of AFM cantilevers with Con A

AFM probes (MLCT) were purchased from Veeco (Camarillo, CA). All probes were soaked with acetone for 5 min for cleaning. After 30 minutes of UV-light irradiation, the cantilevers were incubated with biotinamidocaproyl-labeled biotin-BSA (0.5 mg/mL in 100 mM $NaHCO_3$, pH 8.6; Sigma, St. Louis, MO) overnight at 37 ℃. Then the cantilevers were rinsed three times with PBS, and incubated in streptavidin (0.5 mg/mL in PBS; Pierce, Rockford, IL) for 10 min at room temperature. Following the removal of unbound streptavidin, the cantilevers were incubated in biotinylated Con A (0.5 mg/mL in PBS; Sigma) and then rinsed with PBS before usage.

2.2.3.5 AFM SCFS measurements of rupture forces of integrin $\alpha_4\beta_7$/MAdCAM-1 complex

1 mL of K562 cells from culture media were transferred into 1.5 mL Eppendorf tubes, and centrifuged at 1200 rpm for 3 minutes. Cells were washed twice with 1 mL Wash buffer (150 mM NaCl, 5 mM HEPES, 0.5% BSA and 5 mM EDTA, pH 7.4), then washed twice with 1 mL Buffer A (150 mM NaCl, 5 mM HEPES and 0.5% BSA, pH 7.4). After rinsing, 50ul of cell solution was added into polystyrene Petri dish already containing HBS buffer. Through manually manipulation of Con-A modified AFM probe, a single K562 cell can be picked up via interaction with the triangular area of the C-cantilever of the MLCT probe.

2.3 Results

2.3.1 AFM SMFS measurements of interactions between integrin $\alpha_4\beta_7$ and MAdCAM-1 D1, D2

We used purified MAdCAM-1 D1, D2 and integrin $\alpha_4\beta_7$ proteins to carry out AFM SMFS experiment. Integrin $\alpha_4\beta_7$ was covalently attached to the AFM cantilever and MAdCAM-1 D1, D2 was attached to a silanized cover glass (Figure 2.2). The specificity of the interaction was shown by the adhesion frequency measurement (Figure 2.3). The adhesion frequency was significantly decreased when either the integrin $\alpha_4\beta_7$ or MAdCAM-1 D1, D2 was not present. Also the interaction was abolished by the addition of excess EDTA. Figure 2.2B top trace shows a force scan with rupture forces of the integrin $\alpha_4\beta_7$/MAdCAM-1 D1, D2 bond. The unbinding force f_u of the integrin $\alpha_4\beta_7$/MAdCAM-1 D1, D2 complex is derived from the force jump that accompanies the unbinding of the complex. To increase the occurrence of a single molecule interaction, the contacts between the cantilever and the cover glass were minimized by reducing both the compression force (50-150 pN) and the contact time (0-50 ms).

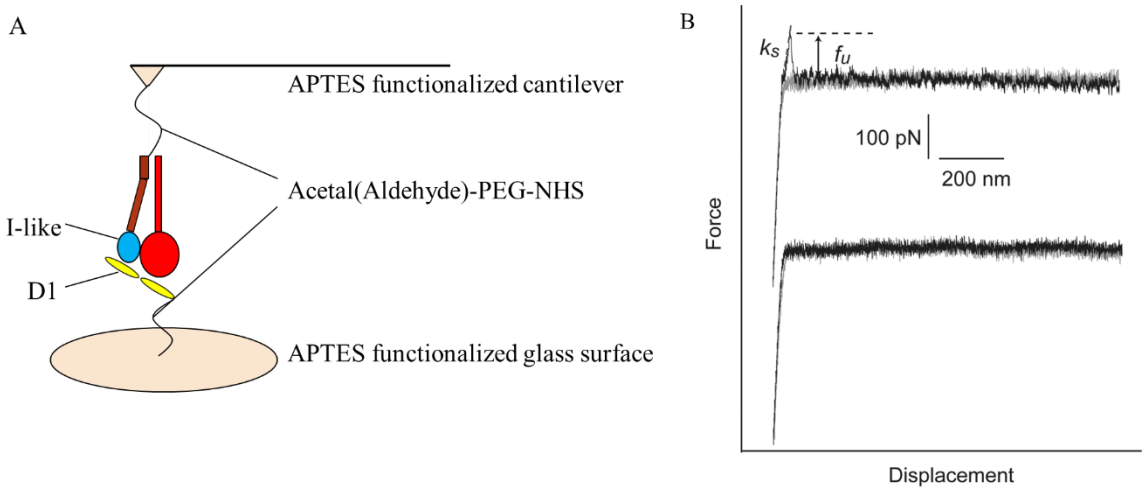

Figure 2.2 Experimental approach of SMFS measurement of interactions between integrin $\alpha_4\beta_7$ and MAdCAM-1 D1, D2. (A) The SMFS experimental system. Integrin $\alpha_4\beta_7$ was

covalently attached to an APTES functionalized cantilever and MAdCAM-1 D1, D2 was attached to an APTES functionalized silanized cover glass via PEG linkers. (B) Typical force scans during experiment. Top trace shows a force scan with rupture forces of the integrin $\alpha_4\beta_7$/MAdCAM-1 D1, D2 bond; bottom trace shows no adhesion. k_s is the system spring which will be used to calculate loading rate. f_u is the rupture force.

2.3.2 Quantitative unbinding force measurements of individual integrin $\alpha_4\beta_7$/MAdCAM-1 D1, D2 complexes

Due to interactions between integrin $\alpha_4\beta_7$ and MAdCAM-1 D1, D2, rupture force curves can be obtained from AFM measurements. On the basis of Hooke's law, rupture force values can be calculated from the spring constant of AFM probe cantilever and the vertical displacement distance of the cantilever, which can be detected by the photodiode from the movement of the laser beam. Through controlling the density of integrin $\alpha_4\beta_7$ coated on cantilever tip and MAdCAM-1 D1, D2 protein coated on the substrate surface, we ascertained conditions containing certain divalent metal cations under which certain probabilistic single force curves showed up during the measurements. In this study, we lowered the amount of integrin $\alpha_4\beta_7$ (100 ug/mL) and MAdCAM-1 D1, D2 (10 ug/mL) protein coated and got a less than 30% frequency of adhesive events during our measurements Figure 2.3.

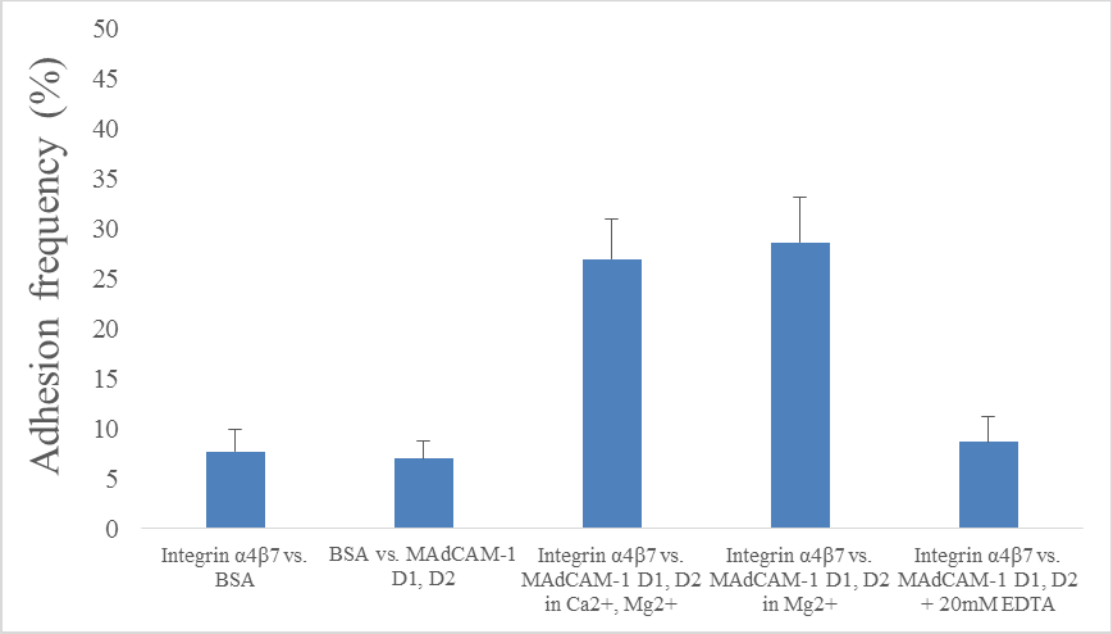

Figure 2.3 Force frequency of adhesion between integrin $\alpha_4\beta_7$ and MAdCAM-1 D1, D2 under different conditions. The data for the negative control groups were recorded under the same contact time and compression force.

Single molecule interactions at a same speed of AFM probe movement (at an average of certain loading rate) were recorded and counted in a histogram (Figure 2.4). The most probable rupture forces under certain average loading rates were acquired and plotted vs. loading rate. Rupture force adhesion changed with loading rate (50-3000 pN/s) and integrin affinity (regulated by divalent metal cation Ca^{2+} and Mg^{2+} in vitro) (Figure 2.4).

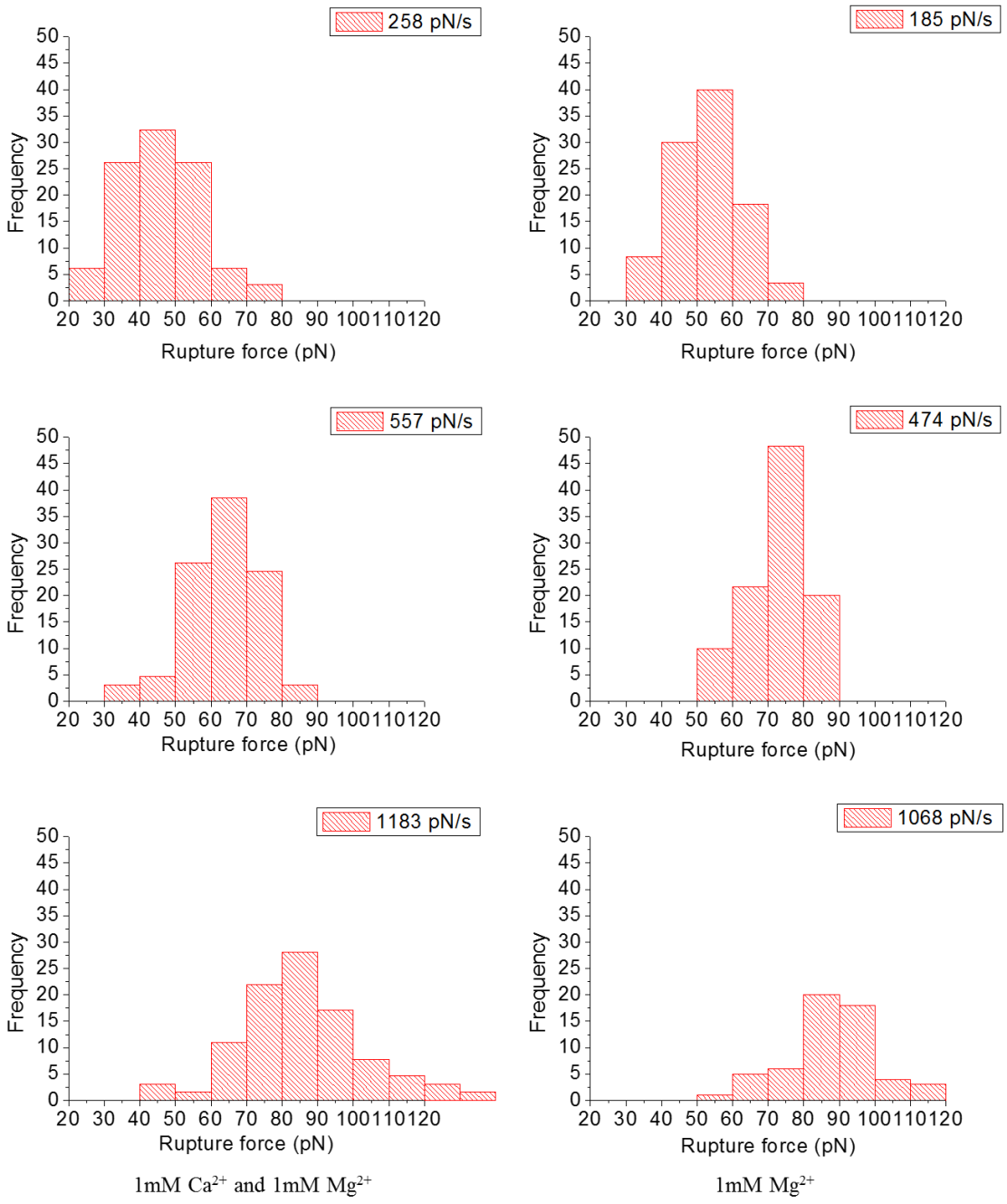

Figure 2.4 Dynamic force spectra of interactions between integrin $\alpha_4\beta_7$ and MAdCAM-1 D1, D2. Rupture force distributions of integrin $\alpha_4\beta_7$ and MAdCAM-1 D1, D2 at different loading rates, in 1mM Ca^{2+} and1mM Mg^{2+} (left) or 1mM Mg^{2+} (right) salt solution.

With the increase of loading rate, the rupture force needed to dissociate integrin $\alpha_4\beta_7$/MAdCAM-1 complex increased to varying degrees. In 1mM Mg^{2+}, when integrin $\alpha_4\beta_7$

was in its high-affinity conformation, interaction forces between integrin $\alpha_4\beta_7$ and MAdCAM-1 D1, D2 were stronger than in 1mM Ca^{2+} and 1mM Mg^{2+}, when integrin $\alpha_4\beta_7$ in its low-affinity conformation. Under similar loading rates, rupture forces changed significantly for integrin $\alpha_4\beta_7$/MAdCAM-1 D1, D2 complex under different ion conditions. In 1mM Ca^{2+} and 1mM Mg^{2+} buffer, the rupture force was about 65 pN at a loading rate of 557 pN/s; in 2mM Mg^{2+} buffer, the rupture force was about 75 pN at a loading rate of 474 pN/s.

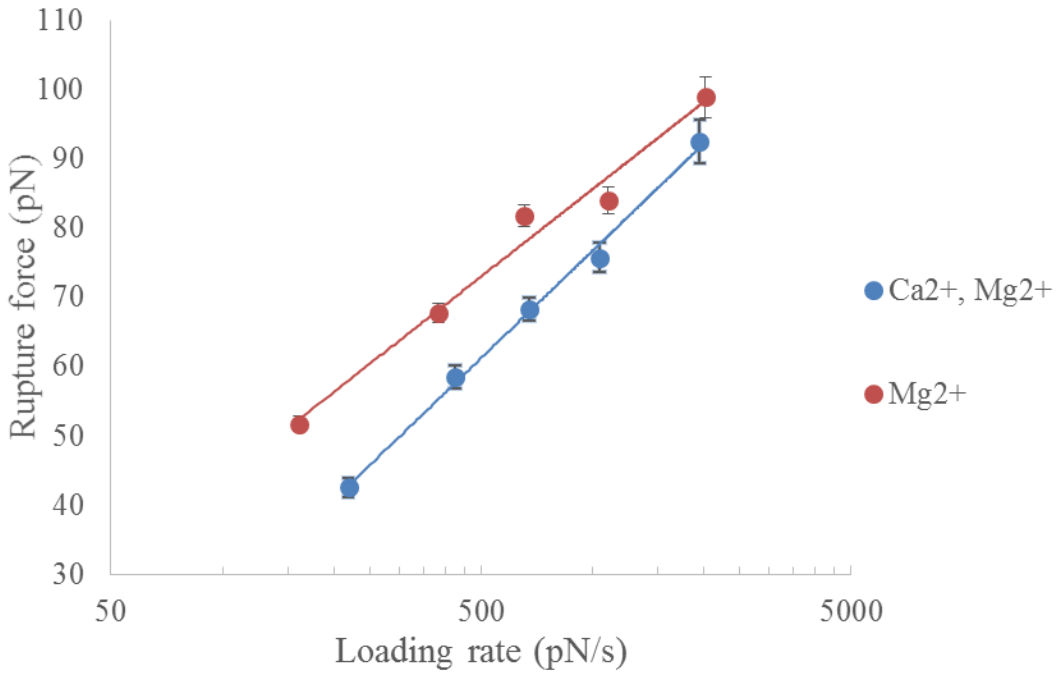

Figure 2.5 Rupture force dynamics of integrin $\alpha_4\beta_7$/MAdCAM-1 D1, D2. Force dynamics of integrin $\alpha_4\beta_7$/MAdCAM-1 D1, D2 in 1mM Ca^{2+} and 1mM Mg^{2+} or in 1mM Mg^{2+}.

2.3.3 Bell model parameters of integrin $\alpha_4\beta_7$/MAdCAM-1 complex dissociation

As described in the introduction, Bell and later Evans et al proposed a theoretical framework:

$$k_{off}(f) = k^{o} \exp\{\frac{f\gamma}{k_B T}\} \qquad [1\text{-}1]$$

$$f^* = \frac{k_B T}{\gamma} \ln\{\frac{\gamma}{k^o k_B T}\} + \frac{k_B T}{\gamma} \ln\{r_f\} \qquad [1\text{-}2]$$

to analyze the adhesion between two cells or between cell and surface when the adhesion is mediated by reversible bonds between specific molecules under external force [66]. The Bell-Evans model has been widely applied to analyze the dissociation of receptor-ligand bonds [70]. After a linear fitting between $f*$ and $\ln r_f$ in the OriginPro program, we computed the Bell parameters of the dissociation between integrin $\alpha_4\beta_7$ and its ligand MAdCAM-1 (Table 2-1).

Table 2-1 Bell parameters of purified integrin $\alpha_4\beta_7$/MAdCAM-1 complex dissociation

	Ca^{2+}+Mg^{2+}	Mg^{2+}
γ (Å)	1.85 ± 0.07	2.21 ± 0.18
k° (s^{-1})	1.43 ± 0.09	0.52 ± 0.12

2.3.4 AFM SCFS measurements of integrin $\alpha_4\beta_7$/MAdCAM-1 mediated K562 cell adhesion

We used established K562 transfectants that stably express human integrin $\alpha_4\beta_7$ on the cell membrane [34] (Figure 2.6) to conduct SCFS experiments and to examine whether the adhesiveness of integrin $\alpha_4\beta_7$ is regulated by metal ions [62]. In addition to K562 transfectants expressing wild type $\alpha_4\beta_7$, we also have three mutants of metal ion binding sites (MIDAS, ADMIDAS and LIMBS) that regulate $\alpha_4\beta_7$ adhesiveness, named S121A, D126A and D217A respectively. This kind of approach was beneficial for studying protein-protein interactions between integrin $\alpha_4\beta_7$ and MAdCAM-1 as integrins are naturally located on the leukocyte membrane. And at the same time, we can avoid non-specific

interactions to a large extent with the usage of purified human MAdCAM-1 coated substrate.

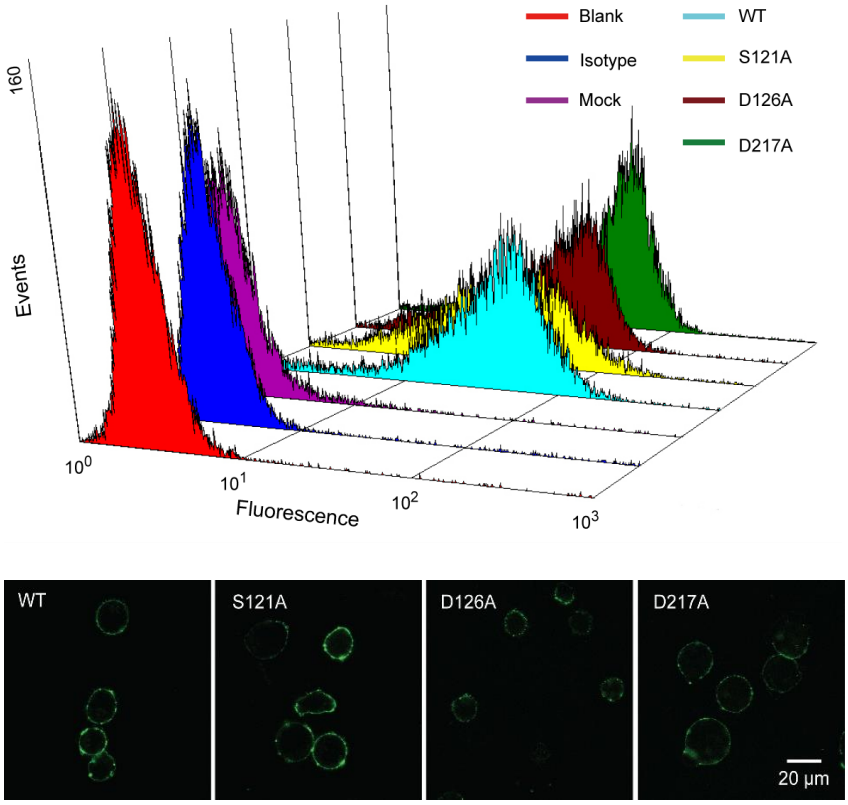

Figure 2.6 Integrin $\alpha_4\beta_7$ expression on K562 stable transfectants. Expression of human integrin $\alpha_4\beta_7$ was detected via flow cytometer (A) and confocal microscope (B). Cells were labeled by Act-1, a specific monoclonal antibody against human integrin $\alpha_4\beta_7$ [67, 68]. (A) Act-1 was not added in blank control (WT $\alpha_4\beta_7$ K562 transfectants); for isotype control, X63, mouse IgG1, was added instead of Act-1 into WT transfectants sample; mock control was K562 cells without integrin $\alpha_4\beta_7$ transfection. Molecular Probes Alexa Fluor 488 labeled goat anti–mouse IgG was used for secondary antibody.

We applied AFM-based single cell force spectroscopy technology to study the biophysical dynamics behind integrin $\alpha_4\beta_7$-mediated leukocyte adhesion. Figure 2.7 illustrates the AFM measurement of $\alpha_4\beta_7$-mediated K562 adhesion on MAdCAM-1 protein coated substrate system and the process of adhering a single living K562 cell onnto the AFM probe. A single living K562 cell transfectant expressing wild type or mutant integrin

$\alpha_4\beta_7$ was adhered onto the concanavalin A (ConA) functionalized cantilever of an AFM probe via manipulation of the probe [40, 44] (Figure 2.7). The single cell was first lowered down to make contact with the MAdCAM-1 coated surface of the cell culture Petri dish for 0.1 second. The compression force applied by the cantilever was approximately 100 pN (typically, 80-150pN). The cell was then pulled away from the surface along with the AFM. Any adhesive interaction formed between $\alpha_4\beta_7$ and MAdCAM-1 protein during the contact time of cell and substrate would break under pulling force generated from the AFM system. Rupture forces can be calculated from the force spectroscopy curves recorded by a two-segmental photodiode from the movement of laser beam reflection coming from the backside of AFM cantilever (Figure 2.7).

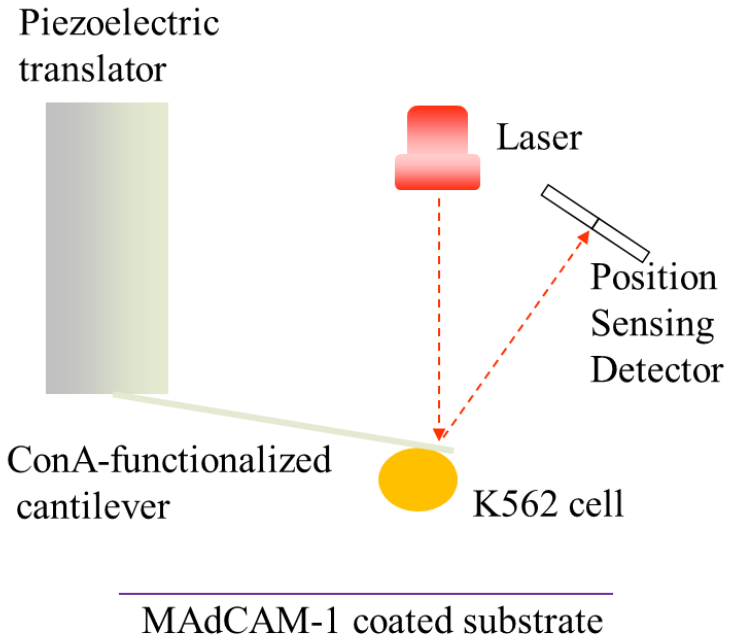

Figure 2.7 Experimental approaches of SCFS measurements of integrin $\alpha_4\beta_7$-mediated K562 adhesion. A k562 cell was attached to the AFM cantilever via interaction between glycoproteins on celluar membrane and ConA functionalized on the cantilever. Cell culture Petri dish surface was coated by MAdCAM-1 protein and then blocked by BSA. Rupture force can be detected by monitoring the laser deflection via a two-segmental photodiode of the AFM setup.

Due to interactions between integrin $\alpha_4\beta_7$ and its ligand MAdCAM-1, rupture force curves can be generated during AFM measurements. Through controlling the density of MAdCAM-1 protein coated on the substrate surface, we ascertained conditions containing specific divalent metal cations under which certain probabilistic single force curves appeared during the measurements. It has been found that more than 83% adhesive events involving single adhesions occurred during such measurements when the adhesion frequency is 30% or less [71]. However, to avoid polymolecular adhesions, we decreased the amount of MAdCAM-1 protein coated and obtained a less than 30% (about 13% on average) frequency of adhesive events during our measurements (Figure 2.8).

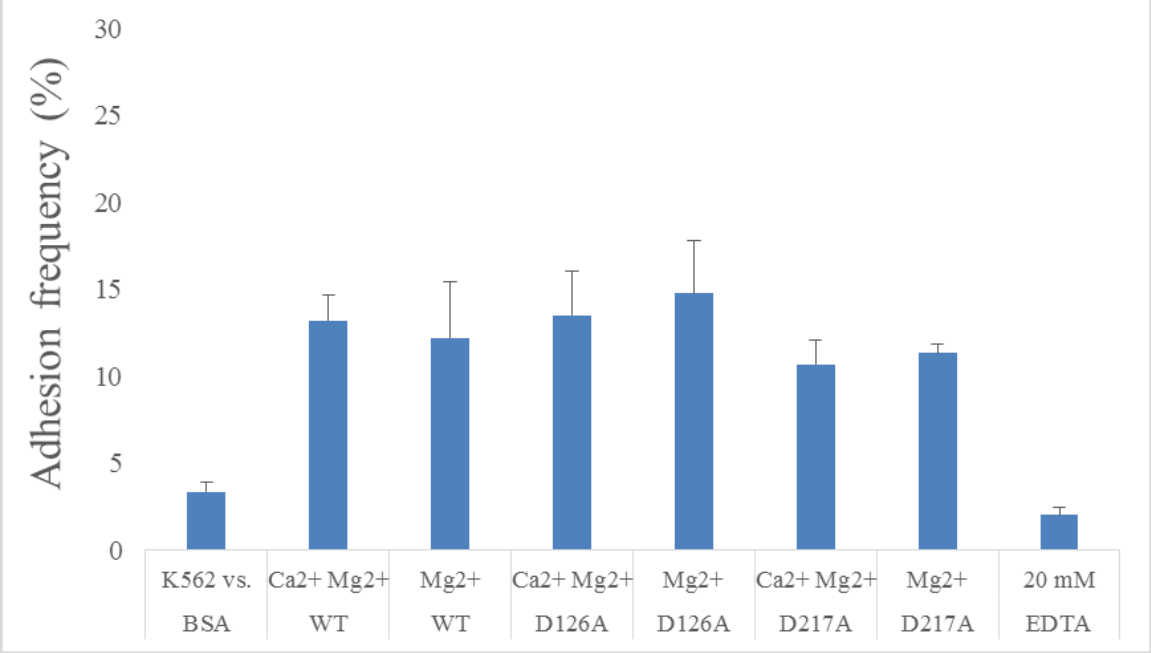

Figure 2.8 Force frequency of adhesion between WT, D126A and D217A integrin $\alpha_4\beta_7$ and MAdCAM-1 under the same contact time and compression force in 1mM Ca^{2+} and 1mM Mg^{2+} or 1mM Mg^{2+} salt solution.

2.3.5 Cytoskeleton anchored bonds and tethered bonds

Two different types of bonds were recorded in SCFS measurements: cytoskeleton anchored bonds (CSK bonds) and tethered bonds. The CSK bonds are anchored to the

cytoskeleton and the rupture of CSK bonds instantaneously following a linear increase of force and then jump to the base line (Figure 2.9 middle trace) [72]. On the other hand, the tethered bonds are not strongly attached to the cytoskeleton and the rupture of tethered bonds follows a constant force plateau (Figure 2.9 top trace). If there are multiple ruptures, the cytoskeleton anchored bonds are generally the first to break in the force curve. Tethered bonds need to be pulled over a certain distance and generally break at the end of the force curve (Figure 2.9 bottom trace). Force spectra of these two types of bonds were investigated.

Cytoskeleton anchored bonds exhibited a linearly increasing force followed by a rupture breaking. The two parameters loading rate (r_f) and rupture force (F_r) are determined from force curves with single cytoskeleton anchored bond ruptures. The loading rate is determined by the system spring from the slope of the force curve just before the bond breaks. The rupture force is determined by the difference between the peak force and the zero force base line in the force curve (Figure 2.9).

Tethered bonds exhibited a constant force plateau followed by a rupture breaking. The bond lifetime and extraction forces were directly obtained from the force curve. The bond life time (τ) is calculated from the tether length and pulling speed. The tether extraction force is determined by the difference between the plateau force and zero force base line in the force curve. It is equal to the amount of force required to pull and extract the tethered bond.

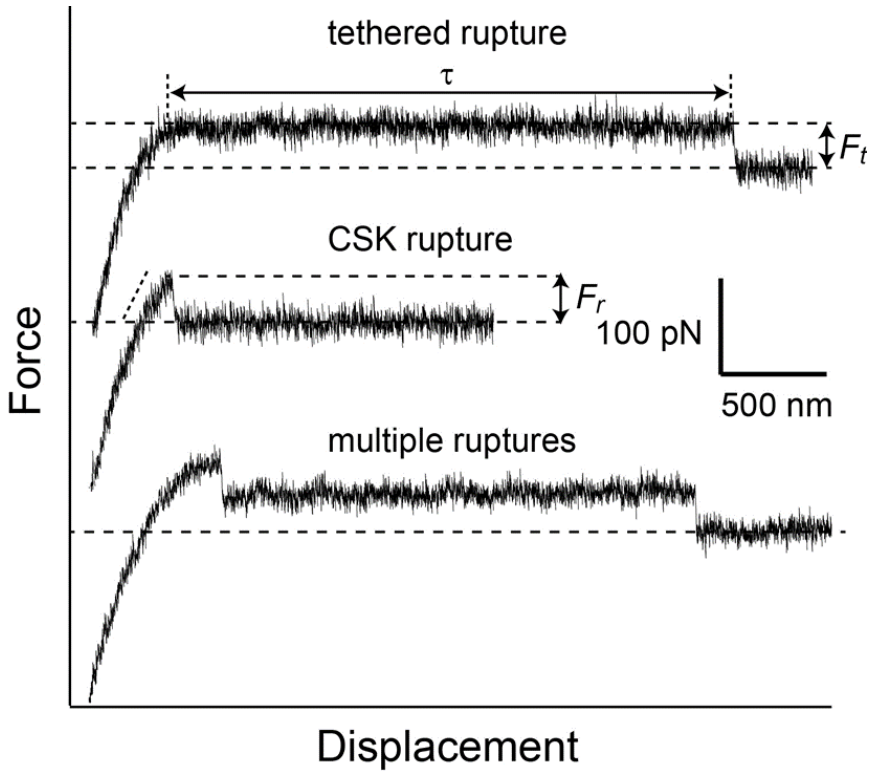

Figure 2.9 Typical force scans during SMFS measurement. Top trace shows a force scan with tethered rupture of the integrin $\alpha_4\beta_7$/MAdCAM-1 D1, D2 bond; middle trace shows a force scan with CSK rupture of the integrin $\alpha_4\beta_7$/MAdCAM-1 D1, D2 bond; bottom trace shows adhesion with multiple integrin $\alpha_4\beta_7$/MAdCAM-1 D1, D2 bond ruptures. F_t is the rupture force for tethered rupture and τ is the lifetime of the tethered bond. F_r is the rupture force for CSK rupture.

2.3.6 Quantitative unbinding force measurements of individual cytoskeleton anchored integrin $\alpha_4\beta_7$/MAdCAM-1 complexes

Single molecule CSK ruptures at a same speed of cell movement with the AFM probe (at an average of certain loading rate) were recorded (Figure 2.10A) and counted in a histogram (Figure 2.10B). Force distributions were fitted according to the Gaussian distribution equation. Mean values of each Gaussian fitting were the most probable rupture forces under certain average loading rates. WT, D126A and D217A $\alpha_4\beta_7$ mediated-K562 cell single force adhesion on 15μg/mL MAdCAM-1 coated Petri dish surface changed with loading rate (40-2000 pN/s) and integrin affinity (regulated by divalent metal cation Ca^{2+}

and Mg^{2+} in vitro) (Figure 2.10B-D). The WT $\alpha_4\beta_7$ K562 transfectant cell had no specific interactions on 1% bovine serum albumin (BSA) coated Petri dish surface or on MAdCAM-1 coated dish with the addition of excess EDTA (Figure 2.8). Additionally, S121A $\alpha_4\beta_7$ K562 transfectant cell had almost no specific interactions on MAdCAM-1 coated surface (data not shown). With the increase of loading rate, the rupture force needed to dissociate $\alpha_4\beta_7$/MAdCAM-1 complex increased to varying degrees. In 1mM Mg^{2+}, when integrin $\alpha_4\beta_7$ was in its high-affinity, interaction forces between WT $\alpha_4\beta_7$ and MAdCAM-1 were stronger than in 1mM Ca^{2+} and 1mM Mg^{2+}, when $\alpha_4\beta_7$ in its low-affinity. The ADMIDAS site mutant, D126A transfectant, had stronger rupture forces than the WT transfectant to some extent, in the same conditions. Whereas, the LIMBS site mutant transfectant had weaker forces than the WT transfectant in 1mM Ca^{2+} and 1mM Mg^{2+} or 1mM Mg^{2+}.

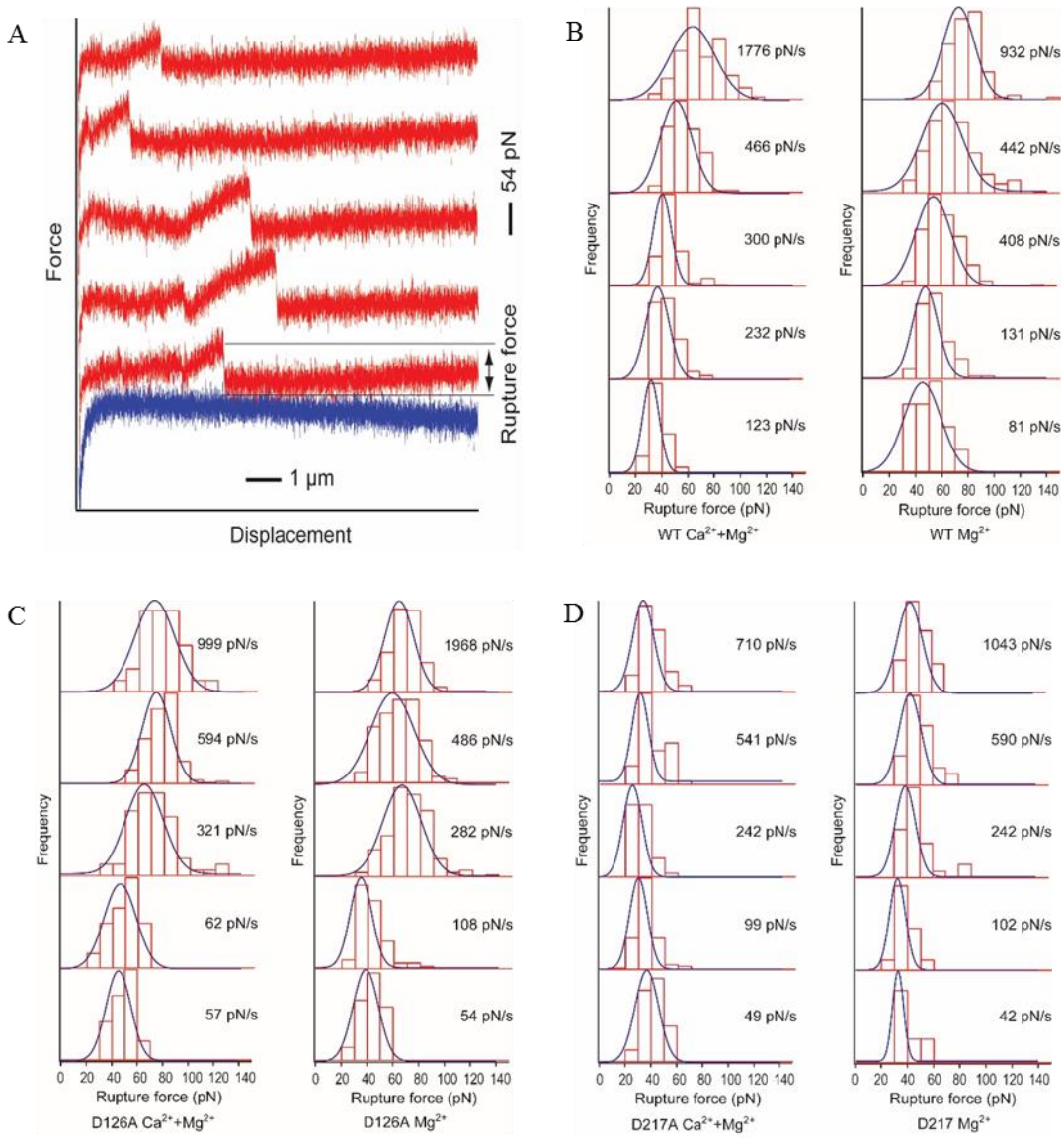

Figure 2.10 Dynamic force spectrum of interactions between integrin $\alpha_4\beta_7$ and MAdCAM-1. （A）Force curves of SCFS measurements on $\alpha_4\beta_7$/MAdCAM-1 interaction in 1mM Mg^{2+}. Red rupture curves come from five individual measurements on the same one cell under loading rate about 442 pN/s. The blue approaching curve was from the same measurement as that of the lowest red curve. Incomplete superposition between horizontal lines of the last pair of curves was due to hydrodynamic force (about 13.6 pN) during such measurements. And the compression force of the probe was about 108pN. Rupture force distributions of (B) WT, (C) D126A and (D) D217A $\alpha_4\beta_7$ and MAdCAM-1 at different loading rates, in 1mM Ca^{2+} and1mM Mg^{2+} or 1mM Mg^{2+} salt solution.

Under similar loading rates, rupture forces changed significantly for WT, D126A and D217A mutants in different ion conditions (Figure 2.11A). For WT $\alpha_4\beta_7$-mediated

K562 cell adhesion on MAdCAM-1, the single adhesion force was about 74 pN at a loading rate of 442 pN/s in 1mM Ca^{2+} and 1mM Mg^{2+} buffer, whereas 65pN at 466 pN/s in 1mM Mg^{2+} buffer. For D126A, the force was about 73 pN at 486 pN/s in 1mM Ca^{2+} and 1mM Mg^{2+}, this was similar to WT in Mg^{2+}; and 88 pN at 594 pN/s in 1mM Ca^{2+} and 1mM Mg^{2+}. For D217A, the forces were 52 pN and 56 pN at 541 pN/s in 1mM Ca^{2+} and 1mM Mg^{2+} and 590 pN/s 1mM Mg^{2+}, respectively. These loading rates applied to K562 cell (442-594 pN/s) were all in the range of estimated physiological loading rates [71].

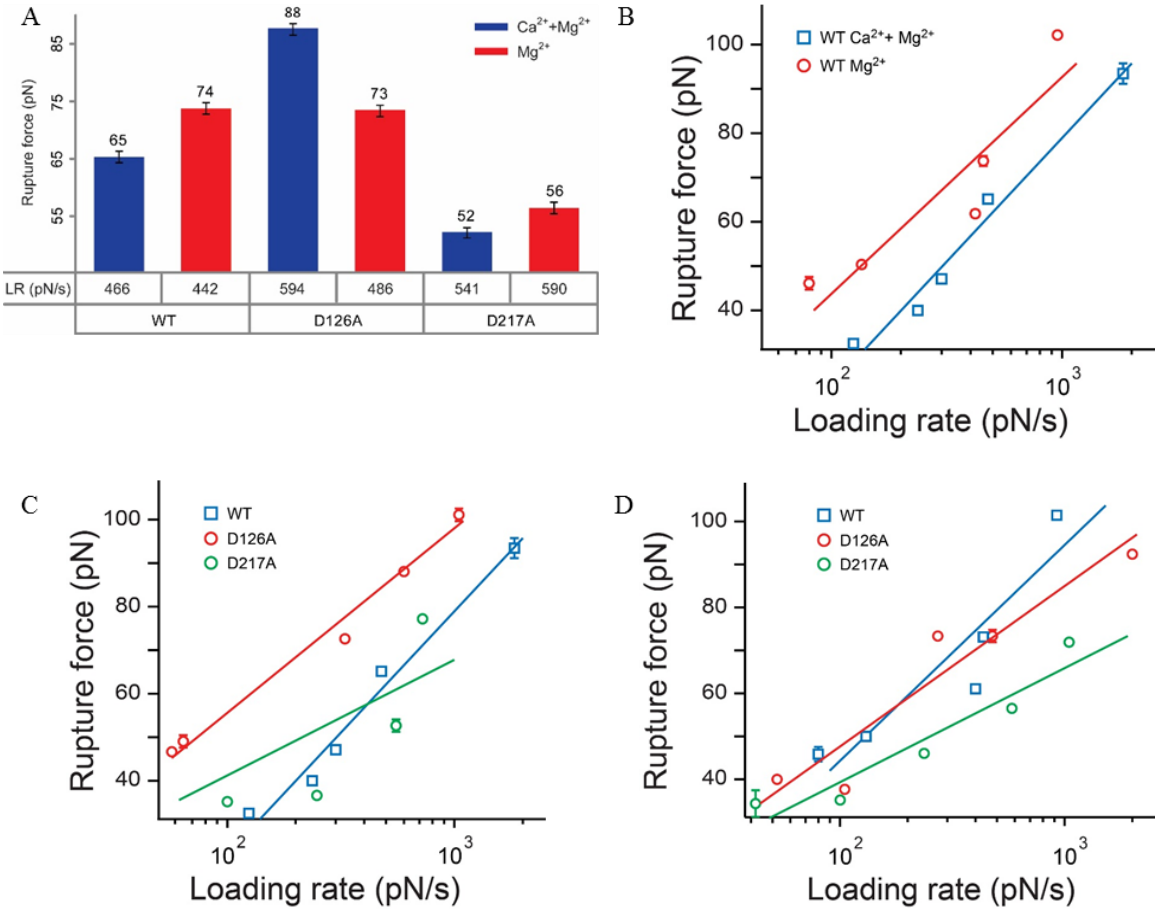

Figure 2.11 Rupture force dynamics of integrin $\alpha_4\beta_7$-mediated K562 single-force adhesion on MAdCAM-1 coated surface. (A) Rupture forces at approximate loading rates. Rupture force values derived from mean values of Gaussian fitting on single force distributions. Bar represent one standard deviation from the Gaussian fitting, respectively. There was a very significant difference ($p<0.01$) between either two force values under Welch two sample t-test except values between WT 1mM Mg^{2+} and D126A 1mM Mg^{2+}, which had a

significant difference ($p<0.05$). T-test was carried out with the usage of R console software. (B) Force dynamics of WT $\alpha_4\beta_7$-mediated K562 adhesion in 1mM Ca^{2+} and 1mM Mg^{2+} or in 1mM Mg^{2+}. Force dynamics of WT, D126A and D217A $\alpha_4\beta_7$-mediated K562 adhesion in 1mM Ca^{2+} and 1mM Mg^{2+} (C) or in 1mM Mg^{2+} (D). Values of every point in (B-D) were applied linear fitting. Vertical bar of every point represents one standard deviation of Gaussian fitting of rupture forces' distribution, respectively. All force values shown or included in these figures had been corrected with hydrodynamic force on the cantilever in our measurements.

After a linear fitting between $f*$ and $\ln r_f$ in the OriginPro program, we calculated Bell parameters of the dissociation between integrin $\alpha_4\beta_7$ and its ligand MAdCAM-1 (Table 2-2).

Table 2-2 Bell parameters of cytoskeleton anchored integrin $\alpha_4\beta_7$/MAdCAM-1 complex dissociation.

CSK bond	WT		D126A		D217A	
	Ca^{2+}+Mg^{2+}	Mg^{2+}	Ca^{2+}+Mg^{2+}	Mg^{2+}	Ca^{2+}+Mg^{2+}	Mg^{2+}
γ (Å)	1.72 ± 0.15	1.98 ± 0.49	2.28 ± 0.17	2.53 ± 0.48	3.49 ± 1.69	3.54 ± 0.63
k° (s^{-1})	1.50 ± 0.20	0.54 ± 0.32	0.25 ± 0.06	0.34 ± 0.20	0.31 ± 0.49	0.3 ±0.18

2.3.7 Quantitative unbinding force measurements of individual tethered integrin $\alpha_4\beta_7$/MAdCAM-1 complexes

The pulling force applied to single tether bonds is dependent on the pulling speed. Tethered bond rupture forces and lifetimes at different pulling speed were recorded and then grouped by rupture forces. The mean tether forces for each group were calculated. And the mean tether lifetimes for each tether group were determined by a cumulative lifetime probability distribution:

$$P(t) = A\exp(-t/\tau) \qquad [2\text{-}1]$$

where P is the probability that the bond survives longer than the time t, τ is the mean lifetime and A is the y-intercept [73]. The mean lifetime of each group was determined

from the exponential probability fits in Figure 2.12. The force spectra were produced by plotting mean lifetime against the determined mean tether extraction forces. Then the force spectra of mean tether lifetimes vs. the mean tether extraction force of tethered integrin $\alpha_4\beta_7$/MAdCAM-1bond in different ions conditions were fit to the Bell model equation.

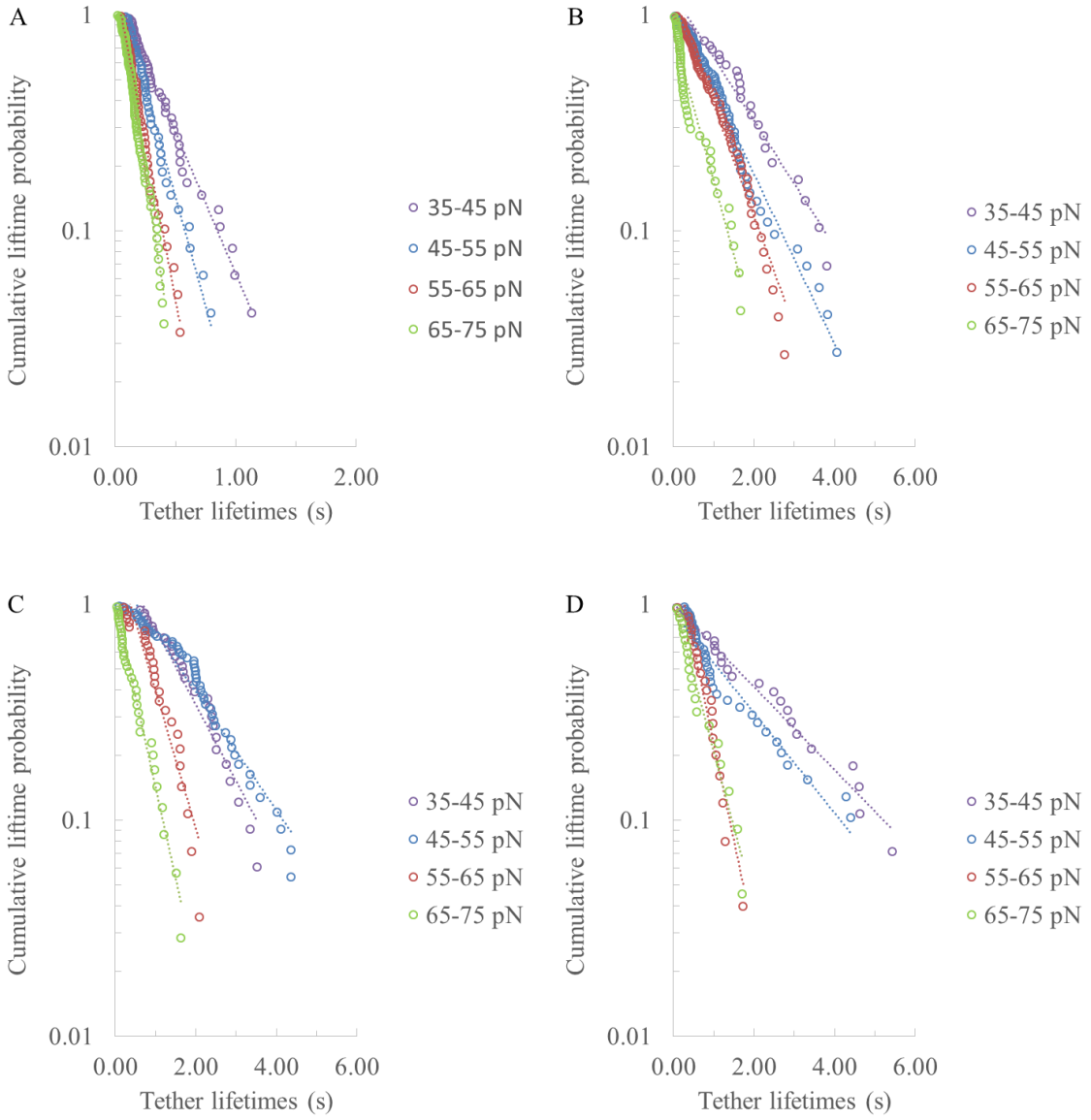

Figure 2.12 Cumulative lifetime probability of tethered integrin $\alpha_4\beta_7$ and MAdCAM-1 bonds. WT integrin $\alpha_4\beta_7$/MAdCAM-1tetherd bond in Ca^{2+} and Mg^{2+} (A) and Mg^{2+} (B); D126A integrin $\alpha_4\beta_7$/MAdCAM-1 tethered bond in Ca^{2+} and Mg^{2+} (C) and Mg^{2+} (D).

With the increase of pulling force, the tethered bond lifetime decreased to varying degrees. In 1mM Mg^{2+}, when integrin $\alpha_4\beta_7$ was in its high-affinity, tethered bonds of WT integrin $\alpha_4\beta_7$ and MAdCAM-1 were stronger and had longer lifetimes than those in 1mM Ca^{2+} and 1mM Mg^{2+}, when integrin $\alpha_4\beta_7$ in its low-affinity. The ADMIDAS site mutant D126A transfectant had stronger tethered bonds than the WT transfectant and longer lifetimes under similar pulling force. Under similar pulling forces, bonds lifetime changed significantly for WT in different ion conditions (Figure 2.13). The tethered bond lifetime of WT integrin $\alpha_4\beta_7$-mediated K562 cell adhesion on MAdCAM-1 was about 0.l5s at 65 pN in 1mM Ca^{2+} and 1mM Mg^{2+} buffer, whereas 0.6s at 70pN in 1mM Mg^{2+} buffer. Interestingly, the lifetime of tethered bond in D126A mutants integrin $\alpha_4\beta_7$/MAdCAM-1 complex did not change in different ion conditions and was very similar to the lifetime of tethered bond in high affinity WT integrin $\alpha_4\beta_7$/MAdCAM-1 complex. The tethered bond lifetime of D126A integrin $\alpha_4\beta_7$-mediated K562 cell adhesion on MAdCAM-1 was 0.5s at 65 pN in 1mM Ca^{2+} and 1mM Mg^{2+} buffer and 0.6s at 70pN in 1mM Mg^{2+} buffer (Figure 2.13). Since in the Bell-Evan's model, an increase in force always shortens the bond lifetime, the bonds that satisfy the Bell-Evan's relationship are the "slip" bonds. It is unclear, however, if the tethered integrin $\alpha_4\beta_7$–MACAM-1 complex behaves as slip, catch or flex bonds.

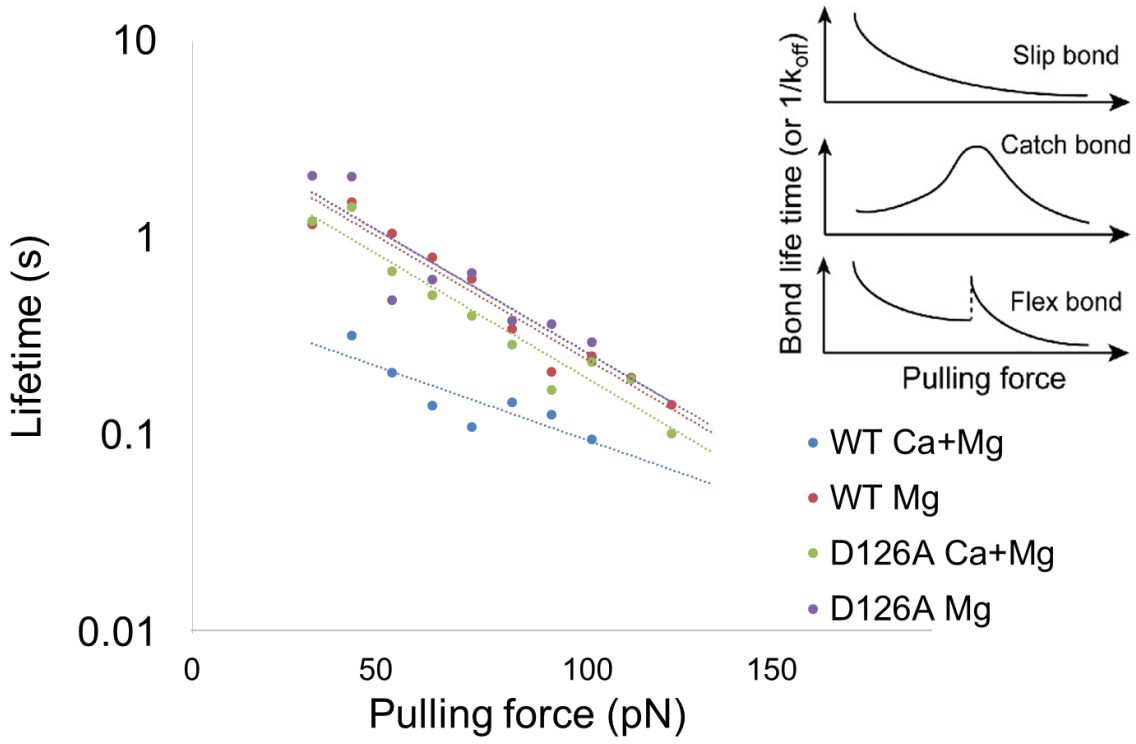

Figure 2.13 Force spectra of single tethered integrin $\alpha_4\beta_7$ and MAdCAM-1 bonds. Force spectra of mean tether lifetime vs. mean tether pulling force. Spectra were fit to the Bell Model. Insert: slip bonds lifetimes shorten exponentially as a function of force. Catch bond lifetimes increase then decrease with force. Flex bond is a two-state slip bond, where a certain pulling force will induce the bond transit from one another slip bond, with an immediate increase of life time upon transition [74, 75].

After fitting the lifetime and pulling force in the OriginPro program, we calculated Bell parameters of tethered bond dissociation between integrin $\alpha_4\beta_7$ and its ligand MAdCAM-1 (Table 2-3).

Table 2-3 Bell parameters of tethered integrin $\alpha_4\beta_7$/MAdCAM-1 complex dissociation.

Tethered	WT		D126A	
	Ca^{2+}+Mg^{2+}	Mg^{2+}	Ca^{2+}+Mg^{2+}	Mg^{2+}
γ (Å)	0.95 ± 0.21	1.12 ± 0.10	1.13 ± 0.11	1.12 ± 0.24
k° (s^{-1})	1.38 ± 0.56	0.28 ± 0.05	0.26 ± 0.06	0.20 ± 0.09

2.4 Discussion

A complicated and efficient mechanism is involved in the recruitment of leukocytes from the main blood stream to sites where inflammation or tissue damage has happened [56]. Specific adhesive molecules, mainly selectins, integrins and their ligands, mediate the selective leukocyte-endothelium interaction. Human integrin $\alpha_4\beta_7$ heterodimer is expressed primarily on mucosal lymphocytes, and also is present on natural killer cells and eosinophils. Integrin $\alpha_4\beta_7$ mediates leukocytes homing into Peyer's patches and intestinal lamina propria through interaction with its main ligand MAdCAM-1 under physiological flow *in vivo* [33, 76-78]. Integrin $\alpha_4\beta_7$ plays different roles in mediating lymphocyte rolling or firm adhesion during their migration on mucosal endothelium.

Previous studies have discovered many features of $\alpha_4\beta_7$ in terms of its structure and biochemical regulation mechanisms [34]. Here we applied AFM-based SMFS and SCFS technology to elucidate the biophysical mechanisms of integrin $\alpha_4\beta_7$ in mediating leukocyte rolling and firm adhesion, which little was known about thus far. During regulation of leukocyte migration, interactions between integrin $\alpha_4\beta_7$ and MAdCAM-1 involve bond-formation, bond-duration and bond-dissociation processes. Through usage of the AFM-based system and application of the Bell-Evans model, we measured rupture forces and obtained Bell parameters for different types of integrin $\alpha_4\beta_7$/MAdCAM-1 complexes: purified protein (Table 2-1), cytoskeleton anchored bond(Table 2-2) and tethered bond(Table 2-3) during the processes of single $\alpha_4\beta_7$/MAdCAM-1 bond dissociation when $\alpha_4\beta_7$ was in its high-affinity or low-affinity state.

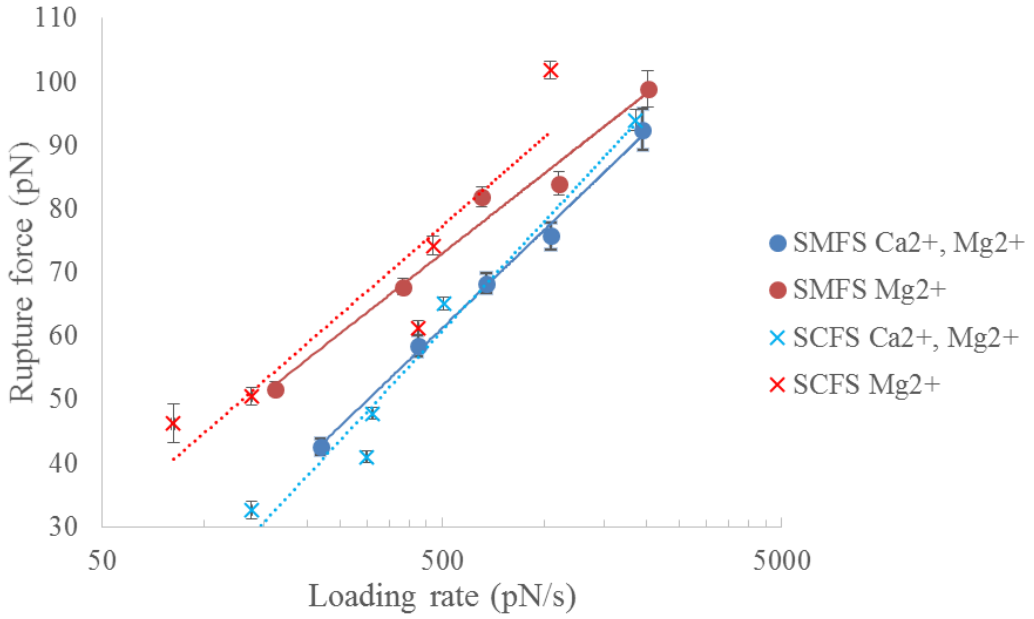

Figure 2.14 Comparison of rupture force dynamics of purified integrin $\alpha_4\beta_7$/MAdCAM-1 D1, D2 and K562 expressed WT integrin $\alpha_4\beta_7$/MAdCAM-1 in 1mM Ca^{2+} and 1mM Mg^{2+} or in 1mM Mg^{2+}. Values of every point were applied linear fitting. Vertical bar of every point represents standard error of the mean.

In general, larger rupture forces were needed to dissociate the high-affinity $\alpha_4\beta_7$ (induced by 1mM Mg^{2+} in vitro) and MAdCAM-1 complex than the low-affinity $\alpha_4\beta_7$ (induced by 1mM Ca^{2+} and 1mM Mg^{2+} in vitro) under different loading rates (40-2000 pN/s) that were mainly in the physiological loading rate range (100-10000 pN/s) [71]. Those rupture forces were similar to the forces needed to break the bonds between purified high affinity integrin $\alpha_4\beta_7$ (induced by 1mM Mg^{2+} in vitro) and low affinity integrin $\alpha_4\beta_7$ (induced by 1mM Ca^{2+} and 1mM Mg^{2+} in vitro) /MAdCAM-1 D1, D2 complex (Figure 2.14). The Bell parameters of integrin of integrin $\alpha_4\beta_7$/MAdCAM-1 complexes were also similar in SMFS and SCFS measurements (Table 2-4).

Table 2-4 Comparison of the Bell parameters of integrin $\alpha_4\beta_7$/MAdCAM-1 complex dissociation in SMFS and SCFS measurements.

	SMFS		SCFS	
	Ca^{2+}+Mg^{2+}	Mg^{2+}	Ca^{2+}+Mg^{2+}	Mg^{2+}
γ (Å)	1.85 ± 0.07	2.21 ± 0.18	1.72 ± 0.15	1.98 ± 0.49
k° (s^{-1})	1.43 ± 0.09	0.52 ± 0.12	1.50 ± 0.20	0.54 ± 0.32

For cytoskeleton anchored bonds, under a loading rate of nearly 450 pN/s, the rupture force of high-affinity $\alpha_4\beta_7$/MAdCAM-1 complex was 74 pN, whereas that of low-affinity complex was 65 pN in the same condition except divalent metal cations which mediated $\alpha_4\beta_7$'s adhesion as high-affinity or low-affinity mimicking the states *in vivo* when the complex is regulating leukocyte firm adhesion or rolling (Figure 2.11A). The rupture forces of the high-affinity mutant (D126A) were the near approximations of the WT in 1mM Mg^{2+}, while those of the low-affinity mutant (D217A) were smaller than those of WT in 1mM Ca^{2+} and 1mM Mg^{2+}. These results indicated that high-affinity complexes were less sensitive to shear flow, at least in terms of bond dissociation.

For tethered bonds, under an extraction force of nearly 70 pN, the lifetime of high-affinity WT $\alpha_4\beta_7$/MAdCAM-1 complex was 0.15s, whereas that of low-affinity complex was 0.6 under different divalent metal cation conditions. The divalent metal cations mediated $\alpha_4\beta_7$'s adhesion as high-affinity or low-affinity, mimicking the states in vivo when the complex is regulating leukocyte firm adhesion or rolling. And the lifetimes of the high-affinity mutant (D126A) were the near approximations of WT in 1mM Mg^{2+}, 0.5s in 1mM Ca^{2+} and 1mM Mg^{2+}, and 0.6s in 1mM Mg^{2+} under the same extraction force of 70 pN. These results indicated that high-affinity complexes had longer lifetime under shear stress in shear flow and were hard to break. In addition, cellular membrane tether bonds

play significant roles in maintaining the cell-substrate adhesion for seconds as they have significant longer lifetimes than CSK bonds.

Chen previously reported that the WT $\alpha_4\beta_7$ integrin mediates rolling adhesion in Ca^{2+} Mg^{2+} and firm adhesion in Mg^{2+}; the ADMIDAS mutants D126A supported only firm adhesion, while the LIMBS mutants D217A mediated only rolling in 293T transfectants and K562 transfectants [34]. We measured the mechanical forces governing $\alpha_4\beta_7$/MAdCAM-1 interactions for the first time. Our results partially explained the biophysical reasons for the flow chamber results (Figure 2.15) in Chen's work, and as well as for the regulation mechanism in vivo. We measured the mechanical forces governing $\alpha_4\beta_7$/MAdCAM-1 interactions for the first time. Meanwhile, data of D126A, D217A and S121A mutants offered good controls to our system and measurements.

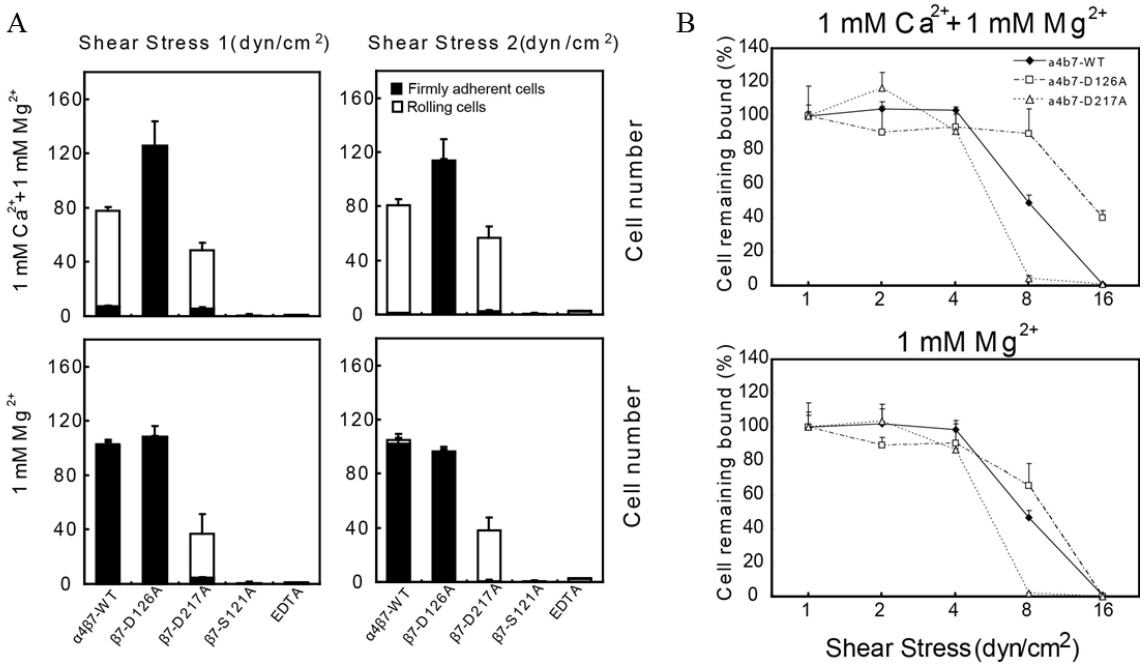

Figure 2.15 Effects of the metal ion-binding site mutations on the adhesive regulation of integrin $\alpha_4\beta_7$ and resistance to shear stress in shear flow. (A) The number of rolling and firmly adherent WT and mutants integrin $\alpha_4\beta_7$ K562 transfectants measured in the 1mM Ca^{2+}, 1m Mg^{2+} or 1mM Mg^{2+} at a shear stress of 1 dyn cm^{-2} or 2dyn com^{-2}. (B) Resistance

to the shear stress. The total number of remaining rolling cells or firm adherent cells at increasing shear stresses was determined as a percentage of adherent cells at 1 dyn cm^{-2}.

Through Bell-Evans model analysis, we obtained Bell parameters of WT, D126A and D217A $\alpha_4\beta_7$/MAdCAM-1 complex dissociation (Table 2-2). For the wild type $\alpha_4\beta_7$/MAdCAM-1 complex, the dissociation constant values (k^o) of the low-affinity complex and the high-affinity complex were 1.50/s and 0.54/s respectively, whereas their positions of transition state (γ) showed little difference. This indicated that the dissociation rate played an important role in integrin $\alpha_4\beta_7$'s affinity. k^o values of D126A and D217A were almost the same and were near that of WT. And γ values of D126A were close to that of WT in Mg^{2+}. However, γ values of D217A were significantly bigger than those of WT and D126A in either Ca^{2+} and Mg^{2+} or Mg^{2+}. This implied that D217A was more sensitive than WT and D126A to the same external force. From the Bell parameters listed in the table, we can also judge the different mechanisms of D126A and D217A affecting the adhesive behavior of $\alpha_4\beta_7$ on MAdCAM-1. By substituting γ and k^o values listed in the table into Equation 1-1, we would get $k_{off}(f)$ as a function of external force (f). Fig. 5A, 5B and 5C depicted the relationships between $k_{off}(f)$ and f of $\alpha_4\beta_7$/MAdCAM-1 complex. We found that dissociation value ($k_{off}(f)$) of the high-affinity complex was smaller than that of the low-affinity complex under the same external pulling force below 200 pN (Figure 2.16A). For the low-affinity or high-affinity complex, D217A always had a bigger $k_{off}(f)$ value than that of WT or D126A under a pulling force between 40 pN and 200 pN (Figure 2.16B,Figure 2.16C), which explains why the D217A transfectant had weaker interactions with a MAdCAM-1 coated dish surface. The dissociation rate plays

important roles for integrin $\alpha_4\beta_7$ in regulating leukocyte migration into Peyer's patches. Our results are the first to give the biophysical parameters of the dissociation process. They provide us with new insight into the molecular mechanism of integrin $\alpha_4\beta_7$-mediated leukocyte rolling and firm adhesion.

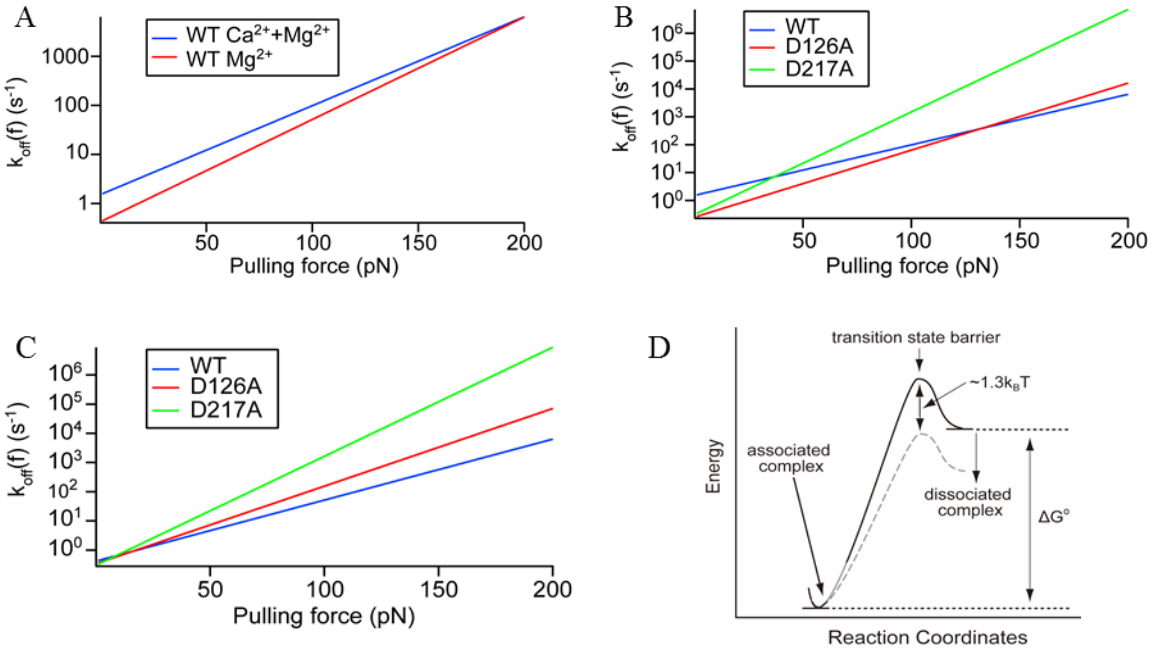

Figure 2.16 Kinetic profiles and energy landscape of $\alpha_4\beta_7$/MAdCAM-1 complex dissociation. Kinetic dissociation profiles of (A) WT $\alpha_4\beta_7$/MAdCAM-1 complex in 1mM Ca^{2+}+1mM Mg^{2+}, (B) WT, D126A and D217A $\alpha_4\beta_7$/MAdCAM-1 complex in 1mM Ca^{2+}+1mM Mg^{2+} and (C) WT, D126A and D217A $\alpha_4\beta_7$/MAdCAM-1 complex in 1mM Mg^{2+}. (D) Energy landscape of WT $\alpha_4\beta_7$/MAdCAM-1 complex dissociation. Gray dotted line represents landscape of low-affinity complex dissociation, whereas black solid line represents that of high-affinity complex dissociation.

The dissociation rate constants can be used to estimate transition state energies with one energy barrier (Figure 2.16D). The energy difference value ($\Delta\Delta G$) between the high-affinity and low-affinity transition state (ΔG_H and ΔG_L) can be calculated with the formula, $\Delta\Delta G = \Delta G_H - \Delta G_L = -k_B T \ln(k_H^o / k_L^o)$. k_H^o and k_L^o are dissociation rate constants of high-affinity complex and low-affinity complex, respectively. The transition state energy needed

for high-affinity complex dissociation is about 1.3 k_BT more than that of low-affinity complex dissociation.

In summary, through SMFS and SCFS measurements on interactions between integrin $\alpha_4\beta_7$ stable transfectant K562 cell and MAdCAM-1 coated dish, we obtained the rupture forces needed to dissociate the $\alpha_4\beta_7$/MAdCAM-1 complex *in vitro* and the Bell parameters of the complex dissociation. Our data is credible with controls such as D126A, D217A and S121A data. Our data demonstrated that dissociation rates under external force make a difference between different bond affinities. This partially explains the biophysical mechanism of $\alpha_4\beta_7$-mediated leukocyte rolling or firm adhesion. To fully understand this mechanism in the aspects of association rate and bond-duration lifetime, we are conducting other single-molecule force spectroscopy approaches on the complex. We want to understand the affinity change when cells receive physiological stimulation, during which process integrin avidity may be involved. There are still many unknown points underlying the biophysical mechanism of integrin-mediated leukocyte migration, which are crucial for understanding integrin functions and for solving problems caused by integrin dysfunction.

2.5 Contribution in Science

Normal homeostasis of the cardiovascular system is strongly dependent on the finely tuned leukocyte adhesive properties, which include transmigration of leukocytes across the blood vessels and homing. Change of cell adhesion properties plays an important role in the pathogenesis of cardiovascular disease. Despite the advances in understanding the structure of cell adhesion molecules and their signal transduction pathways, little is known about their biophysical and biomechanical properties. To this end, direct force

measurements of association and dissociation of individual adhesion molecule-ligand complexes will advance our understanding of the structural and functional basis for cell adhesion in the cardiovascular system.

In this study, I have used SMFS and SCFS to determine the mechanical strength of the low- and high-affinity integrin-ligand interaction on living leukocyte surface. AFM has been used to pull individual integrin-ligand complexes to determine their mechanical strength and force dependent dissociation kinetics under conditions that have given rise to leukocyte rolling and firm adhesion, respectively (Figure 2.16 & Table 2-2). The data suggests that induction of higher affinity states elevates the heights of the energy barriers of integrin complex dissociation, but has minimal effect on the width of the barriers, and that cellular membrane tether bonds play significant roles in maintaining the cell-substrate adhesion for seconds. The results can be used to perform mathematical modeling to better understand leukocyte and immune system behave. The findings could also lead to novel strategies for modulating leukocyte trafficking in different inflammatory and immune disease settings such as atherosclerosis, ischemia/reperfusion injury, myocardial infarction, stroke and autoimmunity.

3 Biophysical mechanism of chemokine –mediated integrin activation

3.1 Motivation

The immune system controls its responses by precisely recruiting lymphocytes from the main bloodstream to the endothelium at target sites in different tissues [79]. There is a recognized multistep paradigm describing the process of leukocyte recruitment. The recruitment involves leukocytes' tethering and rolling, activation, firm adhesion, crawling and transendothelial migration [57, 58]. During the process, homing molecules such as selectins and integrins expressed on lymphocytes membranes interact with ligands on vascular endothelia and target lymphocytes to different tissues [80]. Integrins serve as mediators in exchanging outside-in and inside-out transmembrane signals [18]. These signals instruct leukocytes to perform their functions appropriately. Integrins activation is induced by chemokines acting through G-protein coupled receptors on cell membranes and triggering the binding of intracellular effector proteins, such as talin and kindling, to integrin cytoplasmic domains [81].

Integrin $\alpha_4\beta_7$, also known as LPAM-1 (lymphocyte Peyer's patch adhesion molecule-1), is a homing molecule that targets bloodstream lymphocytes to mucosal tissues, especially in the gut [82]. Integrin $\alpha_4\beta_7$ recognizes multiple ligands: mucosal vascular address in cell adhesion molecule-1 (MAdCAM-1) and vascular cell adhesion molecule-1 (VCAM-1). MAdCAM-1 is the primary ligand, and is expressed on the endothelium of high endothelial venules in the gut and gut-associated lymphoid tissues, such as Peyer's patches and mesenteric lymph nodes (MLNs) [33], while VCAM-1 is widely expressed on stimulated endothelial cells of blood vessels, bone marrow and peripheral lymph nodes

(PLNs) [83]. Previous biochemical studies have shown that integrin $\alpha_4\beta_7$ can be activated by distinct chemokines in a ligand specific manner to mediate selective homing of lymphocytes to endothelial cells expressing either MAdCAM-1 or VCAM-1 in different tissues [84]. However, the kinetic properties and mechanical mechanisms of integrin $\alpha_4\beta_7$ binding and ligand selection are unknown.

Herein, we applied AFM based SCFS technology to study the effects of chemokines on the mechanical properties of interactions between the human integrin $\alpha_4\beta_7$ and its ligands, human MAdCAM-1 or VCAM-1. By attaching a RPMI CXCR3-8866 cell, expressing integrin $\alpha_4\beta_7$ on the cell membrane, to an AFM cantilever, we were able to use AFM to measure the interactions between integrin $\alpha_4\beta_7$ and MAdCAM-1 or VCAM-1 coated on Petri dishes, before and after chemokine stimulation. This approach avoided nonspecific interactions, to the most extent. The chemokines CCL 25 and CXCL10 were used in this study, as they can significantly activate or suppress integrin $\alpha_4\beta_7$ mediated lymphocyte adhesion to either MAdCAM-1 or VCAM-1 [84]. Our study focused on the mechanical forces needed to rupture $\alpha_4\beta_7$/MAdCAM-1 complexes with or without chemokine stimulation. Through Bell model analysis, we demonstrated the different effects of chemokines on biophysical properties of this complex dissociation under physiological force.

3.2 Materials and methods

3.2.1 AFM setup

Single molecule rupture force measurements for integrin $\alpha_4\beta_7$/MAdCAM-1 were conducted using a custom built AFM, as described in Chapter 1. All experiments were

conducted at room temperature (about 25℃) unless noted otherwise. Cantilevers were calibrated over a clean culture dish in PBS buffer using the Igor program. The photodiode position sensitivity was determined by indenting a non-compliant surface. Then a thermal fluctuation method was used to determine the spring constant of the cantilevers. The spring constant values of MLCT cantilevers (Bruker) used in this study were typically 0.01-0.02 N/m.

3.2.2 Cell culture

8866-CXCR3 stable cell lines came from Dr. J. Chen [84]. cDNA construction and expression approaches were depicted previously [34, 84]. Cells were cultured in RPMI 1640 media (Gibco Invitrogen) containing 10% FBS (Biochrom, German), 100U/mL Penicillin-Streptomycin (Gibco), and 2ug/mL Puromysin (Gibco).

3.2.3 Protein immobilization

MAdCAM-1 and VCAM-1 protein cDNA were constructed into the secreting plasmid pHLsec [69]. Constructors were transiently transfected into HEK 293T cells via MegaTran 1.0 reagent (Origene). Secreted proteins with a His-tag protein in EX-Cell serum-free media (JRH Biosciences) were purified with Ni-NTA resins (IBA). 20 μL of 15μg/mL purified MAdCAM-1 or VCAM-1 proteins (diluted in PBS containing 10 mM $NaHCO_3$, pH 8.6) were dropped onto a 35mm Petri dish (Corning) surface and incubated in a wet box at 37℃ for 2 hours. After two washes with PBS, the surface was blocked by 1% BSA in PBS in a wet box at 37℃ for 1 hour. Before usage, the surfacewas washed twice with PBS and then 2 mL serum free RPMI 1640 (Gibco Invitrogen) media was added.

3.2.4 Functionalization of AFM cantilevers with poly-L-lysine

AFM probes (MLCT) were purchased from Veeco (Camarillo, CA). All probes were soaked with acetone for 5 min for cleaning. After 30 minutes of UV-light irradiation, the cantilevers were incubated with poly-L-lysine (5 mg/mL in 100 mM $NaHCO_3$, pH 9.0; Sigma, St. Louis, MO) overnight at 4 ℃. Following the removal of unbound poly-L-lysine, the cantilevers are ready to pick up cells or can be stored in a wet box for up to 3 days.

3.2.5 AFM SCFS measurements of rupture forces of integrin $\alpha_4\beta_7$/MAdCAM-1 or integrin $\alpha_4\beta_7$/VCAM-1 complexes

1 mL of 8866-CXCR3 cells from culture media were transferred into 1.5 mL Eppendorf tubes, and centrifuged at 1200 rpm for 3 minutes. Cells were washed twice with 1 mL Wash buffer (150 mM NaCl, 5 mM HEPES, 0.5% BSA and 5 mM EDTA, pH 7.4), then washed twice with 1 mL Buffer A (150 mM NaCl, 5 mM HEPES and 0.5% BSA, pH 7.4). After above disposal, 50ul of cell solution was added into polystyrene Petri dish already containing RPMI 1640. Through manual manipulation of poly-L-lysine modified AFM probe, a single 8866-CXCR3 cell can be picked up via interaction with the triangular area of the C-cantilever of the MLCT probe.

3.2.6 Chemokine activation

Chemokines CCL25 and CXCL10 were purchased from R&D Systems Inc (Minneapolis, MN). Cells were prestimulated with 0.5 ug/mL soluble chemokines for 5 min before being picked up by a poly-L-lysine functionalized cantilever. All measurements for the same stimulated cell were recorded within 1 h of chemokine stimulation.

3.3 Results

3.3.1 AFM measurements of integrin $\alpha_4\beta_7$ adhesion to its ligands MAdCAM-1 or VCAM-1

As described in Chapter 2, we applied similar AFM-based single cell force spectroscopy technology to study the biophysical dynamics behind integrin $\alpha_4\beta_7$-mediated lymphocyte adhesion. We used established RPMI CXCR-8866 stable cell lines that express human integrin $\alpha_4\beta_7$ on cell membranes to carry out SCFS experiment [84]. Purified human MAdCAM-1 or VCAM-1 coated substrates were used to avoid non-specific interactions to a large extent. Figure 3.1 illustrates the AFM measurements of integrin $\alpha_4\beta_7$ mediated RPMI CXCR3-8866 adhesion on the MAdCAM-1 or VCAM-1 protein coated substrate system and the process of adhering a single, living RPMI CXCR-8866 cell onto an AFM probe. A single, living RPMI CXCR3-8866 cell expressing wild type integrin $\alpha_4\beta_7$ was adhered onto a poly-lysine functionalized cantilever of an AFM probe via manipulation of probe [40, 44] (Figure 3.1). The single cell was first lowered down to contact the MAdCAM-1 or VCAM-1 coated surface of the cell culture Petri dish for 0.1 second. The compression force applied by the cantilever was approximately 150 pN (typically, 100-200pN). Then the cell was pulled away from the surface along with the AFM probe. Any adhesive interactions formed between $\alpha_4\beta_7$ and MAdCAM-1 or VCAM-1 protein during the contact time of cell and substrate would break under the pulling force generated from the AFM system. Rupture forces can be calculated from the force spectroscopy curves recorded by a two-segmental photodiode from the movement of laser beam reflection coming from the backside of the AFM cantilever.

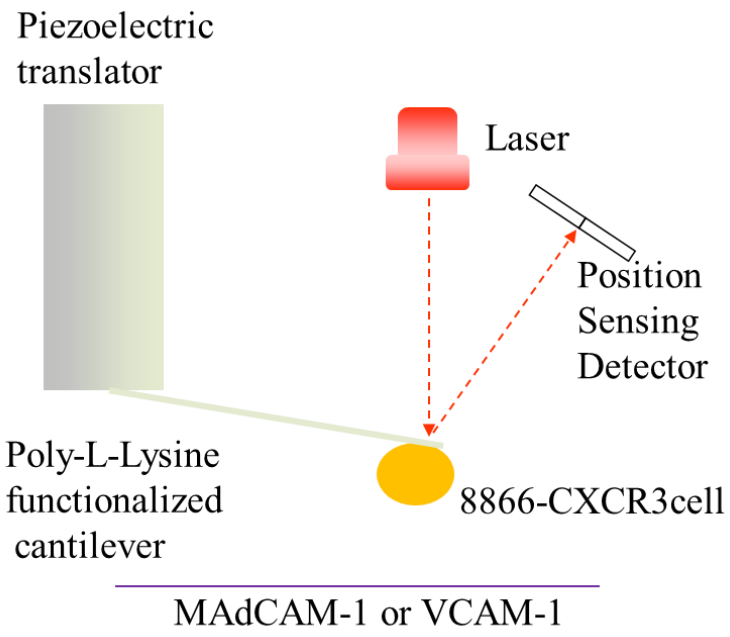

Figure 3.1 Experimental approaches of SCFS measurements of integrin $\alpha_4\beta_7$-mediated 8866-CXCR3 adhesion. An 8866-CXCR3 cell was attached to the AFM cantilever via interaction between negative charges on the celluar membrane and poly-L-lysine functionalized on the cantilever. Cell culture Petri dish surfaces were coated by MAdCAM-1 or VCAM-1 protein and then blocked by BSA. Rupture force can be detected by monitoring the laser deflection via a two-segmental photodiode of the AFM setup.

3.3.2 Chemokine signaling regulates $\alpha_4\beta_7$ integrin activation in a ligand-specific manner

Previous studies have shown that lymphocyte adhesion to the endothelium is prompted by chemokines stimulated integrin activation [85]. Chemokines CCL25 and CXCL10 were tested in this study as they can significantly activate or suppress integrin $\alpha_4\beta_7$ mediated lymphocyte adhesion to either MAdCAM-1 or VCAM-1 [84]. Compared with the adhesion frequency of integrin $\alpha_4\beta_7$ on RPMI 8866-CXCR3 cells to MAdCAM-1 and VCAM-1 before stimulation, the frequency of integrin $\alpha_4\beta_7$ adhesion to MAdCAM-1 was dramatically increased by CCL25 stimulation and that of integrin $\alpha_4\beta_7$ adhesion to VCAM-1 was increased by CXCL10. The frequency of integrin $\alpha_4\beta_7$/MAdCAM-1 adhesion increased from 14% before stimulation to 37% after CCL25 activation; similarly,

the frequency of integrin $\alpha_4\beta_7$/VCAM-1 adhesion increased from 15% before stimulation to 32% after CXCL10 activation under the same conditions. We also saw a trend of increasing rupture forces after chemokine activation. On the contrary, CCL25 suppressed integrin $\alpha_4\beta_7$ adhesion to VCAM-1 and CXCL10 suppressed integrin $\alpha_4\beta_7$ adhesion to MAdCAM-1.

3.3.3 Quantitative unbinding force measurements of individual integrin $\alpha_4\beta_7$/MAdCAM-1 complex

To further quantitatively study the effects of chemokines on interactions between integrin $\alpha_4\beta_7$ and its ligands, MAdCAM-1, rupture forces curves from AFM measurements were recorded and analyzed. Single molecule interactions at a similar loading rate were counted in a histogram and the most probable rupture forces under certain average loading rates were plotted in Figure 3.2. To increase the probability of a single molecule adhesion event for chemokine activation experiments, we reduced the adhesion frequency to less than 30% by lowering the concentration of the coated protein ligand MAdCAM-1 and reducing the contact time.

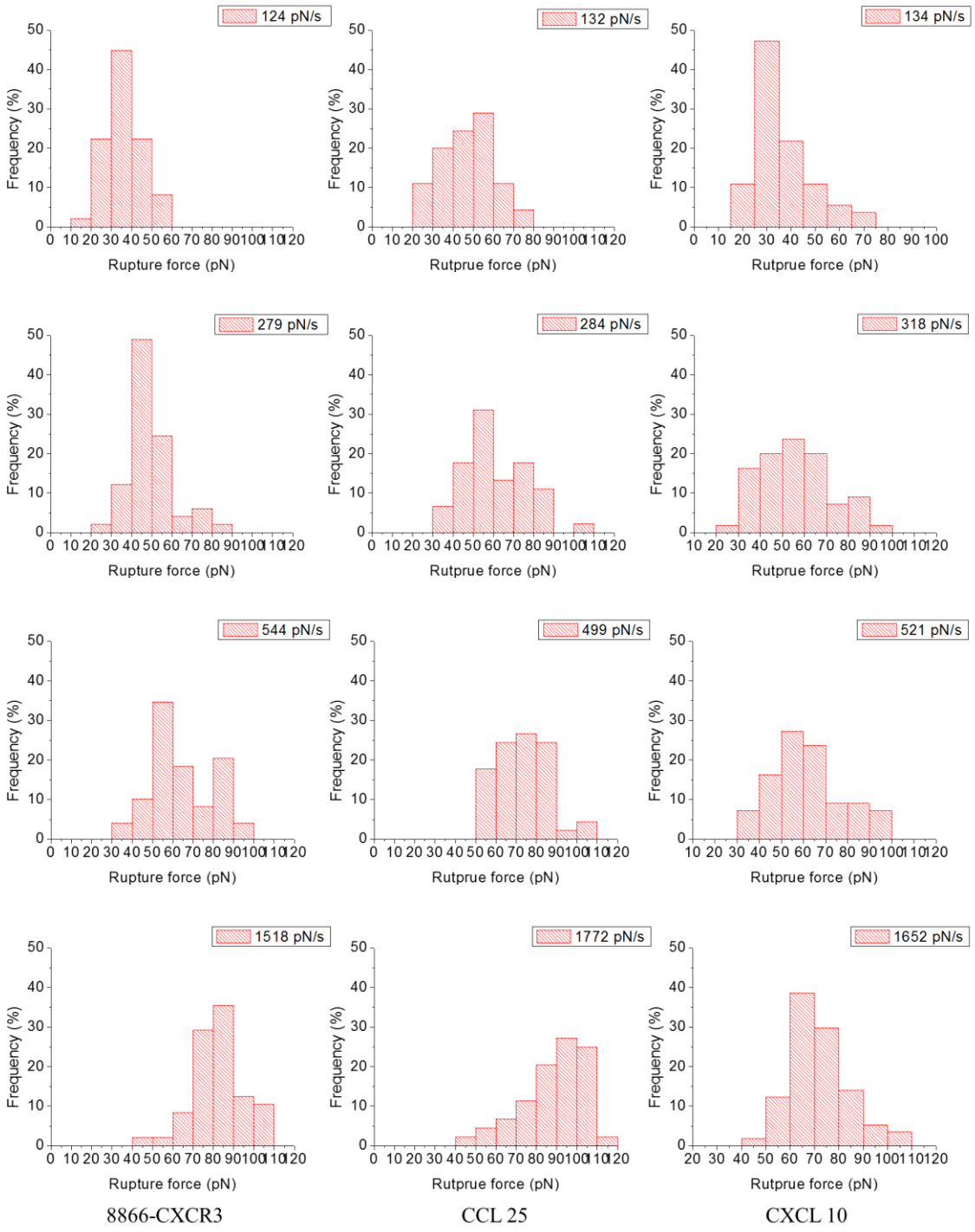

Figure 3.2 Dynamic force spectrum of interactions between integrin $\alpha_4\beta_7$ expressed on 8866-CXCR3 cell surface and MAdCAM-1 under different chemokine stimulation conditions. Rupture force distributions of integrin $\alpha_4\beta_7$ and MAdCAM-1 at different loading rates, without chemokine (left), CCL25 (middle) and CXCL10 (right).

Integrin $\alpha_4\beta_7$ adhesion on a MAdCAM-1 coated Petri dish surface changed with loading rate (50-5000 pN/s) and integrin affinity (regulated by chemokine stimulation) (Figure 3.3). RPMI CXCR3-8866 cells had no specific interactions on a 1% bovine serum albumin (BSA) coated Petri dish surface or on MAdCAM-1/VCAM-1 coated dishes with the addition of excess EDTA. With the increase of loading rate, the rupture force needed to dissociate integrin $\alpha_4\beta_7$/MAdCAM-1 complexes increased to varying degrees.

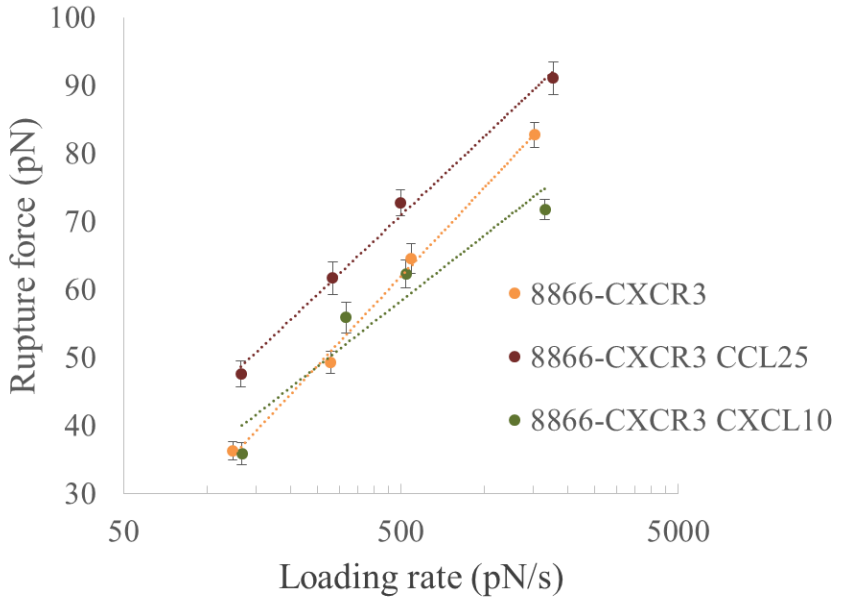

Figure 3.3 Rupture force dynamics of integrin $\alpha_4\beta_7$/MAdCAM-1 under different chemokine stimulation conditions. Force dynamics of integrin $\alpha_4\beta_7$/MAdCAM-1 before and after CCL25 or CXCL10 stimulation.

Under similar loading rates, rupture forces changed significantly before and after chemokine stimulation (Figure 3.4). For integrin $\alpha_4\beta_7$/MAdCAM-1 interactions, the single adhesion force was about 65 pN at a loading rate of 544 pN without chemokine stimulation, 73 pN at a loading rate of 499 pN/s after CCL25 stimulation and 62 pN at a loading rate of 521 pN/s after CXCL10 treatment. These loading rates applied to RPMI CXCR3-8866 cells (499-544 pN/s) were all in the range of estimated physiological loading rates [71].

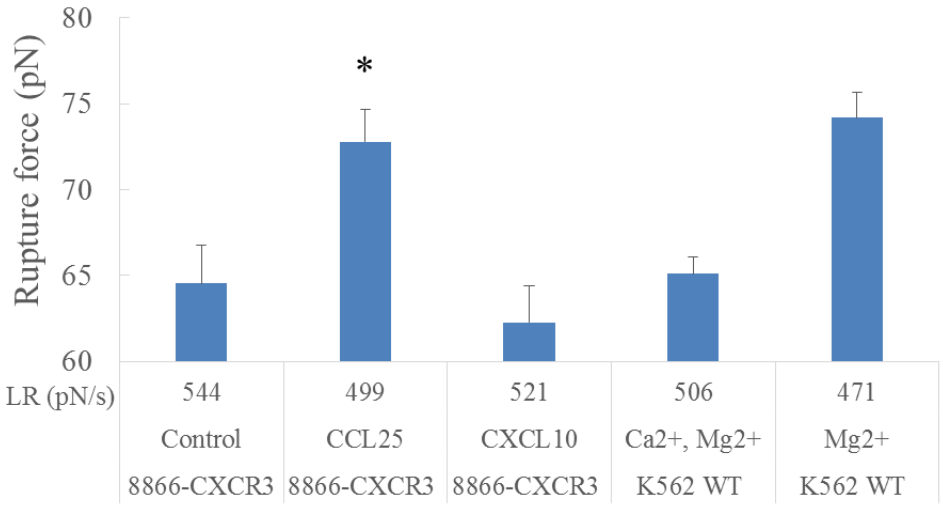

Figure 3.4 Rupture forces at approximate loading rates. There was a very significant difference ($p<0.01$) between Control 8866-CXCR3 and CCL25 treated 8866-CXCR3 cell under Welch two sample t-test (t-Test: Two-Sample Assuming Unequal Variances).

3.3.4 Quantitative unbinding force measurements of individual integrin $\alpha_4\beta_7$/VCAM-1 complex

Similar to MAdCAM-1, integrin $\alpha_4\beta_7$ adhesion on a VCAM-1 coated Petri dish surface changed with loading rate (50-5000 pN/s) and integrin affinity (regulated by chemokine stimulation) (Figure 3.5). With the increase of loading rate, the rupture force needed to dissociate integrin $\alpha_4\beta_7$/VCAM-1 complexes increased to varying degrees.

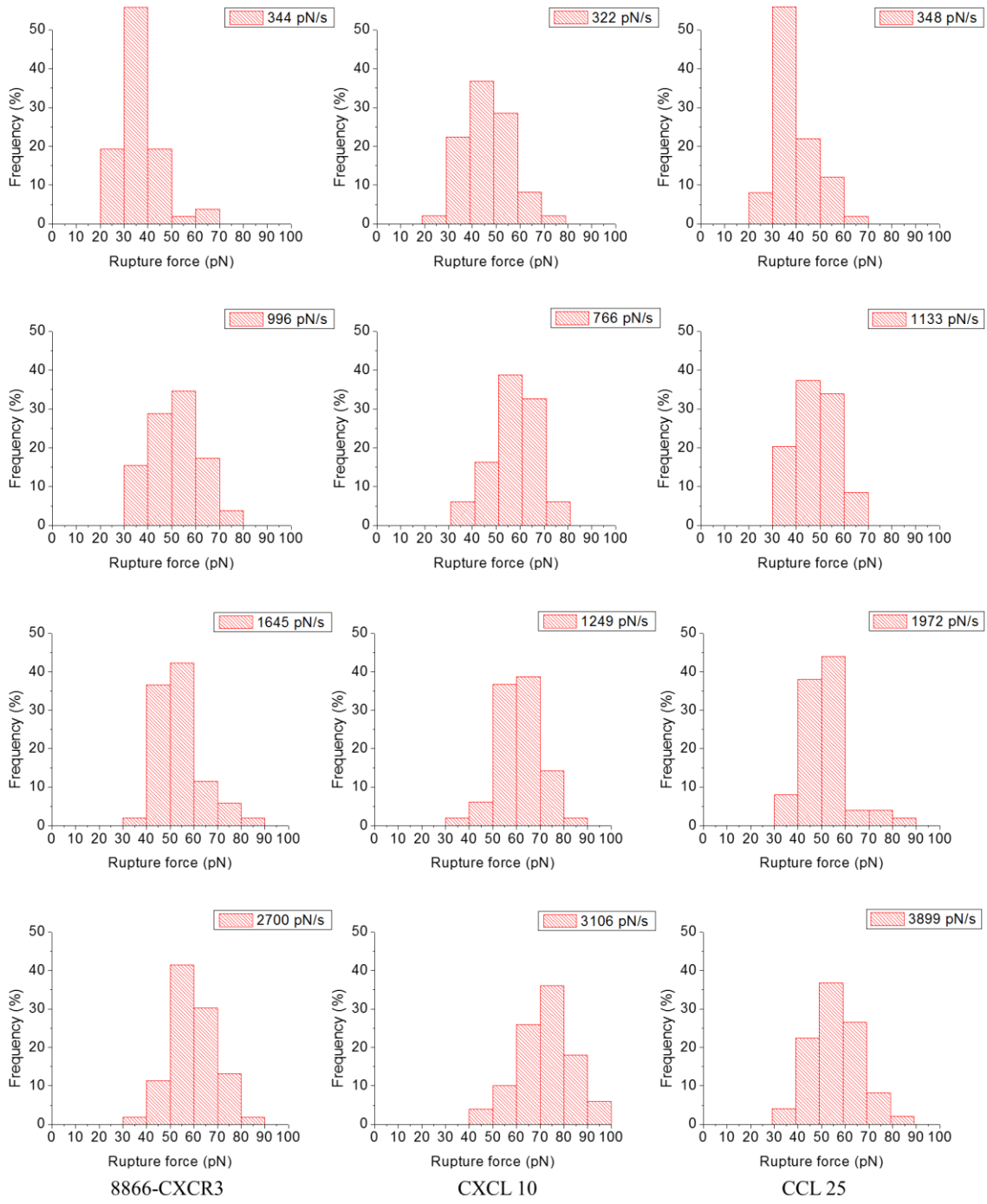

Figure 3.5 Dynamic force spectrum of interactions between integrin $\alpha_4\beta_7$ expressed on 8866-CXCR3 cell surface and VCAM-1 under different chemokine stimulation. Rupture force distributions of integrin $\alpha_4\beta_7$ and VCAM-1 at different loading rates, without chemokine (left), CXCL10 (middle) and CCL25 (right).

Under similar loading rates, rupture forces changed significantly before and after chemokine stimulation (Figure 3.6). For integrin $\alpha_4\beta_7$/VCAM-1 interaction, the single adhesion force was about 51 pN at a loading rate of 996 pN/s without chemokine stimulation, 58 pN at a loading rate of 766 pN/s after CXCL10 stimulation and 48 pN at a loading rate of 1133 pN/s after CCL25 treatment. These loading rates applied to RPMI CXCR3-8866 cell (766-1133 pN/s) were also in the range of estimated physiological loading rates [71].

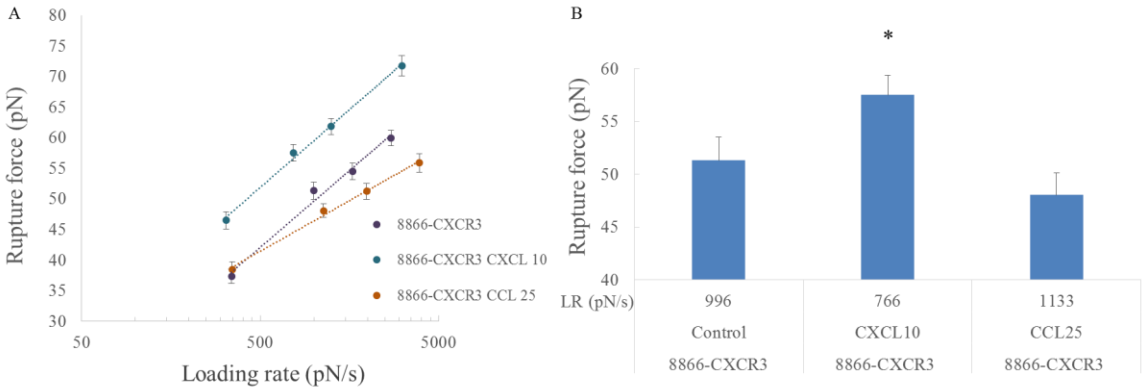

Figure 3.6 Rupture force dynamics of integrin $\alpha_4\beta_7$/MAdCAM-1 under different chemokine stimulation conditions. (A) Force dynamics of integrin $\alpha_4\beta_7$/MAdCAM-1 before and after CXCL10 or CCL25 stimulation. (B) Rupture forces at approximate loading rates. There was a very significant difference ($p<0.01$) between Control 8866-CXCR3 and CCL25 treated 8866-CXCR3 cell under Welch two sample t-test (t-Test: Two-Sample Assuming Unequal Variances).

3.3.5 Bell model parameters of $\alpha_4\beta_7$/MAdCAM-1 and $\alpha_4\beta_7$/VCAM-1 complexes

The Bell-Evans model was used to analyze the adhesion between integrin $\alpha_4\beta_7$ and its ligands, MAdCAM-1 or VCAM-1, with or without chemokine stimulation [86, 87]. After a linear fitting between f^* and $\ln r_f$, we calculated Bell parameters of the dissociation between integrin $\alpha_4\beta_7$ and its ligands MAdCAM-1 and VCAM-1 under different conditions (Table 3-1).

Table 3-1 Bell parameters of integrin $\alpha_4\beta_7$/MAdCAM-1 (A), and integrin $\alpha_4\beta_7$/VCAM-1 (B) complexes dissociation with or without chemokine stimulation.

A

MAdCAM-1	8866-CXCR3	CCL25	CXCL10
γ (Å)	2.19 ± 0.09	2.42 ± 0.14	2.93 ± 0.49
k° (s^{-1})	0.98 ± 0.08	0.45 ± 0.08	0.60 ± 0.32

B

VCAM-1	8866-CXCR3	CXCL10	CCL25
γ (Å)	3.73 ± 0.18	3.70 ± 0.18	5.68 ± 0.32
k° (s^{-1})	1.00 ± 0.28	0.42 ± 0.09	0.22 ± 0.07

3.4 Discussion

The aim of this study was to investigate how chemokine stimulation affects the binding strength and lifetime of individual integrin $\alpha_4\beta_7$/MAdCAM-1 or integrin $\alpha_4\beta_7$/VCAM-1 complexes at the single molecule level. To approach this aim, single molecule force rupture measurements were obtained and analyzed to investigate the dynamic force spectra of integrin $\alpha_4\beta_7$/MAdCAM-1 or integrin $\alpha_4\beta_7$/VCAM-1 complexes with or without chemokine stimulation.

In general, larger rupture forces were needed to dissociate high-affinity integrin $\alpha_4\beta_7$/MAdCAM-1 complex (induced by CCL25) than low-affinity $\alpha_4\beta_7$/MAdCAM-1 complex (induced by CXCL10) under different loading rates (50-5000 pN/s) which were mainly in the range of physiological loading rate (100-10000 pN/s) [71]. And those rupture forces were approximately equal to the forces needed to break the bonds between WT integrin $\alpha_4\beta_7$ on K562 cells and MAdCAM-1 in high affinity integrin $\alpha_4\beta_7$ (induced by 1mM Mg^{2+} *in vitro*) and low affinity integrin $\alpha_4\beta_7$ (induced by 1mM Ca^{2+} and 1mM Mg^{2+} *in vitro*) states (Figure 3.4). For example, under a loading rate of nearly 500 pN/s, the rupture force of an unstimulated integrin $\alpha_4\beta_7$/MAdCAM-1 complex was 65 pN and the

force was the same as the rupture force (65 pN) of low affinity WT integrin $\alpha_4\beta_7$ in 1mM Ca^{2+} and 1mM Mg^{2+}; the rupture force of high-affinity $\alpha_4\beta_7$/MAdCAM-1 complex induced by CCL25 was 73 pN and the force was very similar to the rupture force (74 pN) of high affinity WT integrin $\alpha_4\beta_7$ in 1mM Mg^{2+}. The rupture force of low-affinity integrin $\alpha_4\beta_7$/MAdCAM-1 induced by CXCL10 (62 pN) were a little smaller than that of WT in 1mM Ca^{2+} and 1mM Mg^{2+}. These results indicated that high-affinity complexes were less sensitive to shear flow, as the bond was hard to break. We also saw similar results for the integrin $\alpha_4\beta_7$/VCAM-1 complex. The rupture force was about 51 pN at a loading rate of 996 pN/s without chemokine stimulation, whereas that of high affinity integrin $\alpha_4\beta_7$/VCAM-1 complex induced by CXCL10 was 58 pN at a loading rate of 766 pN/s and low affinity integrin $\alpha_4\beta_7$/VCAM-1 induced by CCL25 was 48 pN at a loading rate of 1133 pN/s in same conditions.

Sun previously reported $\alpha_4\beta_7$ is activated by different chemokines in a ligand-specific manner: stimulation of CCL25 increased integrin adhesion to MAdCAM-1 but suppressed adhesion to VCAM-1, whereas stimulation of CXCL10 increased integrin adhesion to VCAM-1 but suppressed adhesion to MAdCAM-1 [84]. Our results partially explain the biophysical reasons for Sun's flow chamber results, as well as the regulation mechanism *in vivo* [84]. Meanwhile, the rupture force of integrin $\alpha_4\beta_7$/MAdCAM-1 and integrin $\alpha_4\beta_7$/VCAM-1 complexes did not change when the RPMI 8866-CXCR3 cells were stimulated by both CCL25 and CXCL10 at the same time. This is consistent with Sun's work and serves as a control for the opposite regulatory effects of CCL25 and CXCL10.

Through Bell-Evans model analysis, we obtained Bell parameters of the dissociation of integrin $\alpha_4\beta_7$/MAdCAM-1 and integrin $\alpha_4\beta_7$/VCAM-1 complexes with or

without chemokine stimulation (Table 3-1). For the integrin $\alpha_4\beta_7$/MAdCAM-1 complex, the dissociation constant values (k^o) were 0.98/s for the unstimulated cell and 0.45/s for the high-affinity complex stimulated by CCL25, whereas their transition state positions (γ) showed little difference. This indicated that CCL25 activation resulted in a decrease of the dissociation rate of the integrin $\alpha_4\beta_7$/MAdCAM-1 complex and an increase of bond lifetime under the same shear stress. However, although the k^o value of the CXCL10 stimulated integrin $\alpha_4\beta_7$/MAdCAM-1 complex was smaller (0.60/s) compared with the value of 1/s for unstimulated cells, we saw an increase of γ value from 2.19Å to 2.93Å. This implied that the CXCL10 induced integrin $\alpha_4\beta_7$/MAdCAM-1 complex was more sensitive than unstimulated complex to the same external force. From the Bell parameters listed in Table 3-1, we can also judge the different mechanisms of CCL25 and CXCL10 affecting the adhesive behavior of $\alpha_4\beta_7$ to MAdCAM-1. By substituting γ and k^o values listed in the table into Equation 1-1, we would get $k_{off}(f)$ as a function of external force (f). Figure 3.7A depicted the relationships between $k_{off}(f)$ and f of the $\alpha_4\beta_7$/MAdCAM-1 complex. We found that the dissociation value ($k_{off}(f)$) of the high-affinity complex induced by CCL25 was smaller than that of the unstimulated complex under the same external pulling force below 200 pN (Figure 3.7). Also the CXCL10 induced low-affinity complex always had a larger $k_{off}(f)$ value than that of unstimulated or CCL25 induced high-affinity complex under a pulling force between 40 pN and 200 pN (Figure 3.7), which explains why CCL25 induced cells had stronger interactions and CXCL10 stimulated cells had weaker interactions with MAdCAM-1 coated dish surface in the flow chamber experiment [84].

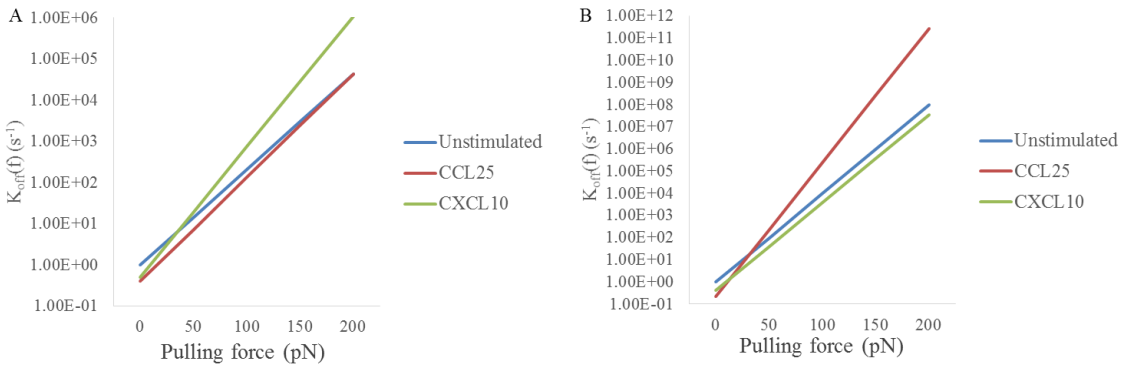

Figure 3.7 Kinetic dissociation profiles of (A) integrin $\alpha_4\beta_7$/MAdCAM-1 complex and (B) integrin $\alpha_4\beta_7$/VCAM-1 complex with or without chemokine stimulation.

In contrast we obtained reverse results for the integrin $\alpha_4\beta_7$/VCAM-1 complex. The dissociation constant values (k^o) were 1.00/s for an unstimulated cell and 0.42/s for the high-affinity complex stimulated by CXCL10, whereas their positions of transition state (γ) showed little difference. This indicated that CXCL10 activation resulted in a decrease of the dissociation rate of integrin $\alpha_4\beta_7$/VCAM-1 complex and an increase of bond lifetime under the same shear stress.

In summary, after CCL25 stimulation, when integrin $\alpha_4\beta_7$ was in its high-affinity state and complexed to ligand MAdCAM-1 but in a low-affinity state complexed to VCAM-1, adhesion between integrin $\alpha_4\beta_7$ and MAdCAM-1 was stronger and interaction between integrin $\alpha_4\beta_7$ and VCAM-1 was weaker, compared to those in unstimulated RPMI 8866-CXCR3 cells. On the contrary, after CXCL10 stimulation, when integrin $\alpha_4\beta_7$ was in its high-affinity state complexed to ligand VCAM-1 but low-affinity state complexed to MAdCAM-1, adhesion between integrin $\alpha_4\beta_7$ and VCAM-1 was stronger and interaction forces between integrin $\alpha_4\beta_7$ and MAdCAM-1 were weaker, compared to those without chemokine treatment. Our results provide important biophysical parameters of the

dissociation process, and partially explain the biophysical mechanism of chemokine regulation of integrin $\alpha_4\beta_7$-mediated leukocyte homing to target tissues.

3.5 Contribution in science

Integrin-mediated lymphocyte homing is a fundamental aspect of our immune system, with important implications on many autoimmune and inflammatory conditions including leukocytosis, and recurrent infections caused by leukocyte adhesion deficiency. While the critical involvement of chemokine-induced affinity regulation of integrin has been established for many years, the underlying mechanism has resisted elucidation.

In this work, I have used the powerful SCFS technique to elucidate the mechanism of integrin affinity regulation by chemokines, as well as the interplay among chemokine signaling, force, integrin affinity and integrin conformation. I have showed that the chemokines CCL25 and CXCL10 have an opposite effect on the affinity of $\alpha_4\beta_7$–MAdCAM-1 interactions. However, the enhancement of lifetime after CCL25 stimulation is less than that of Mg^{2+}, a widely use method to induce high affinity integrin *in vitro*. Furthermore, there seemed to be no catch/flex bond behavior at 80 pN. Therefore, the data demonstrated that the affinity change after chemokine activation is different from the cationic stimulation, suggesting that the SCFS approach might be a suitable technique to study chemokine-induced leukocyte adhesion, and to screen potential drugs to modulate leukocyte trafficking. The results from this project have filled the long-standing knowledge gap on integrin biology, which has broad and important implication for many immune disorders.

4 Sin Nombre virus (SNV) binds to an integrin-GPCR ($\alpha_{IIb}\beta_3$-P2Y$_2$R) complex, and enters the cell with GPCR stimulation.

4.1 Motivation

Hantaviruses cause hemorrhagic fever with renal syndrome (HFRS) and hantavirus cardiopulmonary syndrome (HCPS). Sin Nombre virus (SNV) is a Category A pathogen that causes the most severe form of HCPS with case fatality ratios of 30-50%. Tissue tropism involves the vascular endothelium of the heart, kidney, lung, and lymphoid organs where HCPS is characterized by dysregulation of the endothelial barrier function. Death generally results from low-output cardiogenic shock, and multi-organ failure. Currently, vaccines are not available, nor are there is any approved, effective therapies and treatment of severe disease. Therefore, identification of receptors and their mechanism for enabling hantavirus infection is essential for understanding HCPS pathogenesis, limiting viral entry and spread. Previous studies have identified β_3 and β_1 integrins as the main receptors for pathogenic and non-pathogenic hantaviruses respectively [88]. More recently, β_2 integrin receptors such as Mac-1 ($\alpha M\beta_2$, CD11b/CD18, complement receptor 3 (CR3) and $\alpha X\beta_2$ (CD11c/ CD18), complement receptor 4 (CR4), expressed in leukocytes have been implicated as entry receptors for hantavirus [89]. Interestingly, cell entry through β_2 integrin has been shown to be non-productive in leukocytes, but associated with the release of neutrophil extracellular traps, which contribute to pathogenesis [89].

Pathogenic hantaviruses bind to the plexin-semaphorin-integrin (PSI) domain present at the apex of the bent/inactive form of the human β_3 integrin subunit of $\alpha v\beta_3$ and $\alpha_{IIb}\beta_3$ integrins [90]. The PSI domain is well removed from the site of RGD ligand binding, and to the best of our knowledge, is not used by cellular proteins [91]. In this way, the

evolutionary strategy developed by pathogenic hantaviruses is a novel one for interacting with integrins, which has the potential to reveal new insights into integrin signaling mechanisms.

Integrins recognize narrowly defined structural motifs (e.g. RGD, LDV, etc) expressed on a wide range of extracellular ligands including ECM proteins, counter-receptors and plasma proteins, as well as several components of the cytoskeleton [92-94]. Ligand-occupied integrins, in turn, undergo conformational changes that lead to outside-in activation of integrins [16, 31, 91, 95-97]. It is also worth noting that integrins also bind in cis to other surface moieties including GPI-linked proteins, tetraspanins, members of the immunoglobulin superfamily of cell adhesion molecules and signaling receptors, with which they synergize signal transduction pathways after ligand binding [98-101]. Thus, assembly of proteins on the integrin cytoplasmic domain tails can also occur as a result of signals produced from receptors distinct from integrins. In this way, the assembled complex can activate integrins, change their conformation, and allow enhanced interactions of integrins with ECM ligands, a process termed inside-out signaling [21, 102-105].

Although manipulation of the integrin PSI domain has been shown to elicit integrin activation [106, 107], current data suggest that receptor signaling and post SNV-binding to the PSI domain are insufficient to enable virus internalization. In this regard, one study has shown that polarized epithelial and endothelial cells are susceptible to hantavirus infection exclusively from the apical surface but not the basolateral side [108], even though integrins are sorted to the latter domain [109]. A glycosylphosphatidylinositol-linked protein, CD55/decay-accelerating factor (DAF) which is sorted to the apical surface in polarized cells [110] was implicated as a cell entry co-receptor for pathogenic hantaviruses [108]. In

other studies, complement protein gC1qR/p32 [111], and an unknown 70 kDa protein [112] have been reported to mediate hantavirus infection. However, the functional mechanisms of integrin activation associated with these proteins have not yet been investigated.

We have found that the H319 anti-DAF antibody effectively blocks SNV infection of polarized Vero E6 cells, but poorly inhibits infection of isotropic non-polarized cells [113]. We hypothesized that the cell polarity-dependent blocking of infection with H319 was due to the apical/basolateral domain segregation of components of a signaling complex formed by the integrin and the yet unidentified receptor [98, 99, 114, 115]. We also reasoned that the signaling protein could not directly bind with SNV, due to infection blocking by H319 antibodies in polarized cells. We targeted the $P2Y_2$ receptor ($P2Y_2R$) a member of the purinergic family of G-protein coupled receptors (GPCR), which so far has been reported to interact with α_3 and β_5 integrins through an RGD motif in its first extracellular loop [116]. In polarized cells, $P2Y_2R$ is sorted to the apical surface [117] together with DAF [110] and is segregated from integrins which are sorted to the basolateral membrane domains [109]. Here, we set out to determine whether α_3 integrins engage in signal crosstalk with $P2Y_2R$ to enable SNV infection.

4.2 Materials and methods

4.2.1 Cell Culture and Sin Nombre Virus

CHO K1 cells were grown in F-12K media (Cellgro, Mediatech), 10% FBS, 2mM L-glutamine, and 100 units/mL Penicillin/Streptomycin. CHO A24 and CHO C3 cells were grown in DMEM/F12 HAM mixture (Gibco, Life Technologies) with 10% FBS, 2mM L-Glutamine, 100 units/mL Penicillin/Streptomycin, and 1mg/mL G418 (Sigma). Cells were

maintained at 37°C in a water jacketed 5% CO2 incubator. lines and UV-inactivated Sin Nombre Virus and Fluorescent Labeled SNV were provided by Dr. T. Buranda.

4.2.2 Protein immobilization

Recombinant human $\alpha_{IIb}\beta_3$ integrin (R&D Systems, Minneapolis, MN) was attached to an AFM cantilever (MLCT: Bruker Nano, Camarillo, CA) by covalently crosslinking the two using a heterobifunctional acetal-PEG27-NHS linker as described in previous chapter [118, 119].

4.2.3 Atomic Force Microscopy (AFM) measurements of individual integrin-$P2Y_2R$ interactions

All single-molecule force measurements were conducted using a custom-designed apparatus designed for operation in the force spectroscopy mode [40, 45]. Using a piezoelectric translator, the integrin-functionalized cantilever was lowered onto a $P2Y_2R$-expressing CHO-K1 cell until binding between the integrin and RGD sites occurred. The main objective of these experiments was to determine whether SNV binding to the PSI domain causes a change in affinity at the RGD binding site. The positive control for integrin activation was 2 mM of Mn^{2+} added to the media [120-123]. For SNV assays, the cantilever was pre-incubated with fluorescently labeled neat SNV^{R18}, and a mixture of SNV^{R18} and PSI domain polypeptide [124] to competitively block the interaction between the integrin functionalized cantilever and SNV^{R18}. Association of SNV and the integrin functionalized AFM tip was confirmed by imaging SNV fluorescence on the AFM tip.

The binding interaction between the AFM tip and RGD sites was then determined from the deflection of the cantilever via a position-sensitive two-segment photodiode. To calibrate the cantilever (320 μm long by 22 μm wide triangle), the spring constant at the

tip was characterized via thermally-induced fluctuations. The spring constants (13 ± 3 pN/nm) of the calibrated cantilevers agreed with the values specified by the manufacturer. For each pulling speed, 200 to 500 force curves were recorded, which yielded 50 to 150 unbinding forces. Curve fitting was performed using IGOR Pro or Origin software by minimizing the chi-square statistic for the optimal fit. To enable measurement of a single molecule interaction, the contact time between the cantilever and the sample were minimized to obtain measurements of the unitary $\alpha_{IIb}\beta_3$-RGD unbinding force. An adhesion frequency of ~33% in the force measurements ensured that there was a >83% probability that the adhesion event was mediated by a single bond [52]. The $\alpha_{IIb}\beta_3$-RGD interactions were characterized by the dynamic force spectrum (DFS), which is the plot of most probable unbinding force as a function of the loading rate. The unbinding force was probed at low affinity in the DMEM culture medium (control), the unbinding force of the $\alpha_{IIb}\beta_3$-RGD interaction increased linearly with the logarithm of the loading rate, ranging from 40 to 70 pN over loading rates of 400 to 4,000 pN/s, respectively.

A more detailed analysis of the measurements of the $\alpha_{IIb}\beta_3$-RGD interaction was achieved by fitting the Bell-Evans model [47] to the acquired DFS. The Bell-Evans model, a theory to determine energy landscape properties, describes the influence of an external force on the rate of bond dissociation[46, 47]. According to this model, a pulling force, f, distorts the intermolecular potential of a ligand-receptor complex, leading to a lowering of the activation energy and an increase in the dissociation rate k(f) as follows:

$$K(f) = k^0 \exp\left(\frac{f\gamma}{k_B T}\right) \quad [4\text{-}1]$$

where k^0 is the dissociation rate constant in the absence of a pulling force, γ is the position of the transition rate, T is the absolute temperature, and k_B is the Boltzmann

constant. For a constant loading rate r_f, the probability density for the unbinding of the complex as a function of the pulling force f is given by

$$P(f) = k^0 \exp\left(\frac{\gamma f}{k_B T}\right) \exp\left\{\frac{k^0 k_B T}{\gamma r_f}\left[1 - \exp\left(\frac{f\gamma}{k_B T}\right)\right]\right\} \text{[4-2]}$$

with the most probable unbinding force f^* given by

$$f^* = \frac{k_B T}{\gamma} \ln\left(\frac{\gamma}{k^0 k_B T}\right) + \frac{k_B T}{\gamma} \ln(r_f) \text{ [4-3]}$$

Hence, the Bell model predicts that the most probable unbinding force f* is a linear function of the logarithm of the loading rate. Experimentally, f* was determined from the mode of the unbinding force histograms. The Bell model parameters were determined by fitting Equation 4-3 to the plot of f* versus ln(r_f).

4.3 Results

4.3.1 Binding of SNV to PSI domain of β_3 integrin modulates affinity at the P2Y2R occupied RGD site

Here we used AFM to determine whether the attachment of SNV to the PSI domain triggers integrin activation as measured by a change in affinity at the integrin RGD cis-interaction with $P2Y_2R$. These experiments were carried out using parent CHO-K1 cells. Over the past two decades, atomic force microscopy (AFM) has emerged as an important tool for studying single molecule ligand-receptor interactions, whereby the strength of protein-protein interactions has been measured by a pulling force to induce unbinding [125]. $\alpha_{IIb}\beta_3$- $^{RGD}P2Y_2R$ interactions were studied using the recombinant platelet $\alpha_{IIb}\beta_3$ integrin, attached to an AFM cantilever via an established crosslinking protocol using a hetero-bifunctional PEG linker [125, 126]. Using a piezoelectric translator, the integrin-

functionalized cantilever was lowered onto a $P2Y_2R$-expressing CHO-K1 cell until binding between the integrin and RGD binding site occurred as determined from the deflection of the cantilever via a position-sensitive two-segment photodiode (Figure 4.1A). Figure 4.1C shows ten consecutive pulling force traces, where the 4^{th}, 6^{th} and 9^{th} trace correspond show the specific rupture force of the putative $\alpha_{IIb}\beta_3$- $^{RGD}P2Y_2R$ complex. The unbinding force (Fu) of the $\alpha_{IIb}\beta_3$-$P2Y_2R$ complex was derived from the force jump that accompanies the unbinding of the complex (Figure 4.1B) [125, 126]. For each pulling speed, over 200 force curves were recorded, which yielded 50 to 150 unbinding forces (Figure 4.1; Figure 4.2D). In the same setting $P2Y_2R$ siRNA knockdown CHO-K1 cells were probed by AFM to determine the putative specificity of the $\alpha_{IIb}\beta_3$ -$^{RGD}P2Y_2R$. The overall interaction specificity of the AFM probe was determined by comparing the adhesion frequency measured with an integrin-functionalized probe relative to the PEG linker only probe. The adhesion frequency data, measured under the same experimental conditions and summarized in Figure 4.2A, demonstrate the overall specificity of the $\alpha_{IIb}\beta_3$- $^{RGD}P2Y_2R$ interaction which is manifested by the diminution of adhesion frequency in $P2Y_2R$ knockdown cells relative to the $P2Y_2R$ replete cells. The single molecule unbinding force (F_u) of the $\alpha_{IIb}\beta_3$-RGD site complex was derived from the force jump that accompanied the unbinding of the complex [52].

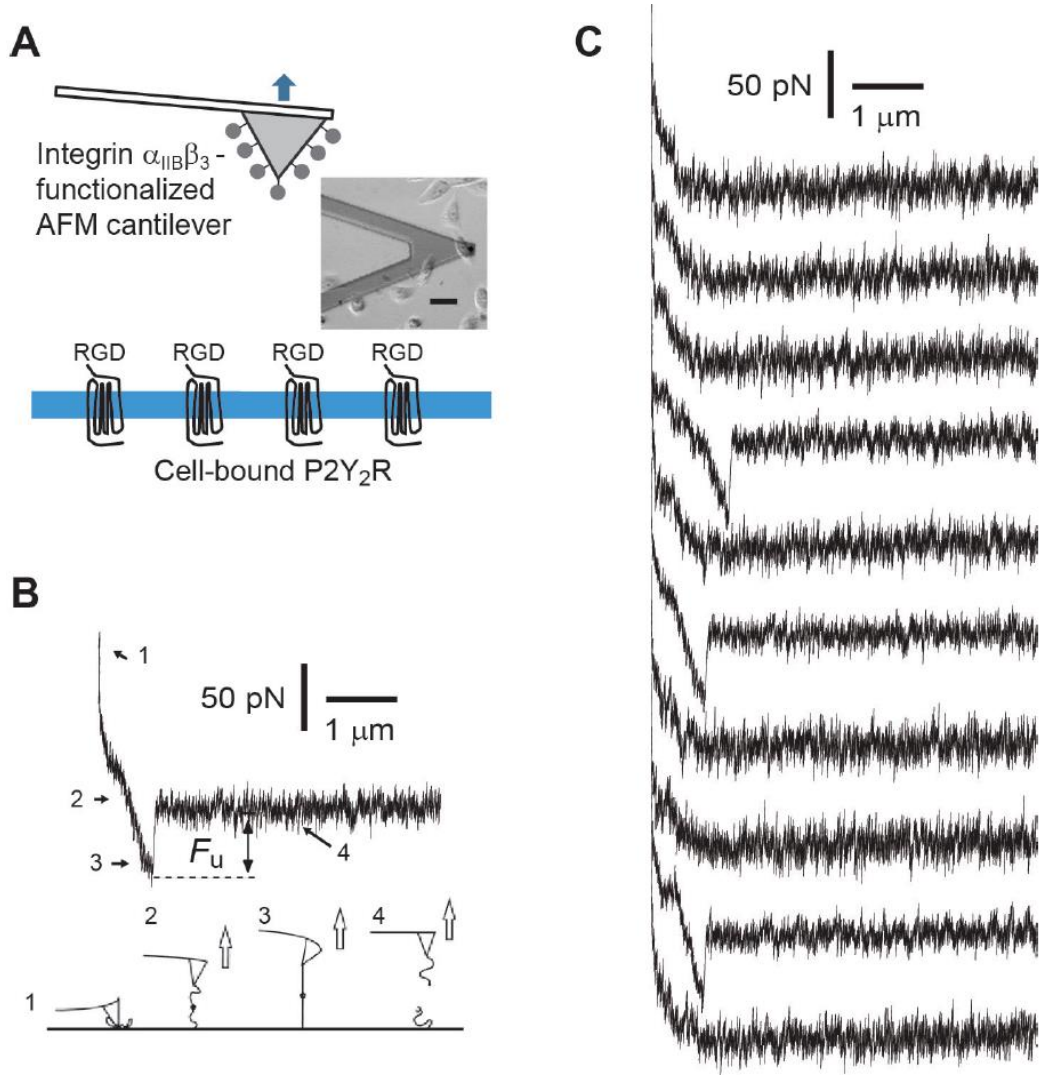

Figure 4.1 Atomic Force Microscopy (AFM) measurements of individual integrin-$P2Y_2R$ interactions. (A) Schematic and bottom view micrograph of AFM micro-cantilever functionalized with $\alpha_{IIb}\beta_3$ above RGD binding sites on CHO-K1 cells. (B) A typical cantilever-CHO-K1 unbinding traces. Fu is the unbinding force. The lower panel shows the 4 stages of stretching and rupturing a single ligand-receptor complex using the AFM: 1) AFM-cell surface engagement 2) retraction 3) extension 4) rupture. (C) To enable measurement of a single molecule interaction, the contact time and indentation force between the cantilever and the sample were minimized to obtain measurements of the unitary $\alpha_{IIb}\beta_3$-$P2Y_2R$ unbinding force. An adhesion frequency of ~33% in the force measurements ensured that there was a >83% probability that the adhesion event was mediated by a single bond [52]. Shown are ten representative consecutive force-displacement (retract) traces between a cantilever tip functionalized with SNV and a CHO-K1 cell under conditions of minimal contact. The 4^{th}, 6^{th} and 9^{th} force curves revealed adhesion.

4.3.2 SNV binding to the PSI domain induced integrin activation

The activation state of $\alpha_{IIb}\beta_3$ is an intrinsic characteristic of the integrin that is independent of the local cell membrane environment [127]. To determine whether SNV binding to the PSI domain induced integrin activation, the integrin-functionalized cantilever was pre-incubated with fluorescently labeled SNV^{R18} particles or a mixture of SNV^{R18} and PSI domain polypeptide to competitively block the interaction between the cantilever and SNV^{R18}. Association of SNV and the AFM tip was confirmed by imaging SNV fluorescence on the AFM tip as shown in Fig. 4B. Mn^{2+} was used as a positive control for integrin activation [21] (Figure 4.2C&D). Analysis of the F_u histograms showed that the distribution of unbinding forces of the PSI peptide-treated sample was bimodal, with each peak corresponding to the most probable force of the control and SNV- or Mn^{2+}-activated integrins, indicating that this could be a combination of F_u profiles for the low and high affinity integrins due to incomplete blocking (Figure 4.2D). As the unbinding forces depend on pulling speed (loading rate) [46, 47] rupture forces were measured over a wide range of loading rates (300-7,000 pN/s) to yield a plot of unbinding forces (F_u) versus loading rate for low and high affinity integrins (Figure 4.2C). The plot is called a dynamic force spectrum (DFS) [52]. Interestingly, the rupture force for SNV activated integrins was comparable to Mn^{2+} activation. Overall the rupture forces required to separate the $\alpha_{IIb}\beta_3$-RGD interactions at low and high affinity were comparable to literature measurements at similar loading rates [128, 129]. These results indicate, for the first time, that SNV engagement of the PSI domain induces integrin activation. This enabled us to next explore the downstream effects of this activation in living cells.

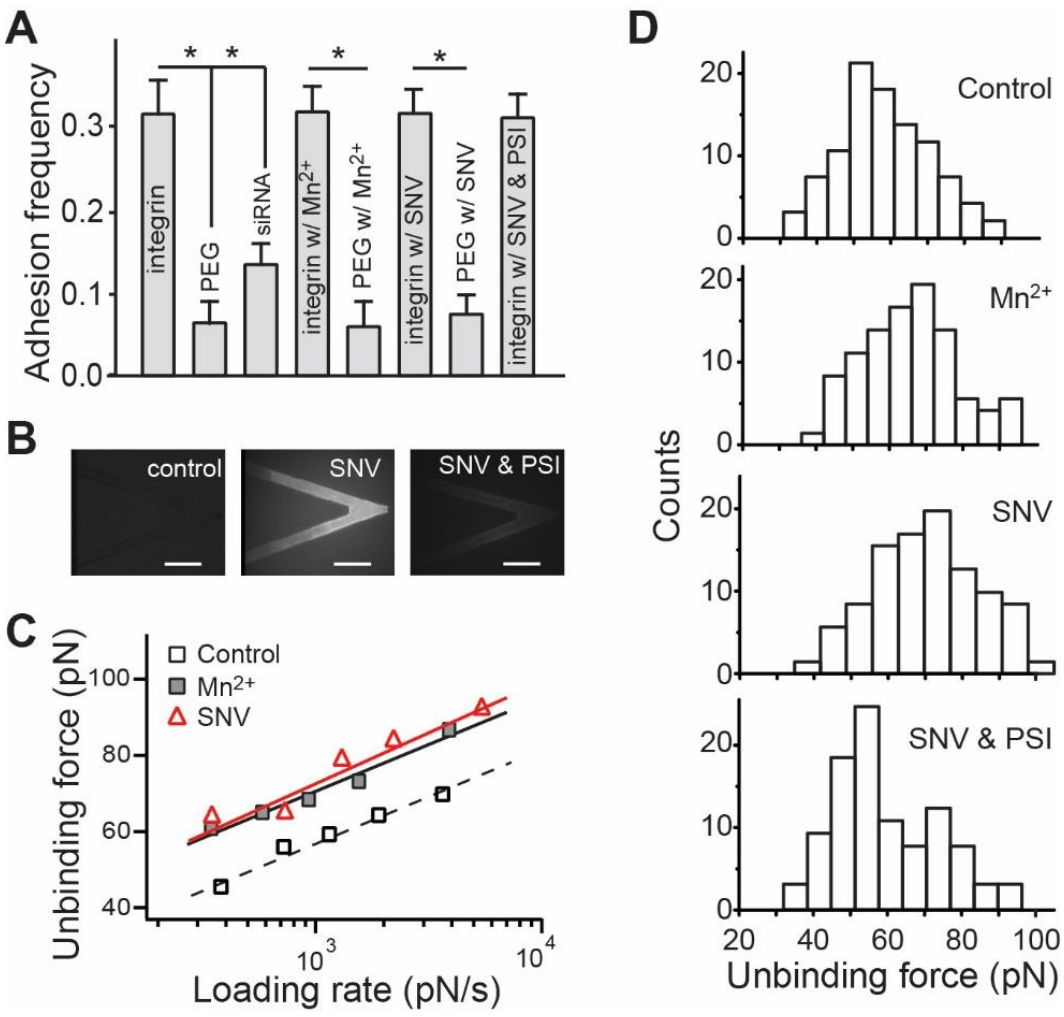

Figure 4.2 Virus binding to PSI domain activates integrin. (A) Adhesion frequency of AFM measurements of integrin-RGD interactions vs. PEG in WT CHO-K1 and siRNA $P2Y_2R$ knockdown cells. Contact force, contact time and retraction speed were 200 pN, 0.15 s and 3.7 um/s, respectively. *P<0.05 between the indicated groups. (B) Fluorescence micrographs (bottom view) of an integrin-functionalized cantilever (left), the same cantilever pre-incubated with fluorescently labeled SNV^{R18} (middle), and with SNV^{R18} and PSI domain polypeptide for blocking SNV binding (right). (C) The dynamic force spectra of the $\alpha_{IIb}\beta_3$- RGD interactions. The Bell-Evans model fit of Fig. 1C revealed a 4-fold decrease in the dissociation rate (or a 4-fold increase of lifetime) for the Mn^{2+} activated integrin (0.10 s^{-1}) compared with that for the resting integrin (0.40 s^{-1}). By assuming the energy difference between two Mn^{2+} activated and resting integrins to be given as $\Delta G_{1,2} = -k_BT \ln(k_1^0/ k_2^0)$, where k_1^0 and k_2^0 are the dissociation rate constants of Mn^{2+} activated and resting integrins, respectively, the data revealed that the integrin activation increased the activation energy by 1.4 k_BT. (D) Histograms of the unbinding forces between $\alpha_{IIb}\beta_3$ and $P2Y_2R$ under the indicated conditions. Loading rates of the histograms were approximately 1000 pN/s.

4.4 Discussion

In the present study, we demonstrate a new function for $P2Y_2R$ as an essential mediator of SNV entry and replication in non-polarized cells. We used single molecule force spectroscopy to show that interaction of SNV with the integrin β_3 PSI domain, results in integrin activation. The canonical model for integrin affinity regulation involves the dynamic equilibrium among three states: inactive, active, and active and ligand-occupied [127, 130]. Transitions between these states involve dynamic allosteric changes. The terminal step is the binding of talin to the cytoplasmic domain of the integrin causing conformational activation of the integrin by inducing a separation of the α and β subunit cytoplasmic domains [95, 104, 127]. Using CHO cell lines, one expressing wild type $\alpha_{IIb}\beta_3$ integrin and another expressing $\alpha_{IIb}\beta_3$ with a loss of function mutation for transmembrane signaling [127, 131, 132], we found that productive infection required full activation of wild type $\alpha_{IIb}\beta_3$ integrin.

Our data also indirectly demonstrated a role for G_s activity in cell entry, which was antagonized by G_i signaling. Although the mechanism by which it is activated is not yet characterized, several studies have established that integrin tension can recruit active G_s proteins to focal adhesions [133, 134]. In the low affinity conformation, the height of the integrin's ligand binding site is comparable to the $P2Y_2R$ binding motif, whereas the allosteric change in conformation of activated integrin can potentially increase the height difference to >100 Å when the integrin is fully activated [135-137]. Previous studies have shown that forces transmitted by integrins regulate many important cellular functions [138-143]. Recent studies have determined that the threshold tension across a single integrin-ligand bond, termed integrin tension, that is transmitted by clustered integrins in motile

focal adhesions (FAs) is on the order of >54 pN [144]. This value is less than the > 70pN unbinding force, measured herein (Figure 4.2D) required to disengage SNV-activated integrin from the $P2Y_2R$, which supports the notion that G_s activating focal adhesions [133, 134] are formed by the integrin tension created by the activated integrin while cis-interacting with $P2Y_2R$. This line of enquiry is worthy of further pursuit.

$P2Y_2R$ is upregulated in a variety of tissues by inflammatory mediators released during infection [145-153] and therefore could be a critical factor in the spread of hantavirus and pathogenesis. ATP and $P2Y_2R$ signaling affects a broad range of biological processes such as the generation of chemotactic signals and/or the activation of different immune cells, causing inflammatory cells such as neutrophils to migrate, proliferate, differentiate, or release diverse inflammatory mediators [145, 154, 155]. More recently, β_2 integrin receptors such as Mac-1 ($\alpha M\beta 2$, CD11b/CD18, complement receptor 3 (CR3) and $\alpha_X\beta 2$ (CD11c/ CD18), and complement receptor 4 (CR4), expressed in leukocytes, have been implicated as entry receptors for hantavirus [89]. Thus, elucidating the role of $P2Y_2R$ as a mediator of hantavirus infection and recruiter of leukocytes to sites of active inflammation could be significant for understanding the pathogenesis of hantavirus infections [156, 157]. $P2Y_2R$ is capable of being treated with drugs and thus provides an opportunity to mitigate the disease [158, 159]. This is likely to result in the identification of potential new targets for discovery and the development of more effective antiviral drugs some of which can be repurposed from existing G-protein specific drugs.

4.5 Contribution in science

Endothelial cells and platelets express β_3 integrins, which are believed to play prominent roles in the pathogenesis of Hantavirus infections. Under normal physiological conditions integrins expressed on the apical surface of vascular endothelial cells and platelets exist in a low-affinity state with respect to extracellular ligand binding and require intracellular signals to bind physiologic ligands. Although manipulation of the integrin PSI domain has been shown to elicit integrin activation, the functional mechanisms of integrin activation associated with SNV virus and proteins have not yet been investigated.

In the present study, we demonstrate a new function for $P2Y_2R$ as an essential mediator of β_3 integrin activation during SNV entry and replication in non-polarized cells. We found that $P2Y_2R$ fulfills this role via an integrin-binding domain (RGD) in its first extracellular loop of $P2Y_2R$. Our results show that SNV binding to the PSI domain prompts an increase in affinity at the $P2Y_2R$ occupied ligand-binding site. The findings of this project provide new insights into integrin activation and how viruses exploit such a pathway to maintain their lifecycle.

5 Conclusions

The research work in this dissertation was focused on analyzing the interactions between integrins and ligands. Single molecule force spectroscopy (SMFS) and single cell force spectroscopy (SCFS) were used to study the mechanical strength and force dependent dissociation kinetics of adhesive bonds formed in integrin-ligand complexes. The Bell-Evans model was used to analyze the data.

In Chapter 2, through SMFS and SCFS measurements on interactions between integrin $\alpha_4\beta_7$ stable transfectant K562 cell and MAdCAM-1 coated dish, we obtained the rupture forces needed to dissociate the $\alpha_4\beta_7$/MAdCAM-1 complex *in vitro* and the Bell parameters of the complex dissociation. Our data demonstrated that dissociation rates under external force make a difference between different bond affinities. The data suggests that induction of higher affinity states elevates the heights of the energy barriers of integrin complex dissociation, but has minimal effect on the width of the barriers, and that cellular membrane tether bonds play significant roles in maintaining the cell-substrate adhesion for seconds. This partially explains the biophysical mechanism of $\alpha_4\beta_7$-mediated leukocyte rolling or firm adhesion. The results can be used to perform mathematical modeling to better understand leukocyte and immune system behave. There are still many unknown points underlying the biophysical mechanism of integrin-mediated leukocyte migration, which are crucial for understanding integrin functions and for solving problems caused by integrin dysfunction.

In Chapter 3, SCFS technique was used to elucidate the mechanism of integrin affinity regulation by chemokines, as well as the interplay among chemokine signaling, force, integrin affinity and integrin conformation. The data showed that the chemokines CCL25 and CXCL10 have an opposite effect on the affinity of $\alpha_4\beta_7$–MAdCAM-1 interactions. However, the enhancement of lifetime after CCL25 stimulation is less than that of Mg^{2+}, a widely use method to induce high affinity integrin *in vitro*. Furthermore, there seemed to be no catch/flex bond behavior at 80 pN. Therefore, the data demonstrated that the affinity change after chemokine activation is different from the cationic stimulation, suggesting that the SCFS approach might be a suitable technique to study chemokine-induced leukocyte adhesion, and to screen potential drugs to modulate leukocyte trafficking. Our results provide important biophysical parameters of the dissociation process, and partially explain the biophysical mechanism of chemokine regulation of integrin $\alpha_4\beta_7$-mediated leukocyte homing to target tissues. The results have filled the long-standing knowledge gap on integrin biology, which has broad and important implication for many immune disorders.

In Chapter 4, we used SMFS to show that interaction of SNV with the integrin β_3 PSI domain, results in integrin activation and demonstrated a new function for $P2Y_2R$ as an essential mediator of β_3 integrin activation during SNV entry and replication in non-polarized cells. We found that $P2Y_2R$ fulfills this role via an integrin-binding domain (RGD) in its first extracellular loop of $P2Y_2R$. Our results show that SNV binding to the PSI domain prompts an increase in affinity at the $P2Y_2R$ occupied ligand-binding site. The findings provide new insights into integrin activation and how viruses exploit such a pathway to maintain their lifecycle.

References

1. Alon, R., D.A. Hammer, and T.A. Springer, *Lifetime of the P-selectin-carbohydrate bond and its response to tensile force in hydrodynamic flow.* Nature, 1995. **374**(6522): p. 539-42.
2. Schreiber, T.H., et al., *Shear flow-dependent integration of apical and subendothelial chemokines in T-cell transmigration: implications for locomotion and the multistep paradigm.* Blood, 2007. **109**(4): p. 1381-6.
3. Ley, K., *Arrest, migration, survival and proliferation of leukocytes and vascular cells: The many faces of chemokine biology - Foreword.* Microcirculation, 2003. **10**(3-4): p. 245-246.
4. Abbassi, O., et al., *Canine neutrophil margination mediated by lectin adhesion molecule-1 in vitro.* J Immunol, 1991. **147**(7): p. 2107-15.
5. Simon, S.I. and C.E. Green, *Molecular mechanics and dynamics of leukocyte recruitment during inflammation.* Annu Rev Biomed Eng, 2005. **7**: p. 151-85.
6. Ley, K., *Arrest chemokines.* Microcirculation, 2003. **10**(3-4): p. 289-95.
7. Shulman, Z., et al., *Lymphocyte crawling and transendothelial migration require chemokine triggering of high-affinity LFA-1 integrin.* Immunity, 2009. **30**(3): p. 384-96.
8. Kim, I., et al., *Vascular endothelial growth factor expression of intercellular adhesion molecule 1 (ICAM-1), vascular cell adhesion molecule 1 (VCAM-1), and E-selectin through nuclear factor-kappa B activation in endothelial cells.* J Biol Chem, 2001. **276**(10): p. 7614-20.

9. Diamond, M.S. and T.A. Springer, *A subpopulation of Mac-1 (CD11b/CD18) molecules mediates neutrophil adhesion to ICAM-1 and fibrinogen.* J Cell Biol, 1993. **120**(2): p. 545-56.

10. Chambers, J.D., et al., *Endocytosis of beta 2 integrins by stimulated human neutrophils analyzed by flow cytometry.* J Leukoc Biol, 1993. **53**(4): p. 462-9.

11. DiVietro, J.A., et al., *Immobilized stromal cell-derived factor-1alpha triggers rapid VLA-4 affinity increases to stabilize lymphocyte tethers on VCAM-1 and subsequently initiate firm adhesion.* J Immunol, 2007. **178**(6): p. 3903-11.

12. Chigaev, A., et al., *Regulation of cell adhesion by affinity and conformational unbending of alpha4beta1 integrin.* J Immunol, 2007. **178**(11): p. 6828-39.

13. Ferreira, A.M., et al., *The p110delta isoform of PI3K differentially regulates beta1 and beta2 integrin-mediated monocyte adhesion and spreading and modulates diapedesis.* Microcirculation, 2006. **13**(6): p. 439-56.

14. Shamri, R., et al., *Chemokine stimulation of lymphocyte alpha 4 integrin avidity but not of leukocyte function-associated antigen-1 avidity to endothelial ligands under shear flow requires cholesterol membrane rafts.* J Biol Chem, 2002. **277**(42): p. 40027-35.

15. Takeyasu, K., et al., *Multiple Forms of the Sodium-Pump in the Chicken - Isolation of Distinct Cdna Clones for the Alpha-Subunit.* Journal of Cell Biology, 1986. **103**(5): p. A52-A52.

16. Luo, B.H., C.V. Carman, and T.A. Springer, *Structural basis of integrin regulation and signaling.* Annu Rev Immunol, 2007. **25**: p. 619-47.

17. Hynes, R.O., *Integrins: versatility, modulation, and signaling in cell adhesion.* Cell, 1992. **69**(1): p. 11-25.

18. Abram, C.L. and C.A. Lowell, *The ins and outs of leukocyte integrin signaling.* Annu Rev Immunol, 2009. **27**: p. 339-62.

19. Yamada, A., et al., *Activation of human CD4 T lymphocytes. Interaction of fibronectin with VLA-5 receptor on CD4 cells induces the AP-1 transcription factor.* J Immunol, 1991. **146**(1): p. 53-6.

20. Roberts, K., et al., *The vitronectin receptor serves as an accessory molecule for the activation of a subset of gamma/delta T cells.* J Exp Med, 1991. **173**(1): p. 231-40.

21. Takagi, J., et al., *Global conformational rearrangements in integrin extracellular domains in outside-in and inside-out signaling.* Cell, 2002. **110**(5): p. 599-11.

22. Legler, D.F., et al., *Superactivation of integrin alphavbeta3 by low antagonist concentrations.* J Cell Sci, 2001. **114**(Pt 8): p. 1545-53.

23. Bednar, B., et al., *Flow cytometric measurement of kinetic and equilibrium binding parameters of arginine-glycine-aspartic acid ligands in binding to glycoprotein IIb/IIIa on platelets.* Cytometry, 1997. **28**(1): p. 58-65.

24. Chan, J.R., S.J. Hyduk, and M.I. Cybulsky, *Chemoattractants induce a rapid and transient upregulation of monocyte alpha4 integrin affinity for vascular cell adhesion molecule 1 which mediates arrest: an early step in the process of emigration.* J Exp Med, 2001. **193**(10): p. 1149-58.

25. Chan, J.R., S.J. Hyduk, and M.I. Cybulsky, *Detecting rapid and transient upregulation of leukocyte integrin affinity induced by chemokines and chemoattractants.* J Immunol Methods, 2003. **273**(1-2): p. 43-52.

26. Constantin, G., et al., *Chemokines trigger immediate beta2 integrin affinity and mobility changes: differential regulation and roles in lymphocyte arrest under flow.* Immunity, 2000. **13**(6): p. 759-69.

27. Grabovsky, V., et al., *Subsecond induction of alpha4 integrin clustering by immobilized chemokines stimulates leukocyte tethering and rolling on endothelial vascular cell adhesion molecule 1 under flow conditions.* J Exp Med, 2000. **192**(4): p. 495-506.

28. Chen, J., et al., *The relative influence of metal ion binding sites in the I-like domain and the interface with the hybrid domain on rolling and firm adhesion by integrin alpha4beta7.* J Biol Chem, 2004. **279**(53): p. 55556-61.

29. Rose, D.M., J.W. Han, and M.H. Ginsberg, *alpha 4 integrins and the immune response.* Immunological Reviews, 2002. **186**: p. 118-124.

30. Carman, C.V. and T.A. Springer, *Integrin avidity regulation: are changes in affinity and conformation underemphasized?* Curr Opin Cell Biol, 2003. **15**(5): p. 547-56.

31. Liddington, R.C. and M.H. Ginsberg, *Integrin activation takes shape.* J Cell Biol, 2002. **158**(5): p. 833-9.

32. Shimizu, Y., D.M. Rose, and M.H. Ginsberg, *Integrins in the immune system.* Adv Immunol, 1999. **72**: p. 325-80.

33. Berlin, C., et al., *alpha 4 integrins mediate lymphocyte attachment and rolling under physiologic flow.* Cell, 1995. **80**(3): p. 413-22.

34. Chen, J., A. Salas, and T.A. Springer, *Bistable regulation of integrin adhesiveness by a bipolar metal ion cluster.* Nat Struct Biol, 2003. **10**(12): p. 995-1001.

35. Moy, V.T., E.L. Florin, and H.E. Gaub, *Intermolecular forces and energies between ligands and receptors.* Science, 1994. **266**(5183): p. 257-9.

36. Lee, G.U., D.A. Kidwell, and R.J. Colton, *Sensing Discrete Streptavidin Biotin Interactions with Atomic-Force Microscopy.* Langmuir, 1994. **10**(2): p. 354-357.

37. Muller, D.J., et al., *New frontiers in atomic force microscopy: analyzing interactions from single-molecules to cells.* Curr Opin Biotechnol, 2009. **20**(1): p. 4-13.

38. Hinterdorfer, P. and Y.F. Dufrene, *Detection and localization of single molecular recognition events using atomic force microscopy.* Nat Methods, 2006. **3**(5): p. 347-55.

39. Benoit, M., et al., *Discrete interactions in cell adhesion measured by single-molecule force spectroscopy.* Nat Cell Biol, 2000. **2**(6): p. 313-7.

40. Zhang, X., E. Wojcikiewicz, and V.T. Moy, *Force spectroscopy of the leukocyte function-associated antigen-1/intercellular adhesion molecule-1 interaction.* Biophys J, 2002. **83**(4): p. 2270-9.

41. Wojcikiewicz, E.P., et al., *Contributions of molecular binding events and cellular compliance to the modulation of leukocyte adhesion.* J Cell Sci, 2003. **116**(Pt 12): p. 2531-9.

42. Hanley, W.D., D. Wirtz, and K. Konstantopoulos, *Distinct kinetic and mechanical properties govern selectin-leukocyte interactions.* J Cell Sci, 2004. **117**(Pt 12): p. 2503-11.

43. Panorchan, P., et al., *Single-molecule analysis of cadherin-mediated cell-cell adhesion.* J Cell Sci, 2006. **119**(Pt 1): p. 66-74.

44. Helenius, J., et al., *Single-cell force spectroscopy.* J Cell Sci, 2008. **121**(Pt 11): p. 1785-91.

45. Zhang, X., et al., *Atomic force microscopy measurement of leukocyte-endothelial interaction.* Am J Physiol Heart Circ Physiol, 2004. **286**(1): p. H359-67.

46. Bell, G.I., *Models for the specific adhesion of cells to cells.* Science, 1978. **200**: p. 618-627.

47. Evans, E. and K. Ritchie, *Dynamic strength of molecular adhesion bonds.* Biophys. J., 1997. **72**: p. 1541-1555.

48. Chen, S. and T.A. Springer, *Selectin receptor-ligand bonds: Formation limited by shear rate and dissociation governed by the Bell model.* Proc Natl Acad Sci U S A, 2001. **98**(3): p. 950-5.

49. Merkel, R., et al., *Energy landscapes of receptor-ligand bonds explored with dynamic force spectroscopy.* Nature, 1999. **397**(6714): p. 50-3.

50. Binnig, G., C.F. Quate, and C. Gerber, *Atomic force microscope.* Phys. Rev. Lett., 1986. **56**: p. 930-933.

51. Ashkin, A., et al., *OBSERVATION OF A SINGLE-BEAM GRADIENT FORCE OPTICAL TRAP FOR DIELECTRIC PARTICLES.* Optics Letters, 1986. **11**(5): p. 288-290.

52. Evans, E., *Probing the relation between force--lifetime--and chemistry in single molecular bonds.* Annu Rev Biophys Biomol Struct, 2001. **30**: p. 105-28.

53. Alon, R., D.A. Hammer, and T.A. Springer, *Lifetime of the P-selectin-carbohydrate bond and its response to tensile force in hydrodynamic flow.[erratum appears in Nature 1995 Sep 7;376(6544):86]*. Nature, 1995. **374**(6522): p. 539-42.

54. Sader, J.E., *Frequency response of cantilever beams immersed in viscous fluids with applications to the atomic force microscope.* Journal of Applied Physics, 1998. **84**(1): p. 64-76.

55. Hutter, J.L. and J. Bechhoefer, *Calibration of Atomic-Force Microscope Tips.* Review of Scientific Instruments, 1993. **64**(7): p. 1868-1873.

56. Kubes, P., *The complexities of leukocyte recruitment.* Semin Immunol, 2002. **14**(2): p. 65-72.

57. Petri, B., M. Phillipson, and P. Kubes, *The physiology of leukocyte recruitment: an in vivo perspective.* J Immunol, 2008. **180**(10): p. 6439-46.

58. Springer, T.A., *Traffic signals on endothelium for lymphocyte recirculation and leukocyte emigration.* Annu Rev Physiol, 1995. **57**: p. 827-72.

59. Riener, C.K., et al., *Simple test system for single molecule recognition force microscopy.* Analytica Chimica Acta, 2003. **479**(1): p. 59-75.

60. Riener, C.K., et al., *Heterobifunctional crosslinkers for tethering single ligand molecules to scanning probes.* Analytica Chimica Acta, 2003. **497**(1-2): p. 101-114.

61. Kamruzzahan, A.S.M., et al., *Antibody linking to atomic force microscope tips via disulfide bond formation.* Bioconjug Chem, 2006. **17**(6): p. 1473-1481.

62. de Chateau, M., et al., *Kinetic and mechanical basis of rolling through an integrin and novel Ca2+-dependent rolling and Mg2+-dependent firm adhesion modalities for the alpha 4 beta 7-MAdCAM-1 interaction.* Biochemistry, 2001. **40**(46): p. 13972-9.

63. Tan, K., et al., *The structure of immunoglobulin superfamily domains 1 and 2 of MAdCAM-1 reveals novel features important for integrin recognition.* Structure, 1998. **6**(6): p. 793-801.

64. Green, N., et al., *Mutational analysis of MAdCAM-1/alpha4beta7 interactions reveals significant binding determinants in both the first and second immunuglobulin domains.* Cell Adhes Commun, 1999. **7**(3): p. 167-81.

65. Dando, J., et al., *A reassessment of the MAdCAM-1 structure and its role in integrin recognition.* Acta Crystallogr D Biol Crystallogr, 2002. **58**(Pt 2): p. 233-41.

66. !!! INVALID CITATION !!!

67. Lazarovits, A.I., et al., *Lymphocyte activation antigens. I. A monoclonal antibody, anti-Act I, defines a new late lymphocyte activation antigen.* J Immunol, 1984. **133**(4): p. 1857-62.

68. Schweighoffer, T., et al., *Selective expression of integrin alpha 4 beta 7 on a subset of human CD4+ memory T cells with Hallmarks of gut-trophism.* J Immunol, 1993. **151**(2): p. 717-29.

69. Aricescu, A.R., W. Lu, and E.Y. Jones, *A time- and cost-efficient system for high-level protein production in mammalian cells.* Acta Crystallogr D Biol Crystallogr, 2006. **62**(Pt 10): p. 1243-50.

70. Zhang, X., et al., *Molecular basis for the dynamic strength of the integrin alpha4beta1/VCAM-1 interaction.* Biophys J, 2004. **87**(5): p. 3470-8.

71. Tees, D.F., R.E. Waugh, and D.A. Hammer, *A microcantilever device to assess the effect of force on the lifetime of selectin-carbohydrate bonds.* Biophys J, 2001. **80**(2): p. 668-82.

72. Tulla, M., et al., *TPA primes alpha2beta1 integrins for cell adhesion.* FEBS Lett, 2008. **582**(23-24): p. 3520-4.

73. Krieg, M., et al., *A bond for a lifetime: employing membrane nanotubes from living cells to determine receptor-ligand kinetics.* Angew Chem Int Ed Engl, 2008. **47**(50): p. 9775-7.

74. Zhu, C. and R.P. McEver, *Catch bonds: physical models and biological functions.* Mol Cell Biomech, 2005. **2**(3): p. 91-104.

75. Kim, J., et al., *A mechanically stabilized receptor-ligand flex-bond important in the vasculature.* Nature, 2010. **466**(7309): p. 992-5.

76. Perez-Villar, J.J., et al., *Expression and function of alpha 4/beta 7 integrin on human natural killer cells.* Immunology, 1996. **89**(1): p. 96-104.

77. Walsh, G.M., et al., *Integrin alpha 4 beta 7 mediates human eosinophil interaction with MAdCAM-1, VCAM-1 and fibronectin.* Immunology, 1996. **89**(1): p. 112-9.

78. Berlin, C., et al., *Alpha 4 beta 7 integrin mediates lymphocyte binding to the mucosal vascular addressin MAdCAM-1.* Cell, 1993. **74**(1): p. 185-95.

79. Butcher, E.C. and L.J. Picker, *Lymphocyte homing and homeostasis.* Science, 1996. **272**(5258): p. 60-6.

80. Mora, J.R. and U.H. von Andrian, *T-cell homing specificity and plasticity: new concepts and future challenges.* Trends Immunol, 2006. **27**(5): p. 235-43.

81. Kinashi, T., *Intracellular signalling controlling integrin activation in lymphocytes.* Nat Rev Immunol, 2005. **5**(7): p. 546-59.

82. Cox, D., M. Brennan, and N. Moran, *Integrins as therapeutic targets: lessons and opportunities.* Nat Rev Drug Discov, 2010. **9**(10): p. 804-20.

83. Berlin-Rufenach, C., et al., *Lymphocyte migration in lymphocyte function-associated antigen (LFA)-1-deficient mice.* J Exp Med, 1999. **189**(9): p. 1467-78.

84. Sun, H., et al., *Distinct chemokine signaling regulates integrin ligand specificity to dictate tissue-specific lymphocyte homing.* Dev Cell, 2014. **30**(1): p. 61-70.

85. De Smedt, T., et al., *CD8alpha(-) and CD8alpha(+) subclasses of dendritic cells undergo phenotypic and functional maturation in vitro and in vivo.* J Leukoc Biol, 2001. **69**(6): p. 951-8.

86. Bell, G.I., *Models for the specific adhesion of cells to cells.* Science, 1978. **200**(4342): p. 618-27.

87. Evans, E. and K. Ritchie, *Dynamic strength of molecular adhesion bonds.* Biophys J, 1997. **72**(4): p. 1541-55.

88. Mackow, E.R. and I.N. Gavrilovskaya, *Hantavirus regulation of endothelial cell functions.* Thromb Haemost, 2009. **102**(6): p. 1030-41.

89. Raftery, M.J., et al., *beta2 integrin mediates hantavirus-induced release of neutrophil extracellular traps.* J Exp Med, 2014. **211**(7): p. 1485-97.

90. Raymond, T., et al., *Pathogenic hantaviruses bind plexin-semaphorin-integrin domains present at the apex of inactive, bent alphavbeta3 integrin conformers.* Proc.Natl.Acad.Sci.U.S.A, 2005. **102**(4): p. 1163-1168.

91. Stewart, P.L. and G.R. Nemerow, *Cell integrins: commonly used receptors for diverse viral pathogens.* Trends Microbiol, 2007. **15**(11): p. 500-7.

92. Humphries, J.D., A. Byron, and M.J. Humphries, *Integrin ligands at a glance.* J Cell Sci, 2006. **119**(Pt 19): p. 3901-3.

93. Plow, E.F., et al., *Ligand binding to integrins.* J Biol Chem, 2000. **275**(29): p. 21785-8.

94. Suehiro, K. and E.F. Plow, *Ligand recognition by beta 3 integrins.* Keio J Med, 1997. **46**(3): p. 111-4.

95. Shattil, S.J., C. Kim, and M.H. Ginsberg, *The final steps of integrin activation: the end game.* Nat Rev Mol Cell Biol, 2010. **11**(4): p. 288-300.

96. Banno, A. and M.H. Ginsberg, *Integrin activation.* Biochem Soc Trans, 2008. **36**(Pt 2): p. 229-34.

97. Arnaout, M.A., B. Mahalingam, and J.P. Xiong, *Integrin structure, allostery, and bidirectional signaling.* Annu Rev Cell Dev Biol, 2005. **21**: p. 381-410.

98. Brown, E.J., *Integrin-associated proteins.* Curr Opin Cell Biol, 2002. **14**(5): p. 603-7.

99. Hemler, M.E., *Integrin associated proteins.* Curr Opin Cell Biol, 1998. **10**(5): p. 578-85.

100. Hemler, M.E., *Tetraspanin functions and associated microdomains.* Nat Rev Mol Cell Biol, 2005. **6**(10): p. 801-11.

101. Termini, C.M., et al., *The membrane scaffold CD82 regulates cell adhesion by altering alpha4 integrin stability and molecular density.* Mol Biol Cell, 2014. **25**(10): p. 1560-73.

102. Shen, B., M.K. Delaney, and X. Du, *Inside-out, outside-in, and inside-outside-in: G protein signaling in integrin-mediated cell adhesion, spreading, and retraction.* Curr Opin Cell Biol, 2012. **24**(5): p. 600-6.

103. Takagi, J., H.P. Erickson, and T.A. Springer, *C-terminal opening mimics 'inside-out' activation of integrin alpha5beta1*. Nat Struct Biol, 2001. **8**(5): p. 412-6.

104. Kim, C., F. Ye, and M.H. Ginsberg, *Regulation of integrin activation.* Annu Rev Cell Dev Biol, 2011. **27**: p. 321-45.

105. Ye, F., et al., *Recreation of the terminal events in physiological integrin activation.* J Cell Biol, 2010. **188**(1): p. 157-73.

106. Xiong, J.P., et al., *A novel adaptation of the integrin PSI domain revealed from its crystal structure.* J Biol Chem, 2004. **279**(39): p. 40252-4.

107. Arnaout, M.A., *Integrin structure: new twists and turns in dynamic cell adhesion.* Immunol Rev, 2002. **186**: p. 125-40.

108. Krautkramer, E. and M. Zeier, *Hantavirus causing hemorrhagic fever with renal syndrome enters from the apical surface and requires decay-accelerating factor (DAF/CD55).* J Virol, 2008. **82**(9): p. 4257-64.

109. Drubin, D.G. and W.J. Nelson, *Origins of cell polarity.* Cell, 1996. **84**(3): p. 335-344.

110. Brown, D.A., B. Crise, and J.K. Rose, *Mechanism of membrane anchoring affects polarized expression of two proteins in MDCK cells.* Science, 1989. **245**(4925): p. 1499-501.

111. Choi, Y., et al., *A hantavirus causing hemorrhagic fever with renal syndrome requires gC1qR/p32 for efficient cell binding and infection.* Virology, 2008. **381**(2): p. 178-183.

112. Mou, D.L., et al., *Cellular entry of Hantaan virus A9 strain: Specific interactions with beta 3 integrins and a novel 70 kDa protein.* Biochemical and Biophysical Research Communications, 2006. **339**(2): p. 611-617.

113. Buranda, T., et al., *Equilibrium and Kinetics of Sin Nombre Hantavirus Binding at DAF/CD55 Functionalized Bead Surfaces.* Viruses-Basel, 2014. **6**(3): p. 1091-1111.

114. Brown, E.J. and W.A. Frazier, *Integrin-associated protein (CD47) and its ligands.* Trends Cell Biol, 2001. **11**(3): p. 130-5.

115. Brown, E., *Integrin-associated protein (CD47): an unusual activator of G protein signaling.* J Clin Invest, 2001. **107**(12): p. 1499-500.

116. Erb, L., et al., *An RGD sequence in the P2Y(2) receptor interacts with alpha(V)beta(3) integrins and is required for G(o)-mediated signal transduction.* J Cell Biol, 2001. **153**(3): p. 491-501.

117. Qi, A.D., S.C. Wolff, and R.A. Nicholas, *The apical targeting signal of the P2Y2 receptor is located in its first extracellular loop.* J Biol Chem, 2005. **280**(32): p. 29169-75.

118. Ebner, A., et al., *A new, simple method for linking of antibodies to atomic force microscopy tips.* Bioconjug Chem, 2007. **18**(4): p. 1176-84.

119. Wildling, L., et al., *Linking of sensor molecules with amino groups to amino-functionalized AFM tips.* Bioconjug Chem, 2011. **22**(6): p. 1239-48.

120. Trache, A., J.P. Trzeciakowski, and G.A. Meininger, *Mg2+ modulates integrin-extracellular matrix interaction in vascular smooth muscle cells studied by atomic force microscopy.* J Mol Recognit, 2010. **23**(3): p. 316-21.

121. Li, F., et al., *Force measurements of the alpha5beta1 integrin-fibronectin interaction.* Biophys J, 2003. **84**(2 Pt 1): p. 1252-62.

122. Zhang, X., E. Wojcikiewicz, and V.T. Moy, *Force spectroscopy of the leukocyte function-associated antigen-1/intercellular adhesion molecule-1 interaction.* Biophysical Journal, 2002. **83**(4): p. 2270-9.

123. Ligezowska, A., et al., *Mechanically enforced bond dissociation reports synergistic influence of Mn2+ and Mg2+ on the interaction between integrin alpha7beta1 and invasin.* J Mol Recognit, 2011. **24**(4): p. 715-23.

124. Buranda, T., et al., *Recognition of decay accelerating factor and alpha(v)beta(3) by inactivated hantaviruses: Toward the development of high-throughput screening flow cytometry assays.* Anal Biochem, 2010. **402**(2): p. 151-60.

125. Hinterdorfer, P. and Y.F. Dufrene, *Detection and localization of single molecular recognition events using atomic force microscopy.* Nature Methods, 2006. **3**(5): p. 347-355.

126. Rankl, C., et al., *Multiple receptors involved in human rhinovirus attachment to live cells.* Proc Natl Acad Sci U S A, 2008. **105**(46): p. 17778-83.

127. Ye, F., C. Kim, and M.H. Ginsberg, *Reconstruction of integrin activation.* Blood, 2012. **119**(1): p. 26-33.

128. Weisel, J.W., H. Shuman, and R.I. Litvinov, *Protein-protein unbinding induced by force: single-molecule studies.* Curr Opin Struct Biol, 2003. **13**(2): p. 227-35.

129. Litvinov, R.I., et al., *Functional and structural correlations of individual alphaIIbbeta3 molecules.* Blood, 2004. **104**(13): p. 3979-85.

130. Frelinger, A.L., 3rd, et al., *Monoclonal antibodies to ligand-occupied conformers of integrin alpha IIb beta 3 (glycoprotein IIb-IIIa) alter receptor affinity, specificity, and function.* J Biol Chem, 1991. **266**(26): p. 17106-11.

131. Luo, B.H., T.A. Springer, and J. Takagi, *A specific interface between integrin transmembrane helices and affinity for ligand.* PLoS Biol, 2004. **2**(6): p. e153.

132. Zhu, J., et al., *Requirement of alpha and beta subunit transmembrane helix separation for integrin outside-in signaling.* Blood, 2007. **110**(7): p. 2475-83.

133. Meyer, C.J., et al., *Mechanical control of cyclic AMP signalling and gene transcription through integrins.* Nat Cell Biol, 2000. **2**(9): p. 666-8.

134. Alenghat, F.J., et al., *Mechanical control of cAMP signaling through integrins is mediated by the heterotrimeric Galphas protein.* J Cell Biochem, 2009. **106**(4): p. 529-38.

135. Takagi, J. and T.A. Springer, *Integrin activation and structural rearrangement.* Immunol Rev, 2002. **186**: p. 141-63.

136. Chigaev, A., et al., *FRET detection of cellular alpha4-integrin conformational activation.* Biophys J, 2003. **85**(6): p. 3951-62.

137. Chigaev, A., et al., *FRET detection of lymphocyte function-associated antigen-1 conformational extension.* Mol Biol Cell, 2015. **26**(1): p. 43-54.

138. Gauthier, N.C., T.A. Masters, and M.P. Sheetz, *Mechanical feedback between membrane tension and dynamics.* Trends Cell Biol, 2012. **22**(10): p. 527-35.

139. Khan, S. and M.P. Sheetz, *Force effects on biochemical kinetics.* Annu Rev Biochem, 1997. **66**: p. 785-805.

140. Puklin-Faucher, E. and M.P. Sheetz, *The mechanical integrin cycle.* J Cell Sci, 2009. **122**(Pt 2): p. 179-86.

141. Orr, A.W., et al., *Mechanisms of mechanotransduction.* Dev Cell, 2006. **10**(1): p. 11-20.

142. Parsons, J.T., A.R. Horwitz, and M.A. Schwartz, *Cell adhesion: integrating cytoskeletal dynamics and cellular tension.* Nat Rev Mol Cell Biol, 2010. **11**(9): p. 633-43.

143. Ross, T.D., et al., *Integrins in mechanotransduction.* Curr Opin Cell Biol, 2013. **25**(5): p. 613-8.

144. Wang, X., et al., *Integrin Molecular Tension within Motile Focal Adhesions.* Biophys J, 2015. **109**(11): p. 2259-67.

145. Idzko, M., D. Ferrari, and H.K. Eltzschig, *Nucleotide signalling during inflammation.* Nature, 2014. **509**(7500): p. 310-7.

146. Ajit, D., et al., *Loss of P2Y(2) nucleotide receptors enhances early pathology in the TgCRND8 mouse model of Alzheimer's disease.* Mol Neurobiol, 2014. **49**(2): p. 1031-42.

147. Seye, C.I., et al., *Functional P2Y2 nucleotide receptors mediate uridine 5'-triphosphate-induced intimal hyperplasia in collared rabbit carotid arteries.* Circulation, 2002. **106**(21): p. 2720-6.

148. Schrader, A.M., J.M. Camden, and G.A. Weisman, *P2Y2 nucleotide receptor up-regulation in submandibular gland cells from the NOD.B10 mouse model of Sjogren's syndrome.* Arch Oral Biol, 2005. **50**(6): p. 533-40.

149. Ratchford, A.M., et al., *P2Y2 nucleotide receptors mediate metalloprotease-dependent phosphorylation of epidermal growth factor receptor and ErbB3 in human salivary gland cells.* J Biol Chem, 2010. **285**(10): p. 7545-55.

150. Peterson, T.S., et al., *Up-regulation and activation of the P2Y(2) nucleotide receptor mediate neurite extension in IL-1beta-treated mouse primary cortical neurons.* J Neurochem, 2013. **125**(6): p. 885-96.

151. Kong, Q., et al., *Interleukin-1beta enhances nucleotide-induced and alpha-secretase-dependent amyloid precursor protein processing in rat primary cortical neurons via up-regulation of the P2Y(2) receptor.* J Neurochem, 2009. **109**(5): p. 1300-10.

152. Fujishita, K., S. Koizumi, and K. Inoue, *Upregulation of P2Y2 receptors by retinoids in normal human epidermal keratinocytes.* Purinergic Signal, 2006. **2**(3): p. 491-8.

153. Ding, L., et al., *The P2Y(2) nucleotide receptor mediates tissue factor expression in human coronary artery endothelial cells.* J Biol Chem, 2011. **286**(30): p. 27027-38.

154. Idzko, M., et al., *Extracellular nucleotide and nucleoside signaling in vascular and blood disease.* Blood, 2014. **124**(7): p. 1029-37.

155. Ayata, C.K., et al., *Purinergic P2Y(2) receptors promote neutrophil infiltration and hepatocyte death in mice with acute liver injury.* Gastroenterology, 2012. **143**(6): p. 1620-1629 e4.

156. Schonrich, G., D.H. Kruger, and M.J. Raftery, *Hantavirus-induced disruption of the endothelial barrier: neutrophils are on the payroll.* Front Microbiol, 2015. **6**: p. 222.

157. Kobak, L., et al., *Hantavirus-induced pathogenesis in mice with a humanized immune system.* J Gen Virol, 2015.

158. Ko, H., et al., *Synthesis and potency of novel uracil nucleotides and derivatives as P2Y2 and P2Y6 receptor agonists.* Bioorg Med Chem, 2008. **16**(12): p. 6319-32.

159. Jacobson, K.A. and J.M. Boeynaems, *P2Y nucleotide receptors: promise of therapeutic applications.* Drug Discov Today, 2010. **15**(13-14): p. 570-8.

Vita

Chenyu Wu

EDUCATION

Lehigh University, Bethlehem, PA, USA
Doctor of Philosophy, May 2016
Bioengineering

Huazhong University of Science and Technology, Wuhan, Hubei, China
Bachelor of Science, June 2010
Biological Sciences

PUBLICATIONS

1 Fu, X. Xu, Y., **Wu, C.**, Moy, V.T., and Zhang, X. "Anchorage-dependent binding of integrin I-domain to adhesion ligands." *Journal of Molecular Recognition*, 2015 Jun 28(6):385-92. doi: 10.1002/jmr.2453.

2 Dong, X., Liao, X., **Wu, C.**, Liu, F., Zhou, J., Zhang, T. "Human Cytomegalovirus Immediate Early Protein 2 Enhances Myocardin-mediated Survival of Rat Aortic Smooth Muscle Cells." *Virus Research*, 2014 Nov 4;192:85-91. doi: 10.1016/j.virusres.2014.08.007.

3 Zhou, J., Liao, X., **Wu, C.**, Li, J., Xiao, R., Zhang, T. "The synergistic effects of cytomegalovirus IE2 and myocardin on cardiomyocyte hypertrophy." *FEBS letters*, 2011 Apr 6;585(7):1082-8. doi: 10.1016/j.febslet.2011.03.007.

4 Zhou, J.*, **Wu, C.***, Wu, Z., Xiao, R., Zhang, T., "The anti-A/H1N1 influenza virus effect of a Chinese Medicinal Prescription-Aitexin." 2011 *International Symposium on Biomedicine and Engineering*, Volume 1, Pages 403-408, 5 August 2011 (*Co-first author)

5 Wu, Z., Zhou, J., **Wu, C.** "The antibacterial activity of a Chinese Medicinal Prescription-Aitexin." 2011 *International Symposium on Biomedicine and Engineerin*g, Volume 2, Pages 446-449, 5 August 2011

6 Dai, Y., Wang, Z., **Wu, C.**, Cheng, C., Tang, W., Li, X., Zhou, J., Zhang, T. Construction and Expression of Human Coagulation Factor IX in the Pichia Pastoris. 2010 4th International Conference on Bioinformatics and Biomedical Engineering (iCBBE), pages 1 – 4, 23 July 2010

PATENT

Wu, Z., Zhang, J., **Wu, C.**, Zhang, Z., Li, X., 2012. A natural aroma Chinese medicinal prescription and its preparation method and application. CN 101700216 B, filed November 27, 2009 and issued April 25, 2012

WORK EXPERIENCE

Herbal-Basic Healthcare Pte, Ltd. Singapore, 2013-2015, Technology Consultant
Caobenxin Technology (wuhan) Co., Ltd. China, 2010-2011, Assistant Product Manager